MAGNETOTELLURIC MEASUREMENTS OF CONDUCTIVITY ANOMALIES IN NORTHERN WISCONSIN

CHARLES T. YOUNG

U. OF WISCONSIN
GEOPHYSICAL & POLAR RESEARCH CENTER

DEPT. OF GEOLOGY & GEOPHYSICS

MADISON, WIS. 53706

WISCONSIN REPORT No. 77-3 DEC., 1977

MAGNETOTELLURIC MEASUREMENTS OF CONDUCTIVITY ANOMALIES IN NORTHERN WISCONSIN

by

Charles Thomas Young

under the supervision of Professor Clarence S. Clay

Four-channel magnetotelluric (MT) measurements in the frequency range 1 to 50 Hz were made, in an array of stations spaced 10 to 1000 meters apart, over linear conductors of copper sulfide and graphitic schist near Ladysmith, Wisconsin. The apparent resistivities and phases for electric field perpendicular to the conductors, for stations away from the conductors, match a flat-layered model consisting of a first layer of 250 ohm-meter material thickness 40 to several hundred meters, a second layer of 1000 ohm-meter material zero to 1000 meters thick, a third layer, very resistive, 25,000 ohm-meters or greater of thickness 10 to 40 kilometers, and a bottom 2000 ohm-meter half-space.

The R-max and R-min data over the conductive schist were modelled by a long narrow conductor or 0.3 ohm meter resistivity having a width of 120 meters, and a depth of 80 meters, buried 40 meters beneath the surface. The minesite model was developed from drill hole data, a resistivity log and nearby DC resistivitiy measurements.

The MT data within a few hundred meters of the conductors show (1) values of R-parallel one tenth or less those at distant stations; (2) values of R-parallel one tenth or less than R-perpendicular at the

same station; (3) alignment of R-max perpendicular to the known strike of the conductor. Beyond a few hundred meters from the conductors, some stations showed scattered orientations, and R-max values only a few percent greater than R-min, probably due to nearby random inhomogeneities. Other stations at similar distances from the central conductor had strong orientations and separation of R-max and R-min indicating proximity to other conductors or local structures which I model with inhomogeneities of high and low conductivity. I found that I had to be closer than about 1/20 skin depth to a conductor in order to detect it.

Approved by Florence S. Law

major professor

TABLE OF CONTENTS

Chapter 1. Introduction

This research applied the digital analysis tensor impedance approach to magentotelluric (MT) analysis of high frequency data (audio frequency magnetotellurics, AMT), using the technique to investigate conductivity anomalies in northern Wisconsin.

I developed sensors and amplifiers to record signals in the frequency 1 to 35 Hz band and modified programs used by Dowling 1968 and 1970 to analyse the data. The field measurements were made in Rusk County, Wisconsin, over a copper mine site, near Ladysmith, Wisconsin, and over other nearby conductors.

The data from two of these traverses, the minesite and Washington township, were computer analyzed to yield tensor apparent resistivities and phases. I interpret the data away from the conductivity anomalies in terms of flat layered earth models; that is, with resistivity a function of depth only, $\rho(z)$, frequently referred to as a one-dimensional model. I present models with resistivity variations in two dimensions, $\rho(x, y)$; that is, models with an infinite strike length, frequently referred to as a two-dimensional model. A third set of traverse data, a reconnaissance study in the Fireside Lakes area, I analyzed for scalar apparent resistivity, phase and coherency. I use these data to indicate broad areas of low resistivity.

Chapter 2. Review of Literature

2.1 AMT Apparatus and Field Technique

MT work in the frequency range 1 Hz to 20 KHz is usually applied to shallow exploration problems such as finding minerals and permafrost: Strangway and Vozoff, 1967; Gineau, 1975; Strangway, Swift and Holmer, 1973. The frequency range is high enough so that analog techniques may be used for frequency analysis and averaging the MT signals. The instrumentation and field techniques for this work have passed through several stages of sophistication. For example, Lepley and Adams, 1966, used an air core coil and a single channel of narrow band filter, rectifier and integrator, measuring electric, E, and magnetic field, H, over separate intervals of time. Others replaced the single channel system with two or more channels so that E and H may be measured simultaneously; for example, Clerc, 1970; Strangway et al., 1973; and Hoover, 1975. It is also possible to use radio stations as a signal source (Clerc, 1970, and Gineau, 1975). Gineau developed mat electrodes which are capacitively coupled to the ground, making continuous-towed profiling possible over smooth ground.

Slankis and Becker, 1969, and Slankis, Telford and Becker, 1972, made two-component telluric and magnetotelluric measurements at a single frequency, 8 Hz, and physically rotated the E and H sensors at several stations. The orientation of resistivity minima and maxima showed good alignment with the known structure, which consisted of a wedge of conductive sediments overlying crystalline bedrock.

Grosskopf, Smith and Bostick, 1974, developed a hybrid analog and digital field system for making four-channel measurements (Figure 2.3.1) using narrowband filters followed by synchronous detectors coupled to a local oscillator. The four channels of signal yield eight in-phase and quadrature outputs which are digitized and entered into a mini-computer. Cross and auto powers are calculated, so that apparent resistivities and phases may be obtained before leaving the field site.

2.2 Telluric Current Method

The telluric current method, used as early as 1939 by Schlumberger, consists of measuring natural a.c. electric potentials over a survey area and relating them to simultaneous measurements at a base station. Recent work has been done by Berdachevski, 1965, and Yungul, 1966. Combined magnetotelluric-telluric work has been done at low frequencies, $f \simeq 1/60$ Hz, by Hermance and Thayer, 1975, and at 8 Hz for mining exploration by Slankis, Telford and Becker, 1972. The main reason for doing combination magnetotelluric-telluric measurements is that a few time-consuming magnetotelluric measurements can be combined with many quicker telluric measurements to improve the quantity of field coverage over that which could be obtained with magnetotellurics, and to improve the quality of the coverage that could be obtained with tellurics alone. Magnetotellurics gives impedance values, or apparent resistivities, whereas tellurics alone gives only relative electric field values or apparent resistivities relative to base station. Hermance illustrates that telluric transfer tensor, relating remote electric

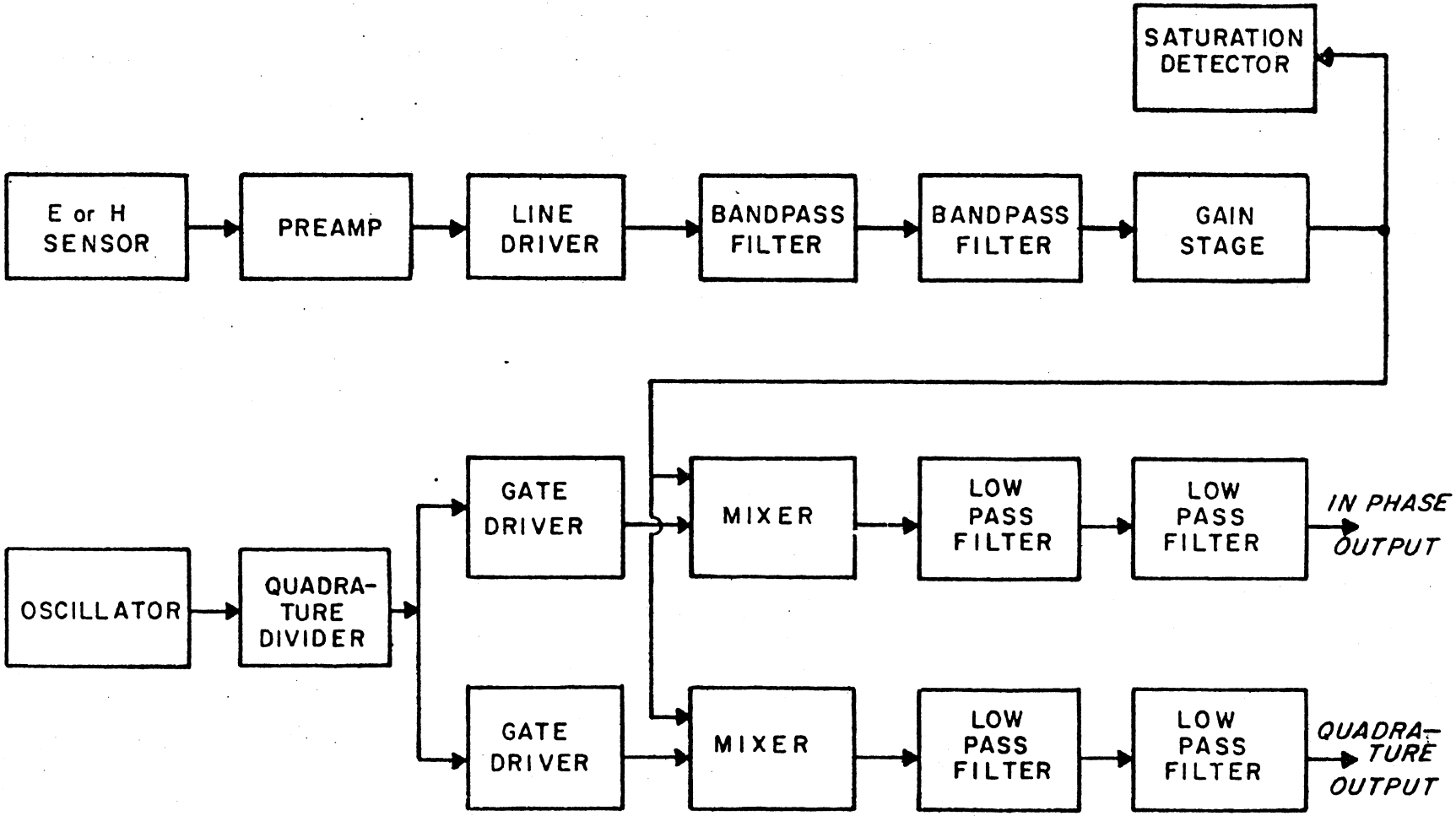

Figure 2.3.1. Audiomagnetotelluric field system of advanced design used by Grosskopf, Smith and Bostick, 1974.

to base electric measurements, can be combined with the base magnetotelluric tensor to give a magnetotelluric impedance tensor at each remote station. He cites experimental evidence for his assumption that the magnetic field varies only slightly over the entire survey region. This assumption appears to be valid for crustal scale, low frequency (below .1 Hz) work. My work shows that for mining scale studies, that is, for shallow conductors in shield areas, the conductive deposits can affect the surface magnetic fields. Even if the hypothesis of constant magnetic field is invalid for certain cases, the telluric current technique is still useful, since the results can still be interpreted as the electric field data.

Chapter 3. Theory

Here I discuss the nature of the magnetotelluric signal sources and define quantities such as impedance, phase and apparent resistivity that will be sought from the electric and magnetic field data. The next chapter contains the computational method by which these data are analyzed to yield the desired quantities.

3.1 Signal Source

The electromagnetic signals which are detected in this experiment are from lightning storms near the equator. The spectrum of the energy emitted is broad, having been measured from 4 Hz to over 400 kHz, (Maxwell, 1966). At the low end of the spectrum the signals exhibit broad resonances, known as Schuman resonances, of approximately 4, 8, 14, 20, and 26 Hz, which are due to the propagation of the signals through the earth ionosphere wave guide. The theory of this wave guide propagation is discussed by Madden and Thompson, 1965.

Ideally, for magnetotellurics, one wants vertically incident plane waves. In fact, due to the high effective index of refraction of the conducting earth, near-horizontal incidence waves are refracted to vertical at the earth's surface. In addition to direction of propagation, the electric and magnetic fields should be measured far enough away from the source so that the E/H ratio is not dependent on the source distance of source geometry. In free space, this distance would be the plane wave region. Over a conducting earth, Bannister (1969) shows that "the measurement distance must only be greater than seven skin depths for the ratio of horizontal electrical

and magnetic fields at the earth's surface to be determined primarily by the surface impedance of the earth". This distance can be thought of as marking the start of the effective plane wave region. For northern Wisconsin, signals at 10 Hz coming from sources more distant than 25 kilometers satisfy this condition, given an earth resistivity of 5000 ohm meters.

I measured electric and magnetic fields of these signals to determine the surface impedance of the earth, defined in the next section.

3.2 Impedance Tensor and Apparent Resistivity

Here I define the surface scalar and tensor impedance and scalar and tensor apparent resistivity. Knowing these quantities, one can interpret the resistivity structure under the measurement site. Section 3.3 contains examples of theoretical apparent resistivity profiles over two two-dimensional structures. The discussion here is based on Word, Smith and Bostick, 1970; Sims, 1969; Madden, 1963; Vozoff, 1972; and Swift, 1972.

The horizontal components of the electric and magnetic fields (E and H) are related by an impedance tensor Z, with components Z_{XX}, Z_{XY}, Z_{YX}, Z_{YY}.

$$E_X = Z_{XX}H_X + Z_{XY}H_Y$$

$$E_Y = Z_{YX}H_X + Z_{YY}H_Y \qquad 3.2.1$$

The MKS units here are E-volts/meter, H-Amps/meter, Z ohms. For an inhomogeneous earth, the components of Z are functions of frequency and orientation or coordinate axes. The method of estimating the components from field data is discussed in Chapter 4.

In the case of the homogeneous earth, Z is independent of orientation, Z_{XX} and $Z_{YY} = 0$, $Z_{YX} = -Z_{YX}$, and Z has the value

$$Z = E_X/H_Y = \sqrt{j\omega\mu\rho} \qquad 3.2.2$$

ρ = resistivity of homogeneous earth in ohm meters

μ = permeability of the medium in Henrys/meter. The permeability of most rocks is equal to that of free space, $\mu_o = 4\pi \times 10^{-7}$ H/m

ω = angular frequency = $2\pi f$

$j = \sqrt{-1}$

In this case, H is orthogonal to E and has a phase lag of 45°. The skin depth in the earth is expressed by

$$\delta = \left(\frac{2\rho}{\omega\mu}\right)^{1/2} \simeq 500\ (\rho/f)^{1/2} \text{ meters} \qquad 3.2.3$$

and represents the depth at which the wave is attenuated to 1/e of its amplitude at the surface.

This homogeneous earth case is used to define apparent resistivity, ρ_a,

$$\rho_a = \frac{1}{\mu\omega}\left(\frac{E_X}{H_Y}\right)^2 \quad \text{or} \quad \frac{1}{\mu\omega}\,|Z|^2 \qquad 3.2.4$$

Customary geophysical electric and magnetic field units are mv/km for electric field and gamma for magnetic field where 1 gamma = $10^{-9}/\mu_o$ ampere/meter. Using these units the apparent resistivity, Equation 3.2.4, becomes

$$\rho_a = \frac{1}{5f}|Z|^2 \qquad \text{where } Z = E_i/H_j \qquad 3.2.5$$

$$i,j = X,Y \text{ or } Y,X$$

with

f = frequency in Hz

The apparent resistivity for a homogeneous earth or flat-layered earth is independent of the orientation of the measurement axis. The variation of apparent resistivity and phase of E to H with frequency for a layered earth and the techniques of data interpretation are discussed in Keller and Frischknecht (1967), pages 214 to 227.

The apparent resistivity defined by Equation 3.2.4 is usually called the <u>scalar</u> apparent resistivity, with phase equal to the phase difference of E_X and H_Y. The <u>tensor</u> apparent resistivity is similarly defined as

$$\rho_{aij} = \frac{1}{5f}|Z_{ij}|^2 \qquad i, j = X \text{ or } Y \qquad 3.2.6$$

Where the Z_{ij} are defined in Equation 3.2.1. The phase of the tensor resistivity is the phase of the corresponding impedance element. These impedances are used to interpret the resistivity structure under the measurement site. I give examples in the next section of theoretical responses over two two-dimensional structures: (1) a

fault between two blocks of different resistivities; (2) a narrow vertical conductor with overburden.

3.3 Polarization Modes over a Two-dimensional Earth

Structures such as faults, dikes or fold belts are frequently the subject of geophysical investigation. In many cases such structures are approximately two-dimensional, meaning that there is little or no variation along one horizontal axis, such as, along the strike of a fault or along the axis of a fold belt. Using the tensor magnetotelluric method, it is possible to determine the orientation of such structures by rotating the coordinate system to find minimum and maximum apparent resistivities. If the axes of measurement are aligned with the structure, Z_{YX} and Z_{XY} are the impedances of the E-perpendicular and E-parallel modes of propagation, respectively, as in Figure 3.3.1. These modes are decoupled from each other. For a perfectly two-dimensional earth components Z_{XX} and Z_{YY} are zero when the measuring axes are aligned with the structure. For geometry which is only approximately two-dimensional, Z_{XX} and Z_{YY} are considerably smaller than Z_{XY} and Z_{YX}. In the event that the measurement axes are not aligned with the structure, the impedances must be mathematically rotated using the formulas given in section 3.5

3.3.1 Apparent resistivities over a fault

In the case of a simple two-dimensional model of a fault or contact consisting of adjacent blocks of different resistivities, Figure 3.3.1.1, the E-perpendicular apparent resistivity is discontinuous across the fault while the E-parallel value shows a

STRIKE ALONG Y AXIS

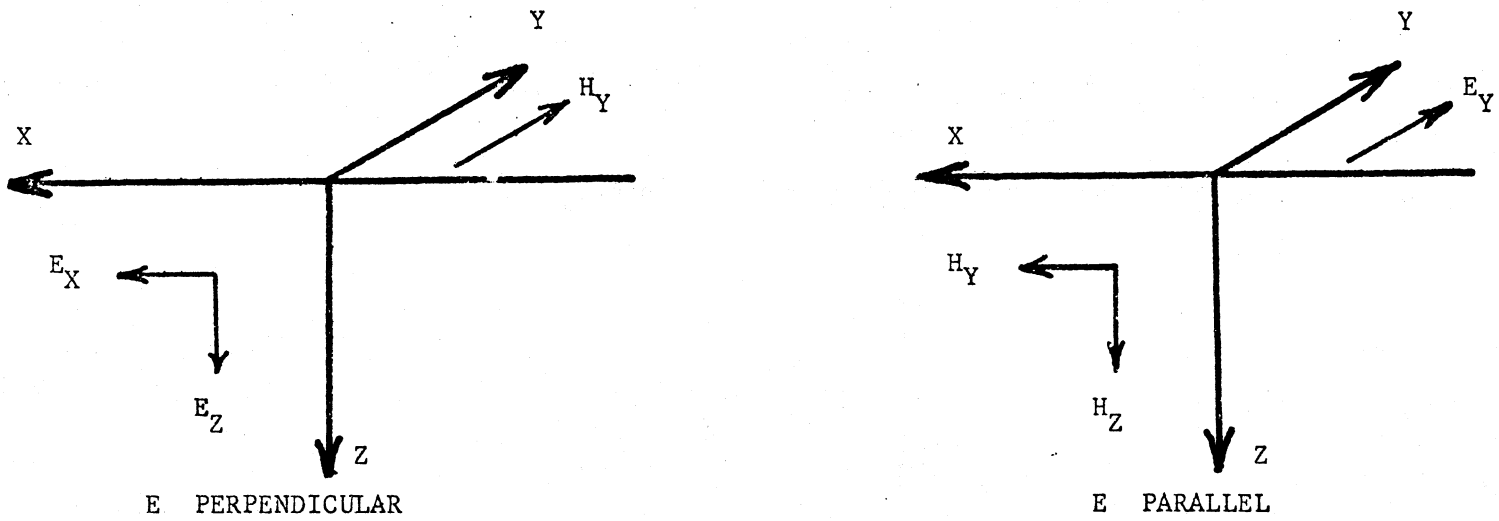

Figure 3.3.1 Magnetotelluric polarization modes. From Swift, 1971.

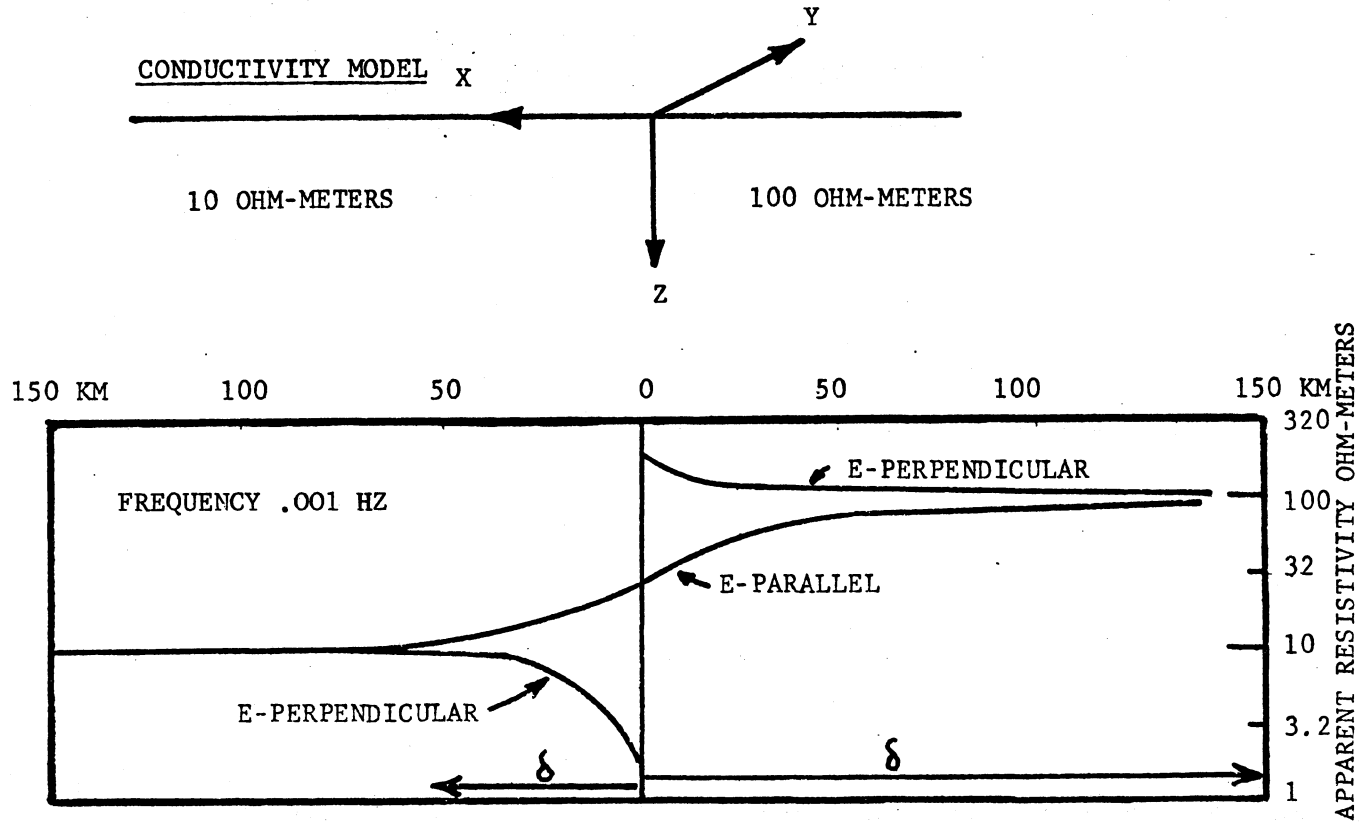

Figure 3.3.1.1. Theoretical apparent resistivities across a fault, from Swift, 1971. E-parallel and E-perpendicular or R-parallel and R-perpendicular refer to results using electric field measured along X or Y axis respectively, using axes as labelled on uppermost figure. Skin depth in each block shown by δ in lower figure.

smooth transition from the homogeneous earth value on one side of the fault to the homogeneous-earth value of the other side (Swift, 1971).

3.3.2 Apparent resistivities over a narrow conductor

Figure 3.3.2.1 gives theoretical R-perpendicular and R-parallel profiles over a buried narrow vertical conductor at a frequency of 1000 Hz. The R-perpendicular anomaly is narrow, approximately the width of the conductor. The R-parallel anomaly is considerably wider. Even though this model is calculated for a different frequency than the fault model, they may be compared by skin depth, which is indicated on the figure or in the caption. The significance of the skin depth here is that it provides a scaled measure of how near an MT site must be to a fault or conductor to detect it. For example, for the buried conductor of Figure 3.3.2.1 for a factor of two contrast from the asymptotic value, an MT station must be within 600 meters of the conductor to detect it for R-parallel, and for R-perpendicular the station must be on top of the conductor.

3.4 Rotation of Axes to find Orientation of Structure

The estimates of Z from an experiment must be rotated mathematically to mind maximum and minimum values for Z_{XY} and Z_{YX}, respectively. For a two-dimensional structure, rotation finds the principal axes. The general rotation rule for the Z tensor is

$$Z'_{XY} = \frac{Z_{XY} - Z_{YX}}{2} + \frac{Z_{XY} + Z_{YX}}{2} \cos 2\Phi - \frac{Z_{XX} - Z_{YY}}{2} \sin 2\Phi \qquad 3.4.1$$

$$Z'_{YX} = -\left\{\frac{Z_{XY} - Z_{YX}}{2}\right\} + \frac{Z_{XY} + Z_{YX}}{2} \cos 2\Phi - \frac{Z_{XX} + Z_{YY}}{2} \sin 2\Phi \qquad 3.4.2$$

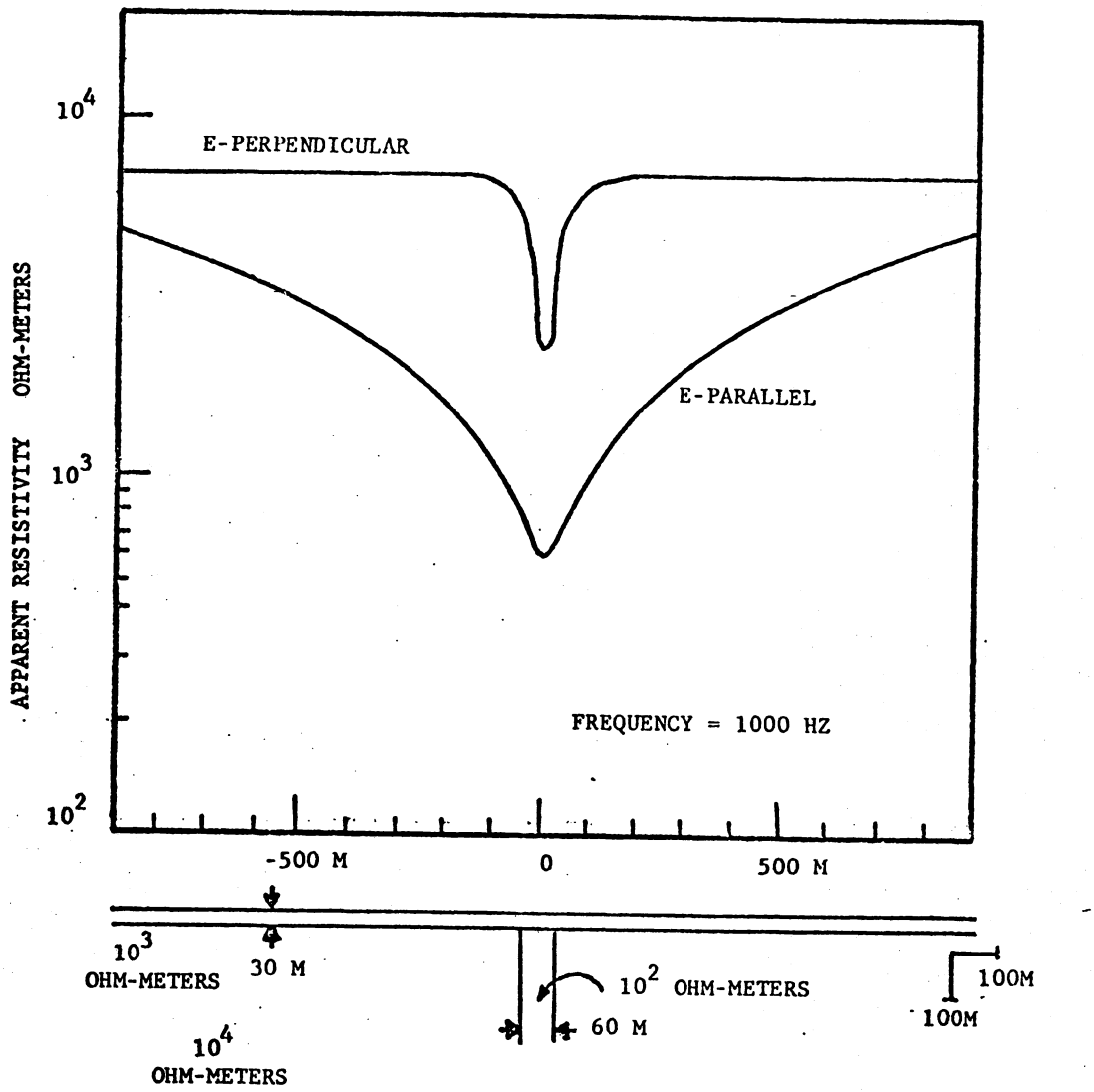

Figure 3.3.2.1. Theoretical response across a buried narrow vertical conductor, from Ward et al., 1974. Skin depth in 10^4 ohm-meter host rock is 1581 meters.

where the primes refer to results in the rotated reference frame and Φ is the angle of rotation. For the correct value of Φ, Z_{XY} is maximized and Z_{YX} is minimized, or vice versa. The impedances for E-parallel and E-perpendicular modes of propagation will be equal to Z_{XY} and Z_{YX}, or vice versa.

It is not necessary to rotate by increments and check Z_{XY} and Z_{YX} for inflections to find Φ. The angle of the rotated axes may be found directly by the following relationship (Sims, 1969):

$$4\Phi = \tan^{-1} \frac{2\,(ac + bd)}{(a^2 + b^2) - (c^2 + d^2)} \qquad 3.4.3$$

where

$$Z_{XX} - Z_{YY} = a + jb \qquad Z_{XY} + Z_{YX} = c + jd$$

Evaluating Φ in equation 3.4.3 yields four angles 90 degrees apart. Comparing the resultant values of Z_{XY}, Equation 3.4.1 for these rotations, one can identify two directions, 180 degrees apart, as the orientation of Z-max and the other two directions as the orientation of Z-min.

One in-line pair of directions indicates strike of the structure, but from the impedance analysis alone there is no way to tell which of the pairs is the strike in a single site.

It would be useful if there were some way to tell from observations of a single station whether the Z maximum direction or the Z minimum direction were the strike of the structure, that is, the direction along which the resistivity does not vary. The vertical magnetic field, if measured simultaneously with the horizontal electric field, can be used to determine strike.

For cases of resistivity structure consisting of anything other than plane layers, the vertical component of the magnetic field will be non-zero. This result follows directly from the appropriate Maxwell equation,

$$\vec{\nabla} \times \vec{E} + \frac{\mu}{c} \frac{\partial \vec{H}}{\partial t} = 0 \qquad 3.4.4$$

which has a vertical component of

$$\frac{\partial E_Y}{\partial X} - \frac{\partial E_X}{\partial Y} + \frac{\mu}{c} \frac{\partial H_Z}{\partial t} = 0 \qquad 3.4.5$$

showing that horizontal variations in the electric field caused by conductivity changes give rise to a vertical component of the magnetic field.

The empirical relationship that relates the vertical magnetic field to the horizontal electric field is given by

$$H_Z = Y_{ZX} E_X + Y_{ZY} E_Y \qquad 3.4.6$$

This equation defines the admittance tensor, Y, which can be found from H_Z, E_X, and E_Y data. The magnitude of Y is related to the horizontal inhomogeneity of the earth by equation 3.4.6. The components of Y are sensitive to coordinate rotation, as is the impedance tensor Z. Word, Smith and Bostick (1970) show that the rotation of the y-axis which maximizes Y_{ZY} is found by

$$2\Phi_{max} = \tan^{-1} \frac{2\,(ac + bd)}{(a^2 + b^2) - (c^2 + d^2)} \qquad 3.4.7$$

where

$$Y_{ZY} = a + jb \qquad Y_{ZY} = c + jd$$

The 2 Φ term yields two in-line directions. Φ max uniquely identifies strike direction.

Chapter 4. Estimation of Tensor Components from the Data

I recorded four channels of data, E_X, E_Y, H_X, and H_Y, using the apparatus that will be described in Chapter 5. These data were analyzed using the statistical techniques described in this chapter, yielding estimates of scalar or rotated tensor apparent resistivity and phase.

4.1 The Use of Autopowers and Coherencies to Determine Tensor Components

The components of the impedance tensor Z may be estimated from n independent data sets, that is, n successive time series. There is more than one possible way to calculate each component of Z. In my data analysis I will use two solutions for Z, Z^E and Z^H, which minimize noise on the electric and magnetic channels, respectively. Z^E and Z^H will be averaged and the coordinate system will be rotated to find maximum and minimum impedances. The results will be expressed as rotated tensor apparent resistivities and phases. The following description of the statistical techniques follows Sims, 1969, and Bentley, 1973. Additional details, computer programs and run directions are on file at the University of Wisconsin Geophysical and Polar Research Center.

Suppose I have n consecutive measurements of E_X, H_X, and H_Y at a given frequency and I desire to estimate the elements Z_{XX} and Z_{YY}. These tensor components can be found by minimizing the sum of the squares of the differences between E_X and E_X predicted from the values of H_X and H_Y, that is, to minimize the quantity

$$\Psi = \sum_{i=1}^{n} (E_{Xi} - Z_{XX}H_{Xi} - Z_{XY}H_{Yi})(E^*_{Xi} - Z^*_{XX}H^*_{Xi} - Z^*_{XY}H^*_{Yi}) \qquad 4.1.1$$

where * indicates complex conjugate.

The Z_{XX} which minimizes this quantity is found by setting to zero the derivatives of Ψ with respect to the real and imaginary parts of Z_{XX}.

$$\frac{\partial \Psi}{\partial Re Z_{XX}} = \sum \left\{ -(H_{Xi})(E_{Xi}^* - Z_{XX}^* H_{Xi}^* - Z_{Xi}^* H_{Yi}^*) - (E_{Xi} - Z_{XX}H_{Xi} - Z_{XY}H_{Yi})(H_{Xi}) \right\} = 0$$

$$\frac{\partial \Psi}{\partial Im Z_{XX}} = \sum \left\{ -(H_{Xi})(E_{Xi}^* - Z_{XX}^* H_{Xi}^* - Z_{XY}^* H_{Yi}^*) + (E_{Xi} - Z_{XX}H_{Xi} - Z_{XY}H_{Yi})(H_{Xi}) \right\} = 0$$

4.1.2

Adding the two equations and dividing by two yields

$$\sum_{i=1}^{n} H_{Xi}^* E_{Xi} = Z_{XX} \sum_{i=1}^{n} H_{Xi} H_{Xi}^* + Z_{XY} \sum_{i=1}^{n} H_{Yi} H_{Xi}^* \qquad 4.1.3$$

Similarly, setting to zero the derivatives of Ψ with respect to the real and imaginary part of Z_{XY} yields

$$\sum_{i=1}^{n} E_{Xi} H_{Yi}^* = Z_{XX} \sum_{i=1}^{n} H_{Xi} H_{Yi}^* + Z_{XY} \sum_{i=1}^{n} H_{Yi} H_{Yi}^* \qquad 4.1.4$$

Two more equations relating Z_{XX} and Z_{XY} to cross and auto products of field quantities are also given by Sims ,1969,

$$\sum_{i=1}^{n} E_{Xi} E_{Xi}^* = Z_{XX} \sum_{i=1}^{n} H_{Xi} E_{Xi}^* + Z_{XY} \sum_{i=1}^{n} H_{Yi} E_{Xi}^* \qquad 4.1.5$$

$$\sum_{i=1}^{n} E_{Xi} E_{Yi}^* = Z_{XX} \sum_{i=1}^{n} H_{Xi} E_{Yi}^* + Z_{XY} \sum_{i=1}^{n} H_{Yi} E_{Yi}^* \qquad 4.1.6$$

These auto and cross products such as $\Sigma\, E_{iY}\, E_{iY}^{*}$, $\Sigma\, H_{iY}\, E_{iY}^{*}$ are auto and cross power density spectra. There are many methods for determining these quantities from a digitized time series. My method, as described by Sims, 1969, involves taking the discrete Fourier transform using the fast Fourier transform algorithm (FFT), computing the products for each harmonic and averaging neighboring harmonics to obtain the desired bandwidth. My program averages harmonics to produce spectra with frequencies spaced logarithmically. The four equations for Z_{XX} and Z_{XY} give six possible solutions for each unknown. Sims shows that two of the six solutions are unstable, and that of the four remaining, two are biased up by noise on the electric channel and the two others are biased down by noise on the magnetic channel. My analysis uses two of these solutions, one called Z^{E}, biased up by electric channel noise, the other, Z^{H}, biased down by magnetic channel noise. These are averaged for my final value of Z which is used to calculate rotated tensor values.
Some authors and programs use the coherency notation, others use cross and auto powers. I present both forms for Z^{E}_{XY}; the two are related by $\mathrm{coh}(AB) \equiv \langle AB \rangle / [\langle AA^{*} \rangle^{1/2} \langle BB^{*} \rangle^{1/2}]$ where the brackets are defined as averaging over n independent data:

$$\langle AB \rangle \equiv \frac{1}{n} \sum_{i=1}^{n} A_i B_i$$

For example, the two forms for Z_{XY} that we use are

$$Z^{E}_{XY} = \frac{\langle H_X E_X^{*} \rangle \langle E_X E_Y^{*} \rangle - \langle H_X E_Y^{*} \rangle \langle E_X E_X^{*} \rangle}{\langle H_X E_X^{*} \rangle \langle H_Y E_Y^{*} \rangle - \langle H_X E_Y^{*} \rangle \langle H_Y E_X^{*} \rangle} \qquad 4.1.7$$

$$= \frac{\langle E_X E_X^* \rangle^{1/2}}{\langle H_Y H_Y^* \rangle^{1/2}} \left\{ \frac{\text{coh}(H_X E_X^*)\,\text{coh}(E_X E_Y^*) - \text{coh}(H_X E_Y^*)}{\text{coh}(H_X E_X^*)\,\text{coh}(E_Y E_Y^*) - \text{coh}(H_X E_Y^*)\,\text{coh}(H_Y E_X^*)} \right\} \qquad 4.1.8$$

$$Z^H_{XY} = \frac{\langle E_X E_X^* \rangle^{1/2}}{\langle H_Y H_Y^* \rangle^{1/2}} \left\{ \frac{\text{coh}(E_X H_Y^*) - \text{coh}(H_X H_Y^*)\,\text{coh}(E_X H_X^*)}{1 - |\text{coh}(H_X H_Y^*)|^2} \right\} \qquad 4.1.9$$

The equations for the other impedance elements are similarly found (expressed only in coherencies):

$$Z^H_{XX} = \frac{\langle E_X E_X^* \rangle^{1/2}}{\langle H_X H_X^* \rangle^{1/2}} \left\{ \frac{\text{coh}(E_X H_X^*) - \text{coh}(E_X H_Y^*)\,\text{coh}(H_Y H_X^*)}{1 - |\text{coh}(H_X H_Y)|^2} \right\} \qquad 4.1.10$$

$$Z^H_{YX} = \frac{\langle E_Y E_Y^* \rangle^{1/2}}{\langle H_X H_X^* \rangle^{1/2}} \left\{ \frac{\text{coh}(E_Y H_X^*) - \text{coh}(E_Y H_Y^*)\,\text{coh}(H_Y H_X^*)}{1 - |\text{coh}(H_X H_Y^*)|^2} \right\} \qquad 4.1.11$$

$$Z^H_{YY} = \frac{\langle E_Y E_Y^* \rangle^{1/2}}{\langle H_Y H_Y^* \rangle^{1/2}} \left\{ \frac{\text{coh}(E_Y H_Y^*) - \text{coh}(E_Y H_X^*)\,\text{coh}(H_X H_Y^*)}{1 - |\text{coh}(H_X H_Y^*)|^2} \right\} \qquad 4.1.12$$

$$Z^E_{YX} = \frac{\langle E_Y E_Y^* \rangle^{1/2}}{\langle H_X H_X^* \rangle^{1/2}} \left\{ \frac{\text{coh}(E_Y E_X^*)\,\text{coh}(H_Y E_Y^*) - \text{coh}(H_Y E_X^*)}{\text{coh}(H_X E_X^*)\,\text{coh}(H_Y E_Y^*) - \text{coh}(H_X E_Y^*)\,\text{coh}(H_Y E_X^*)} \right\} \qquad 4.1.13$$

$$Z^E_{YY} = \frac{\langle E_Y E_Y^* \rangle^{1/2}}{\langle H_Y H_Y^* \rangle^{1/2}} \left\{ \frac{\text{coh}(H_X E_X^*) - \text{coh}(H_X E_Y^*)\,\text{coh}(E_Y E_X^*)}{\text{coh}(H_X E_X^*)\,\text{coh}(H_Y E_Y^*) - \text{coh}(H_X E_Y^*)\,\text{coh}(H_Y E_X^*)} \right\} \qquad 4.1.14$$

$$Z^E_{XX} = \frac{\langle E_X E_X^* \rangle^{1/2}}{\langle H_X H_X^* \rangle^{1/2}} \left\{ \frac{\text{coh}(H_Y E_Y^*) - \text{coh}(E_X E_Y^*)\,\text{coh}(H_Y E_X^*)}{\text{coh}(H_X E_X^*)\,\text{coh}(H_Y E_Y^*) - \text{coh}(H_X E_Y^*)\,\text{coh}(H_Y E_X^*)} \right\} \qquad 4.1.15$$

4.2 Conditions Under Which Tensor Impedance Reduces to Scalar Impedance

There are some instances where I would want to substitute the scalar impedance for the tensor value. This substitution would be necessary if I were working with two-channel apparatus which gives only scalar values, or if at a given measurement site one channel of instrumentation malfunctioned, leaving me with only three good channels of data. It has been my plan all along to set up the measurement axes parallel to and perpendicular to the strike of geological structures I am studying. The tensor resistivities reduce to the scalar values in such cases.

Considering the terms in Z^E_{XY} and Z^H_{XY}, Equations 4.1.8 and 4.1.9:

1. coh $(H_X H_Y)$ should go to zero if the signals are randomly polarized;
2. coh $(E_X H_X)$, coh $(E_X H_Y^*)$ and coh $(E_X E_X^*)$ should be zero if the apparatus is aligned with structure, detecting separate modes of propagation.

Removing these quantities from Z^E_{XY} and Z^H_{XY} yields, in both cases.

$$Z_{XY} = \frac{\langle E_X E_X^* \rangle^{1/2}}{\langle H_Y H_Y \rangle^{1/2}} \operatorname{coh}(E_X H_Y^*) \qquad 4.2.1$$

For my analysis, I calculate the scalar impedance, Z_X by

$$Z_X = \frac{\langle E_X E_X^* \rangle^{1/2}}{\langle H_Y H_Y^* \rangle^{1/2}} \qquad 4.2.2$$

with scalar apparent resistivity, R_X,

$$R_X = \frac{1}{5f} Z^2 \qquad 4.2.3$$

phase Θ,

$$\theta = \tan^{-1} \frac{\text{Im coh}\,(E_X H_Y^*)}{\text{Re coh}\,(E_X H_Y^*)} \qquad 4.2.4$$

and coherency, $\text{coh}\,(E_X H_Y^*)$, the scalar impedance Z_Y, R_Y, Θ_Y and coherency are similarly defined for the signal pairs E_X, H_Y.

4.3 Tests for Quality of Data

For a flat-layered earth high coherency of orthogonal E-H pairs, averaged over several data strings is a criterion for acceptable data. In addition, I want the coherency of H_X to H_Y to be low, indicating that I am averaging electromagnetic waves with different polarizations. Low H_X H_Y coherency is desirable because the data strings are more likely to be statistically independent, and the denominators in Equations 4.1.8, 4.1.13 to 4.1.15 will be a little less than one.

For more complicated earth structure, high coherency of E, H pairs is no longer a good measure of data quality. Instead, one must use E E-predicted coherency, which measures for all the data sets analyzed, how well the Z values predict E from the corresponding values of H.

E E-predicted coherency is defined by Swift, 1967, as

$$\text{coh}(E_i^P, E_i) \equiv \frac{\langle E_i^P E_i \rangle}{\langle E_i^P E_i^P \rangle^{1/2} \langle E_i E_i \rangle^{1/2}} \qquad i = X \text{ or } Y \qquad 4.3.1$$

where $$E_i^P \equiv Z_{iX} H_X + Z_{iY} H_Y$$ 4.3.2

and $$\langle E_i^P, E_i^* \rangle = Z_{iX} \langle H_X E_i^* \rangle + Z_{iY} \langle H_Y E_i^* \rangle$$ 4.3.3

expressing 4.3.1 in terms of 4.3.3 and other coherencies, 4.3.4

$$\mathrm{coh}\left(E_i^P, E_i\right) = \frac{|H_X| Z_{iX} \mathrm{coh}(H_X E_i^*) + |H_Y| Z_{iY} \mathrm{coh}(H_Y E_i^*)}{\left[|Z_{iX}|^2 |H_X|^2 + |Z_{iY}|^2 |H_Y|^2 + 2|H_X||H_Y| R_e\left(Z_{iX} Z_{iY} \mathrm{coh} H_X H_Y^*\right)\right]^{1/2}}$$

Since I am calculating the Z elements using the Z^E and Z^H forms in Equations 4.1.7 to 4.1.15, there are two values for each coh (E_X^P, E_X) and coh (E_Y^P, E_Y). A value of E E-predicted coherency near unity should be obtained for good data. Low values of E E-predicted coherency would be caused, for example, by circuit noise or local magnetic fields or currents.

4.4 Correction of Digitized Data to Yield Field Quantities

The digitized time series must be converted to the frequency domain and corrected for the response of the system to yield field quantities, milivolts per kilometer for the electric field, gamma for the magnetic field. The values of the Fourier series of each data segment are multiplied by the appropriate system response factor A_e or A_h where, for the electric channel:

$$A_e = (D.F.) \frac{1}{\ell \times G_E \times SK} \times 10^6 \times \frac{1}{B}$$ 4.4.1

D.F. = Digitizer factor = full scale digitizer imput voltage/ full scale digital value. Typically 2.5 v / 1024

ℓ = Electrode separation

G_E = Electric channel gain at 10 Hz

SK = Digitizer skew factor, complex number of unity magnitude with phase equal to 150 microsecond delay per channel, (counting the first channel as zero).

B = Complex system response for that channel interpolated from table, magnitude normalized to unity at 10 Hz

and for the magnetic channel:

$$A_h = (D.F.) \frac{1}{C.F. \times G_H \times SK} \times 10^6 \times \frac{1}{B} \qquad 4.4.2$$

where

C.F. = Coil sensitivity at 10 Hz

and

G_H = Magnetic channel gain at 10 Hz

Chapter 5. Instrumentation

The basic nature of the signals dictates what bandwidth, sensitivity and noise levels are required for the apparatus. The spherics are random noise, at low signal levels, and in a spectrum full of strong powerline interference from the 60 Hz fundamental and harmonics. Theoretically digital frequency analysis could separate out the powerline interference, but I found that in practice there was not sufficient dynamic range in the amplifiers and tape recorder to accommodate both the strong interference and the weak signals over the original bandwidth of 1 to 5000 Hz. Furthermore, the very sharp 60 Hz notch active filters originally used after the first stage of amplification were not satisfactory, probably due to the non-linear response of the input stage to the strong 60 Hz interference. I reduced the bandwidth to 1 to 50 Hz, below all powerline interference. Here, the specially constructed magnetic detection coil lacked the sensitivity required for the weak signals, and that the magnetic channel was still saturated by 60 Hz interference.

My final instrumentation system used the large, 2m long, 70 Kg, coils designed for low frequency MT, Hill and Bostick, 1972. To reduce powerline interference at the sensors, these coils were resonated at mid-band (about 11 Hz). The resistance of the windings and the metal coil cases damp the resonance to give a bandwidth appropriate to the experiment.

Both the electric and magnetic channels needed passive 60 Hz notch filters as close to the sensor outputs as possible. The electric channels have twin-tee passive notch filters in each differential input line and the magnetic channels have similar filters after the preamplifiers. To reduce interference further I operated the equipment from batteries: the amplifiers were powered by a d.c. to d.c. converter operating from a storage battery; the tape recorder had a built-in inverter operating from the same storage battery. The oscilloscope, which was not used while recordings were being made, was powered by a 120v 60 Hz inverter from another storage battery.

A method of checking the system for proper operation was needed. Since the signals are random noise, it was not possible, by a simple visual inspection of an oscilloscope trace of the amplifier output to discriminate between circuit noise and signal. However, since there are two indentical electric channels and two identical magnetic channels, I found that it was easy to tell that signals, and not circuit noise, were being received by placing the two electrode pairs or two coils on the ground parallel or antiparallel. Circuit noise would be uncorrelated, but incident electromagnetic signals should be highly correlated. This test works well in the field with a two-channel oscilloscope. I also tape recorded and computer analyzed data taken with parallel sensors and found that the coherency of the parallel signals was higher than .9 for frequencies from about 1 to 45 Hz.

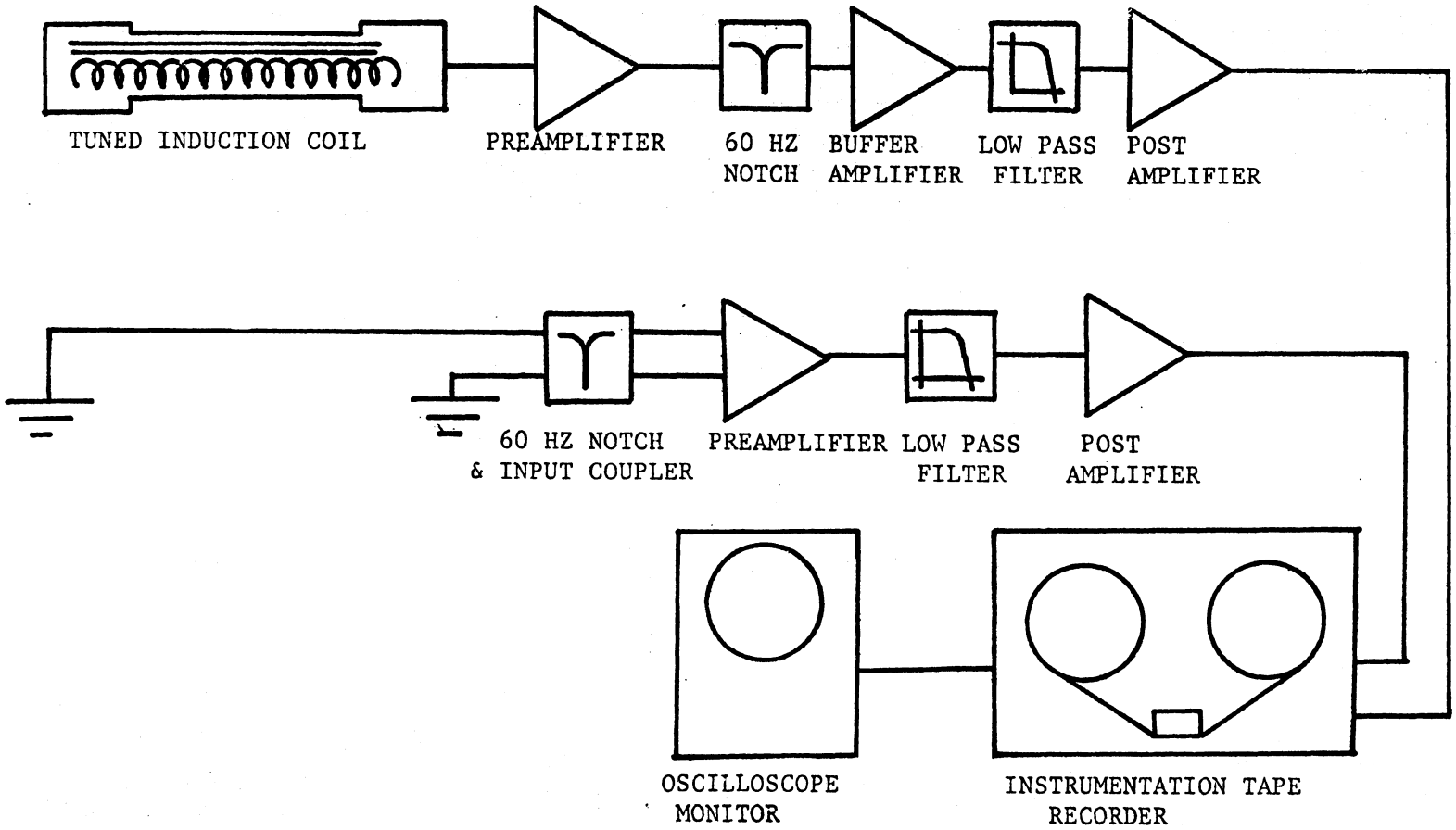

Figure 5.1 Field apparatus for audiomagnetotellurics. Only one of each of the two E and H channels are shown.

5.1 Electric and Magnetic Sensors

Electric sensors are brass stakes driven into the ground 50 meters apart. Sometimes special conditions required a shorter spacing. Such cases are discussed in Chapter 6 under field procedure. A pair of 40 centimeter long, 1 cm diameter brass stakes exhibit a mutual contact resistance around 2000 ohms in damp soil, rising to 20,000 ohms in gravel or sandy soil. The amplifiers described below can tolerate these source resistence changes. Low-frequency magnetotellurics use porous-pot electrodes to avoid polarization affects; in my case metal stakes are adequate because beyond the first stage, the amplifiers are A.C. coupled, which blocks the d.c. component dut to polarization.

The magnetic sensors are mu-metal core induction coils designed for low frequency magnetotelluric work, Hill and Bostick, 1962. These coils, when used unresonated, have a sensitivity of about $135\mu v\ \gamma^{-1}\ Hz^{-1}$ which is sufficient to receive the signals in the band of interest. However, the coils are subject to 60 Hz power line interference. To reduce this problem I resonated the coils with .33 mfd capacitors to mid-band, approximately 11 Hz. This modification increased the sensitivity at mid-band by a factor of two and significantly reduced the powerline interference.

5.2 Amplifiers and Filters

The magnetic channel preamplifier, Figure 5.2.1 uses an Analog Devices 521 integrated circuit instrumentation amplifier. The feedback resistors are chosen to give gains of 10 or 300. Each pre-

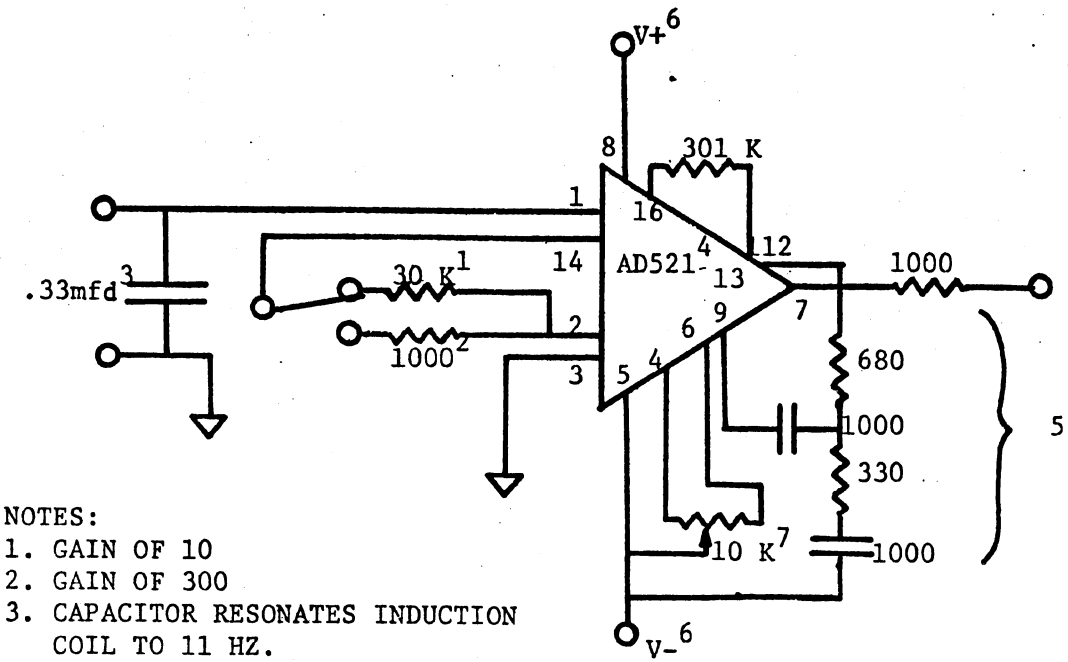

NOTES:
1. GAIN OF 10
2. GAIN OF 300
3. CAPACITOR RESONATES INDUCTION COIL TO 11 HZ.
4. MANUFACTURED BY ANALOG DEVICES, INC.
5. NETWORK SETS BANDWIDTH AT 1000 HZ.
6. SEPARATE DUAL 12 VOLT LANTERN BATTERY SUPPLY FOR EACH CHANNEL.
7. OFFSET CONTROL.

Figure 5.2.1 Magnetic channel preamplifier. Values of resistors are in ohms, capacitor values if greater than unity are picofarads, if less than unity, microfarads.

amplifier is powered individually by lantern batteries for isolation. The input circuit noise level is less than one microvolt peak-to-peak over a 50 Hz bandwidth. Following the preamplifier are notch filters and buffer amplifiers, Figure 5.2.2. Following the buffer are the low pass filters, Figure 5.2.3, and post amplifiers, Figure 5.2.4, which are identical in all four channels.

The electric channel preamplifier, Figure 5.2.5 is a Datel 200C instrumentation amplifier, with switch selectable gains of 10 or 700. The input impedance of the amplifier is greater than 10^7 ohms and the input noise level less than one microvolt over the 50 Hz bandwidth.

The passive notch filters and D.C. offset adjust Figure 5.2.6, comprise an input coupler for the electric channel preamplifier. These components reduce the electric channel input impedance to about 40,000Ω and the common mode rejection to 43 db. The notch filters are needed to avoid saturation or distortion in the amplifiers due to 60 Hz interference.

5.3 Calibration of System

In order to correct the Fourier coefficients of the data to yield field quantities, as discussed in Chapter 4, the gain and phase shift of the entire detection and recording system must be known as accurately as possible. At first I used sine waves to calibrate the system, but found that the calibration could be done more accurately using my computer analysis programs and pseudo-random test signals. The technique is discussed by Anderson, Finnie and Roberts, 1967. The analysis program, MAGTEL, was

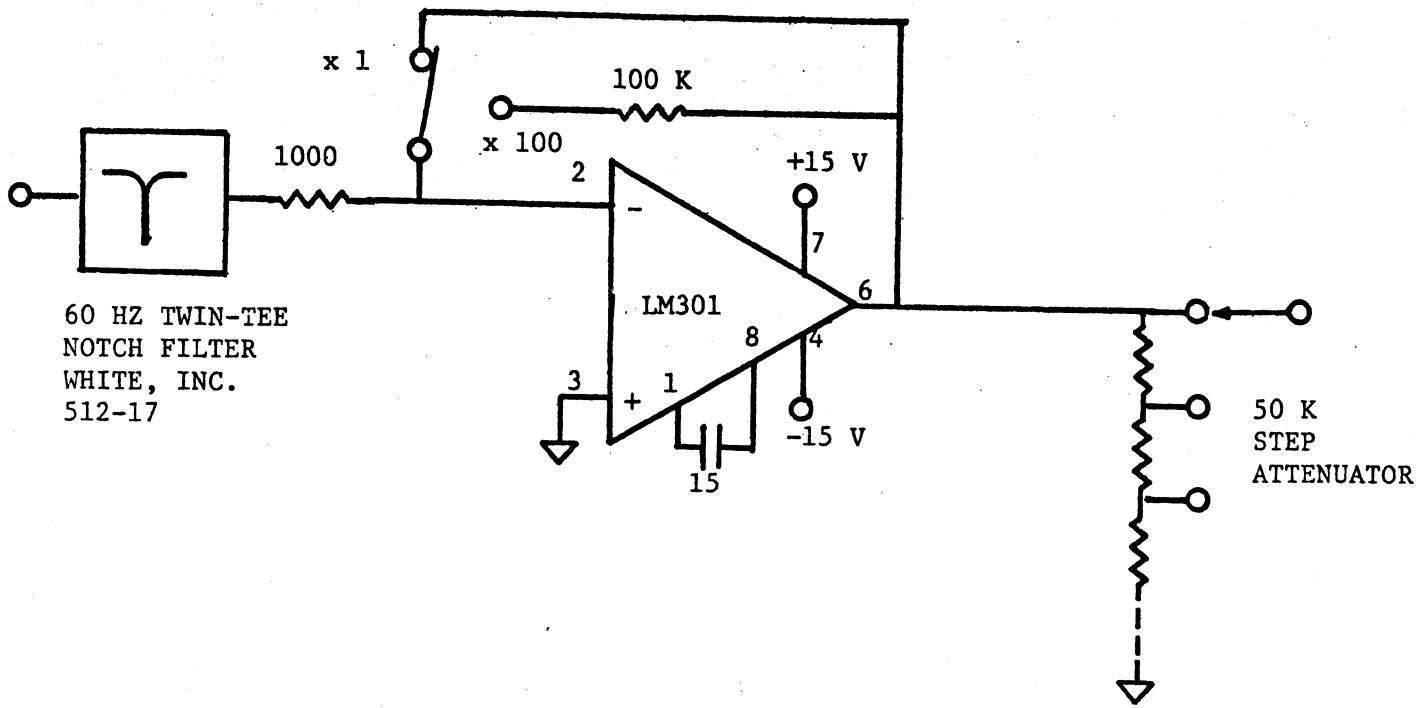

Figure 5.2.2 Magnetic channel notch and buffer amplifier. Capacitor value in picofarads. Resistor values in ohms.

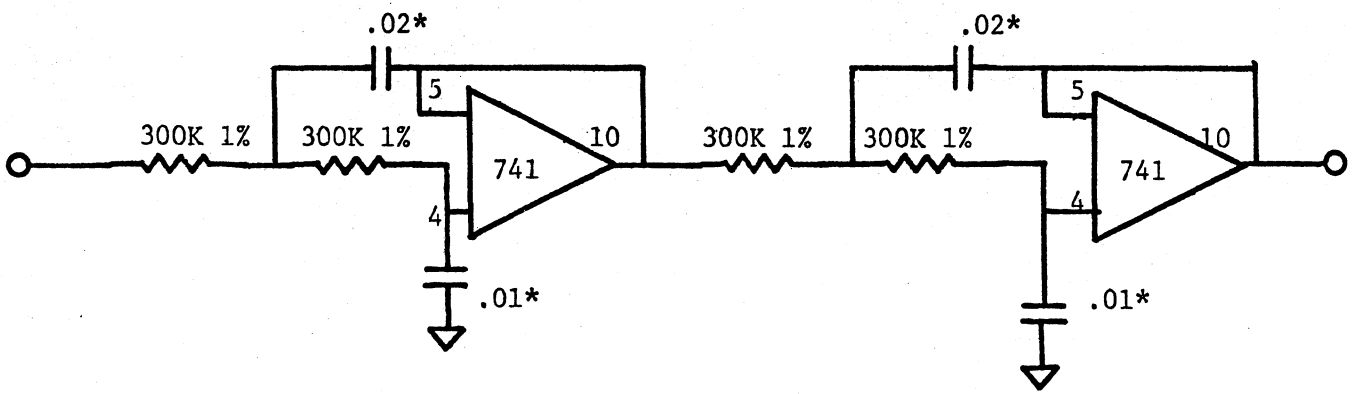

+15 V TO PINS 11
-15 V TO PINS 6

*CAPACITOR VALUES MATCHED TO WITHIN ONE PERCENT

Figure 5.2.3. Low pass filter. Resistor values are in ohms. Capacitor values in microfarads

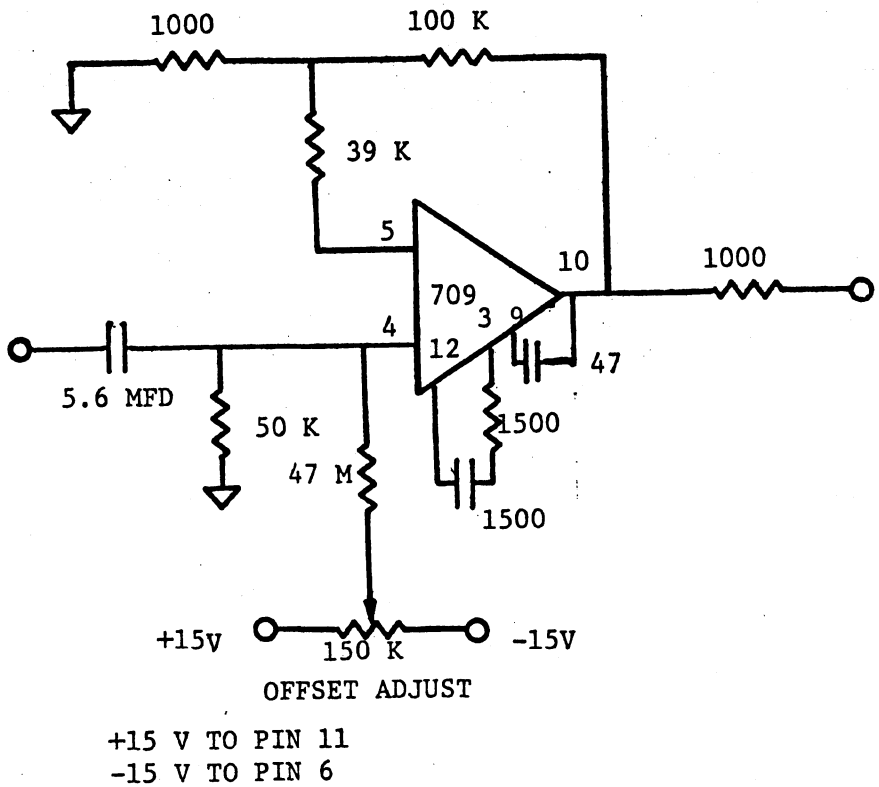

Figure 5.2.4. Post amplifier. Resistor values in ohms. Capacitor values in picofarads except as noted.

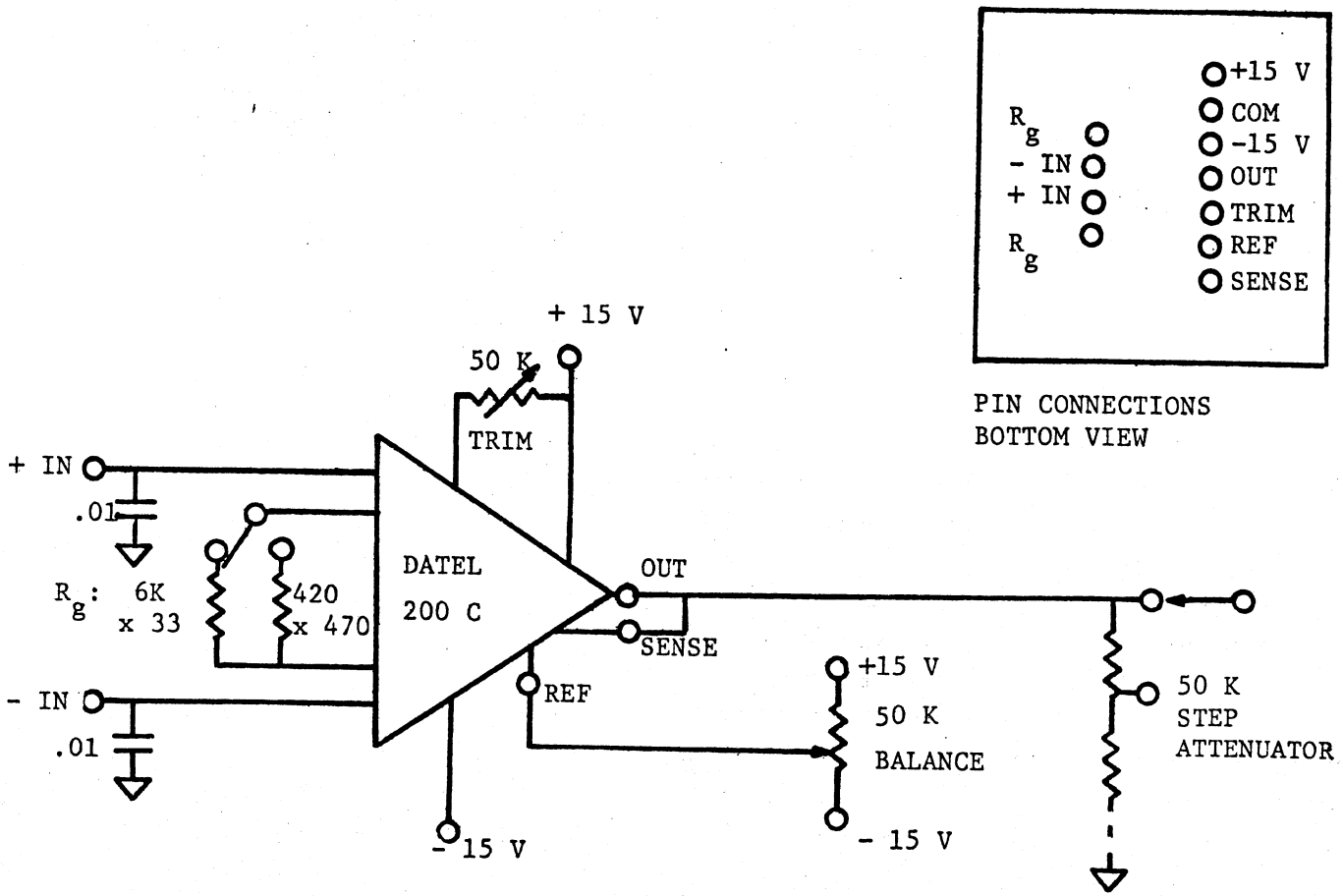

Figure 5.2.5. Electric channel preamplifier. Resistor values in ohms. Capacitor values in microfarads.

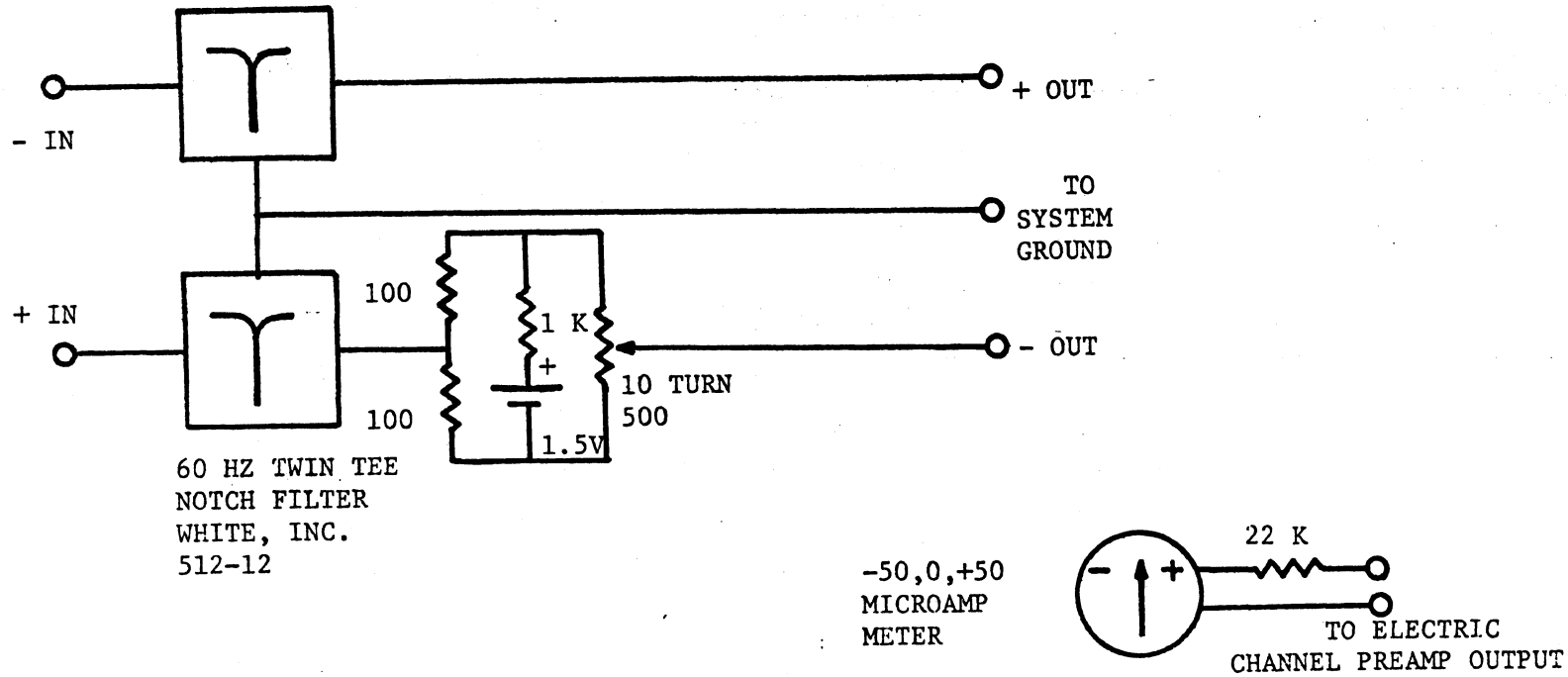

Figure 5.2.6. Electric channel input coupler and balance monitor. Resistor values in ohms.

temporarily modified to set phase corrections to zero and amplitude corrections to unity. One or two channels contained the pseudo-random test signal, the other channels contained the amplifier outputs. The phase shifts listed in the program output then represents phase difference between the recorded input and output of the recording system. Since MAGTEL prints out signal powers, square roots were calculated to find voltage ratios for the gains. For the filter correction tables used in the analysis programs, the gain was normalized to unity at 10 Hz.

5.3.1 Electric channel calibration

The gain and phase shift of the electric channel amplifiers was determined as described above. A block diagram of the apparatus is shown in Figure 5.3.1.1, the results in Figure 5.3.1.2.

5.3.2 Magnetic channel calibration

The induction coils were calibrated in a uniform magnetic field created inside a solenoid. The solenoid was 3.5 meters long, 32 centimeters in diameter and had one turn per centimeter of length, similar to the one used by Word, Smith and Bostick, 1970. The magnetic field inside a solenoid is given by

$$B = \mu_o in$$

where $\mu_o = 4\pi \times 10^{-7}$ weber per amp-meter or Henry per meter

i = current in amps

n = number of turns per unit length

B = magnetic field in Webers per meter^2

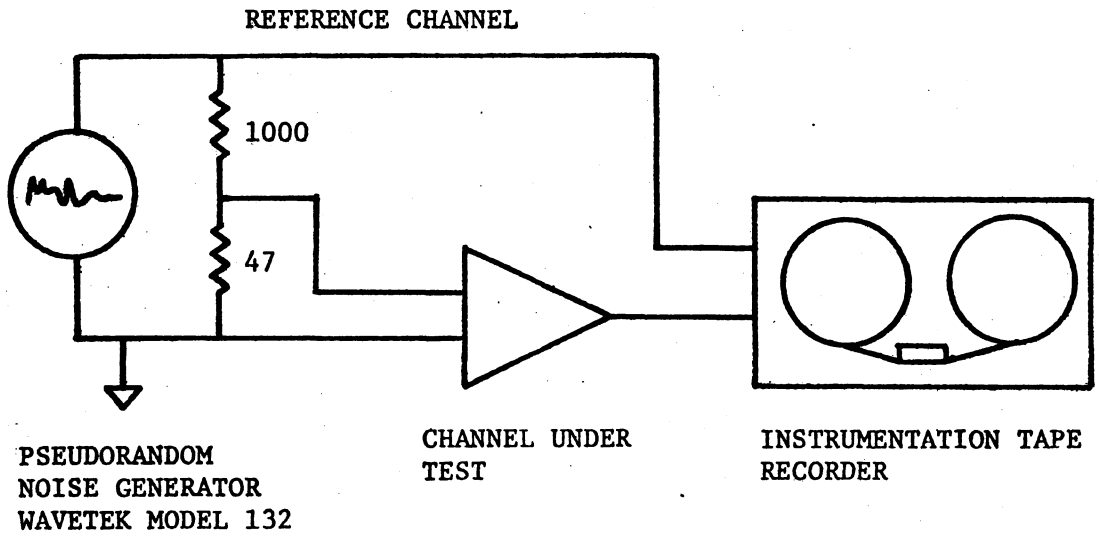

Figure 5.3.1.1. Calibration of amplifier using pseudorandom noise.

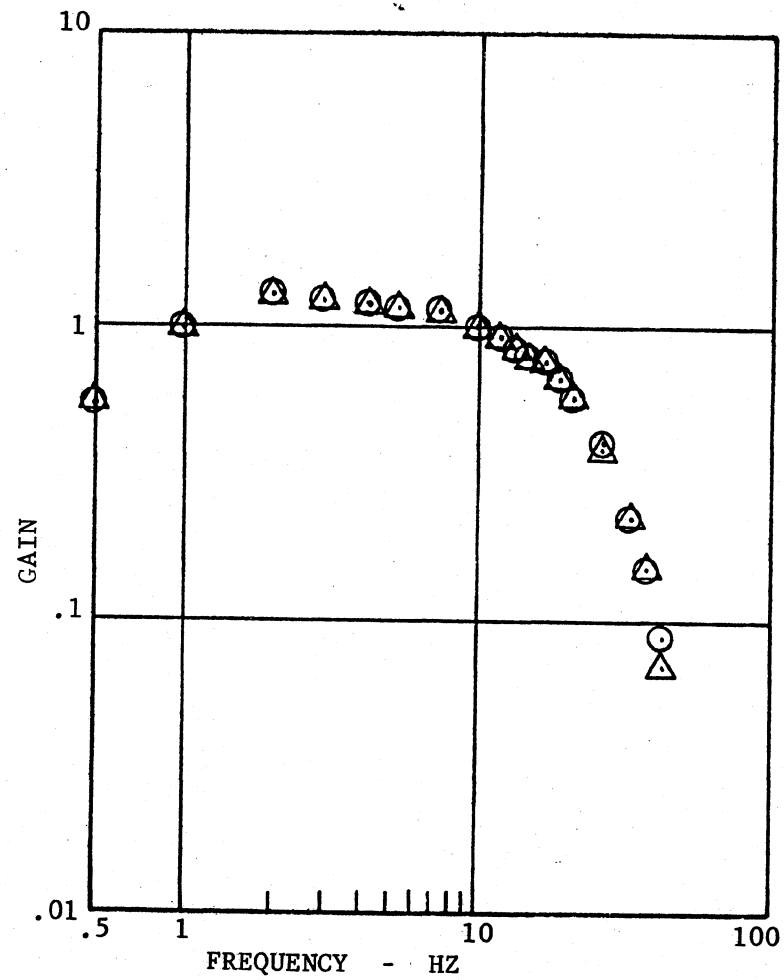

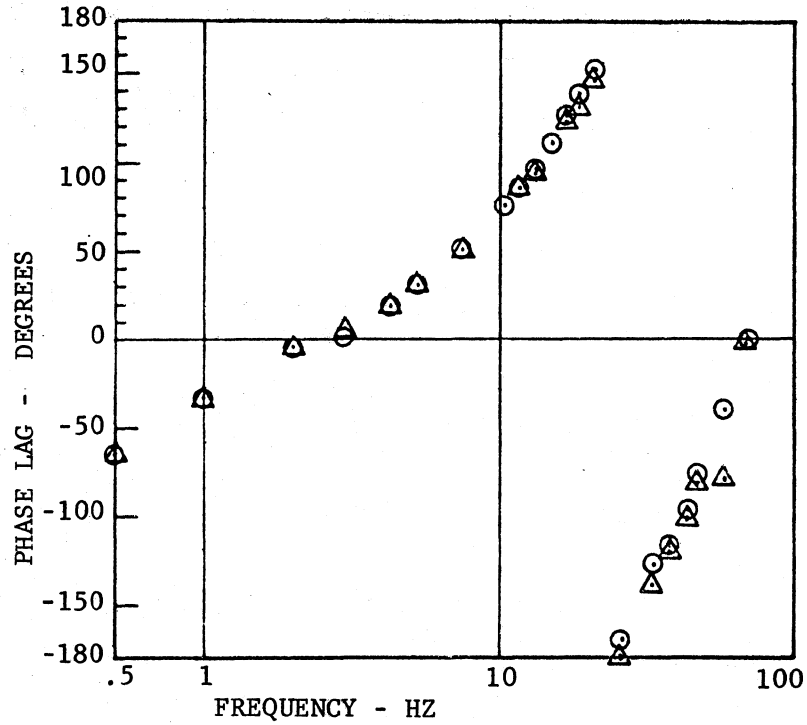

Figure 5.3.1.2 Amplitude and phase response of electric channels. Amplitude is normalized to unity at 10 Hz. Circles are Channel 1, E_X, triangles are Channel 2, E_Y.

Remembering that 10^9 gamma = 1 weber per meter^2, the magnetic field in this solenoid is 125,00 gamma per amp. The current through the solenoid is monitored by measuring the voltage across a series resistor.

The magnetic channel calibration required two steps: (1) determination of the absolute sensitivity of the induction coil. (2) Determination of system phase response and gain relative to a pseudo-random test signal.

I determined the absolute sensitivity of the sensor coil with sine waves energizing the solenoid. A four-pole low pass filter with corner frequency at 40 Hz was used to filter out 60 Hz interference, and the filter output was viewed on an oscilloscope. The sensitivity of both sensor coils at 10 Hz is 2300 plus or minus 100 microvolts per gamma.

System phase and gain were determined with pseudo-random noise using the experimental apparatus in Figure 5.3.2.1 similar to the electric channel calibration. The results are shown in Figure 5.3.2.2. The magnetic channel amplifiers were tested separately from the coils using the same techniques as Section 5.3.1. The responses, not shown, were nearly identical to the electric channels.

I determined the gain of each amplifier at each field site by injecting sine waves of known amplitude into the amplifier inputs, to give a mid-scale reading on the tape recorder recording level meter. These recorded calibration signals were measured on the oscilloscope in the field and later digitized in the laboratory to calculate gain at each site.

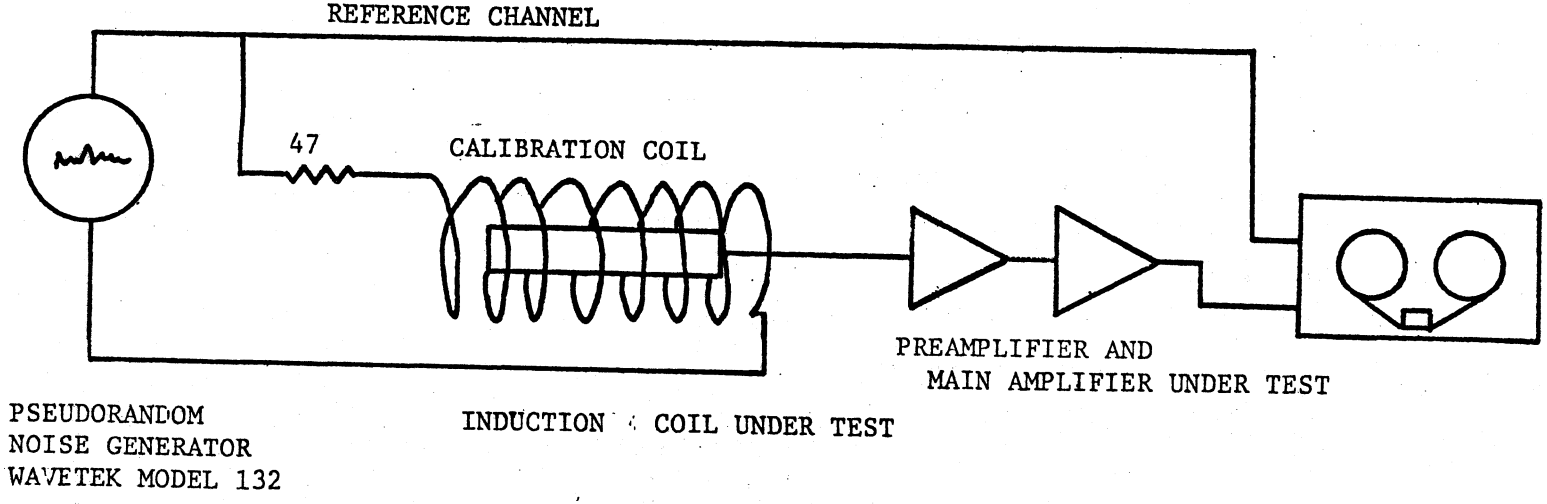

Figure 5.3.2.1 Calibration of magnetic channel using pseudorandom noise.

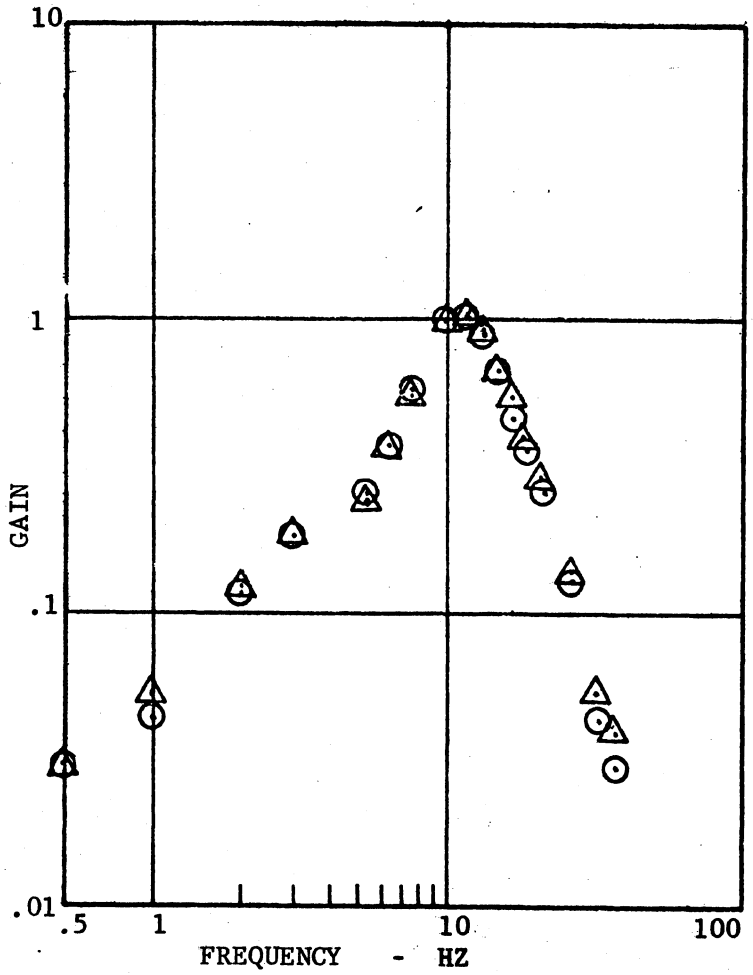

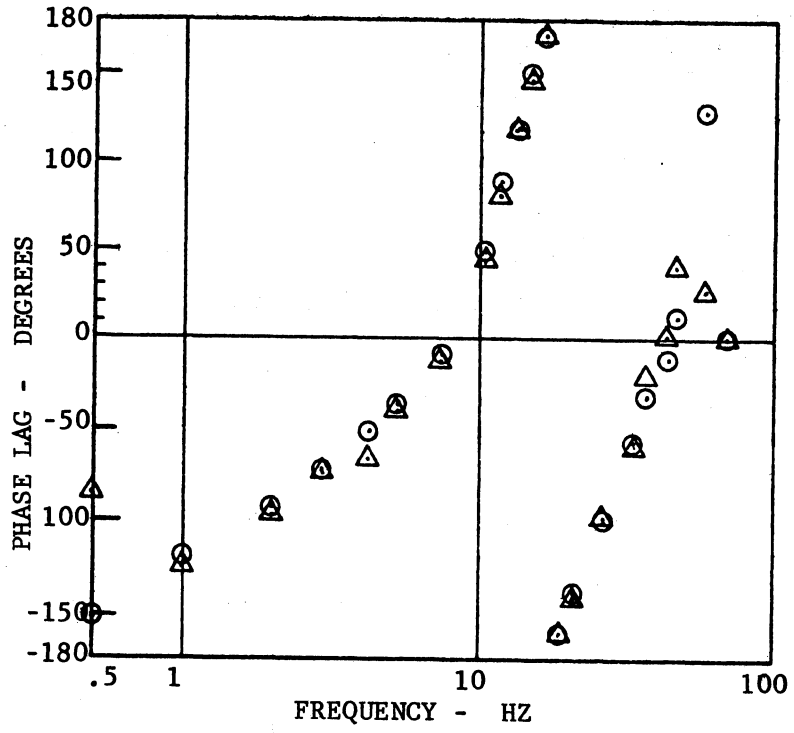

Figure 5.3.2.2 Amplitude and phase response of magnetic channel including resonated induction coil. Amplitude is normalized to unity at 10 Hz. Circles are Channel 3, H_X, triangles are Channel 4, H_Y.

After the field season, the calibration was retested using pseudo-random noise and computer analysis as described above. I found no significant changes in gain or phase response.

Chapter 6. Field Program

The magnetotellurics apparatus described in Chapter 5 was used for a series of measurements in Rusk County, Wisconsin, investigating the Kennecott copper deposit near Ladysmith and nearby bands of graphitic schist conductors.

6.1 Geology of Field Area

The bedrock in Rusk County lies at depths of a few meters to tens of meters and consists of Precambrian age rocks, metasediments, metavolcanics and intrusives mapped in Figure 6.1.1. Dutton and Bradley, 1970; Sims, 1976 and May,1976. These rocks are found in northeasterly trending steeply dipping folds, covered by Cambrian sandstones and glacial till. The copper deposit, within box MS on Figure 6.1.1, is found in a band of metavolcanics approximately one mile south of Ladysmith, which lies immediately northwest of a band of interbedded graphitic schist and volcanic flows. The known geology of each site is described in Chapter 8.

6.2 Geophysics of Field Area

DC, transient EM and MT soundings have been conducted in northern Wisconsin, giving a gross layered earth structure described here. Sternberg and Clay's (1977) Figure 6.2.1 summarizes DC soundings from diverse parts of northern Wisconsin, showing a conductive layer tens to hundreds of meters thick overlying a thick highly resistive layer. These data with spacings up to 50 kilometers do not penetrate deeper than this layer, indicating that its resistivity must be above 10^5 ohm meters. EM and MT soundings penetrate the resistive layer,

Figure 6.1.1. General Precambrian geology of Rusk County, Wisconsin, from May, 1976, with Index map in upper left hand corner. The metasediment region also contains the electrical conductors determined by airborne electromagnetic measurements. Drill holes made to follow up the airborne measurements found interbedded graphitic schists and metamorphosed volcanic flows. (Personal communication, Edwarde May of Flambeau Mining Corp. and P.M. Wright of Kennecott Exploration). Boxes marked W, MS and FSL correspond to station location maps, Figures 8.1.1, 8.2.1, and 8.3.1, for data stations at the minesite, Washington township and Fireside Lakes area respectively.

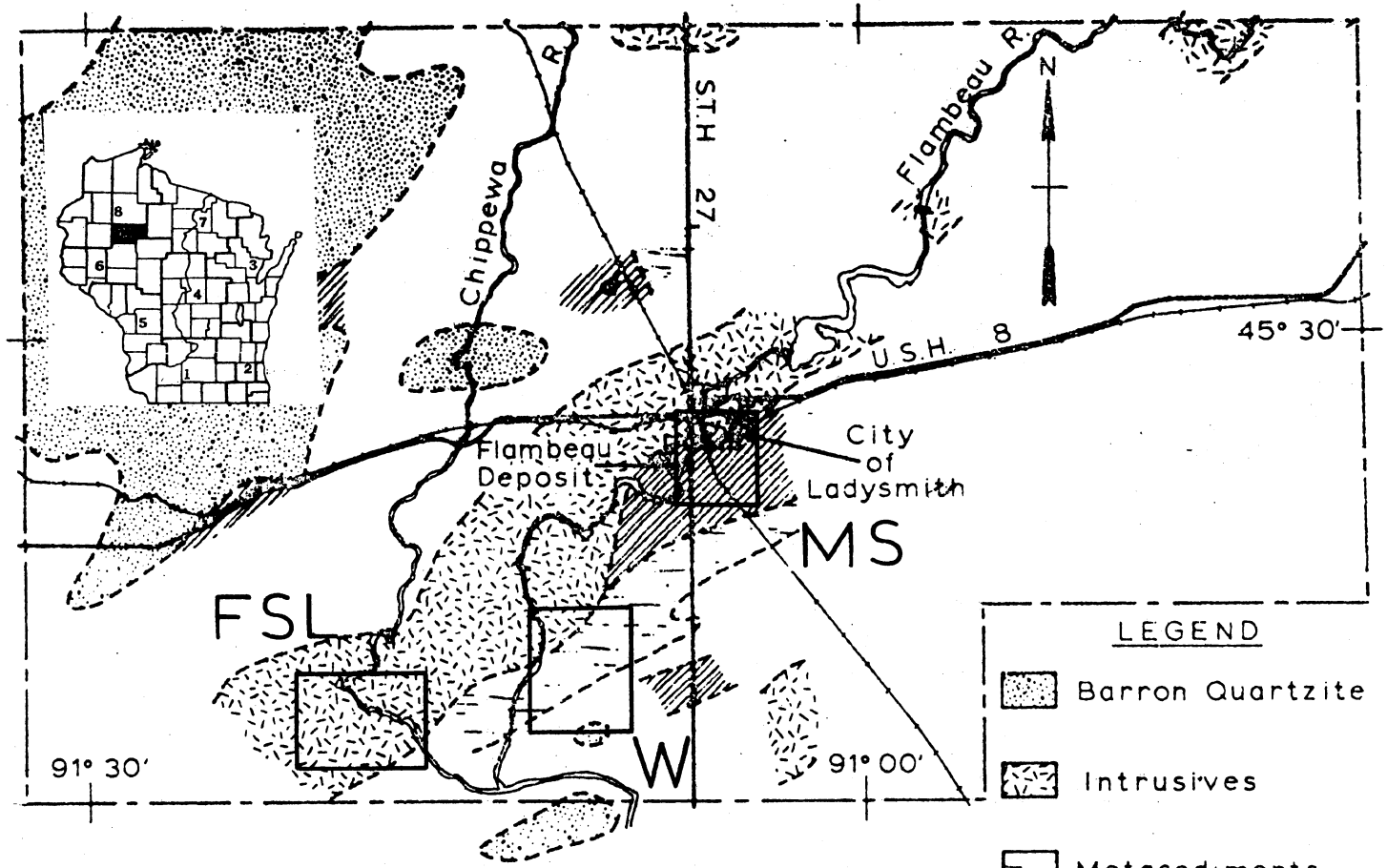

GENERAL PRECAMBRIAN GEOLOGY
of
RUSK COUNTY, WISCONSIN

showing a conductive lower layer, Kan, 1975; Sternberg, 1977, and Dowling, 1970. Sternberg and Clay also report a 20 kilometer wide zone of multiple conductors, the Flambeau Anomaly, which lies roughly along 46° N latitude and extends east of 91° longitude for more than 100 kilometers, or from 50 kilometers north of Ladysmith to about 150 kilometers northeast of Ladysmith. Dowling Site 4 MT sounding layered model, 50 kilometers east of Ladysmith, south of the Flambeau Anomaly and Sternbergs EM transient interpretations of soundings a few kilometers north of the Flambeau Anomaly are summarized in Figure 6.2.1, showing a gross structure of low-high-low resistivity layering.

In Rusk County, numerous magnetic dip needle anomalies, Hotchkiss, 1929, and electrical conductors are oriented generally northeast (45°) parallel to the strike of most structures. Schwenk's 1976 map of airborne EM conductivity anomalies, Figure 6.2.2 covers two of my field areas. The anomalies continue at least 20 kilometers to the southwest, through the Fireside Lakes area, P.M. Wright, Kennecott Exploration, telephone conversation. The pattern of multiple elongated parallel conductors is similar to the Flambeau Anomaly.

6.3 Field Procedure

The locations of my magnetotelluric profiles are shown by the boxes in the area map of Figure 6.1.1.

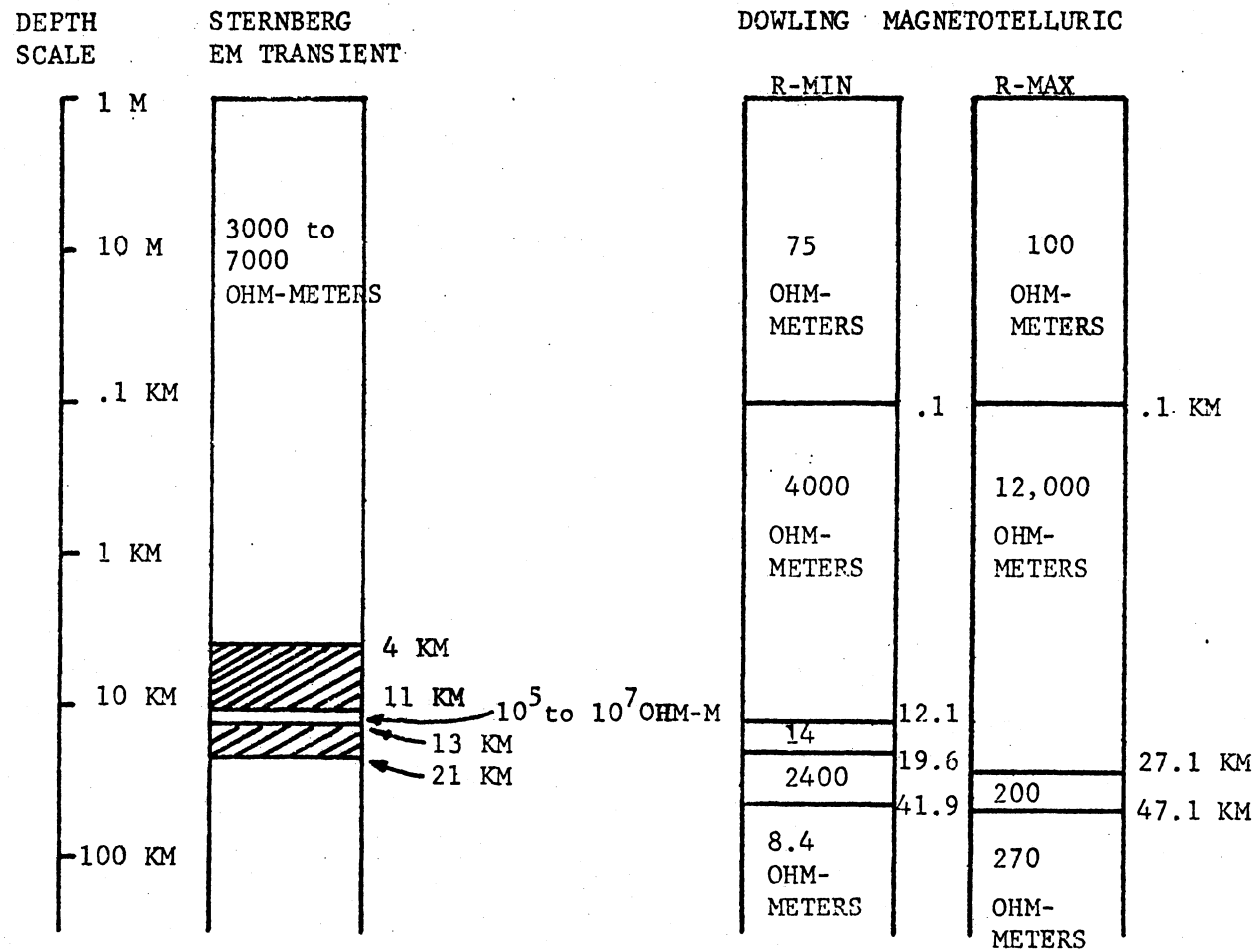

Figure 6.2.1. Layered models of electromagnetic and magnetotelluric sounding in northern Wisconsin. Shaded area in EM transient model shows range of depths for interfaces. From Sternberg and Clay, 1977 and Dowling 1970.

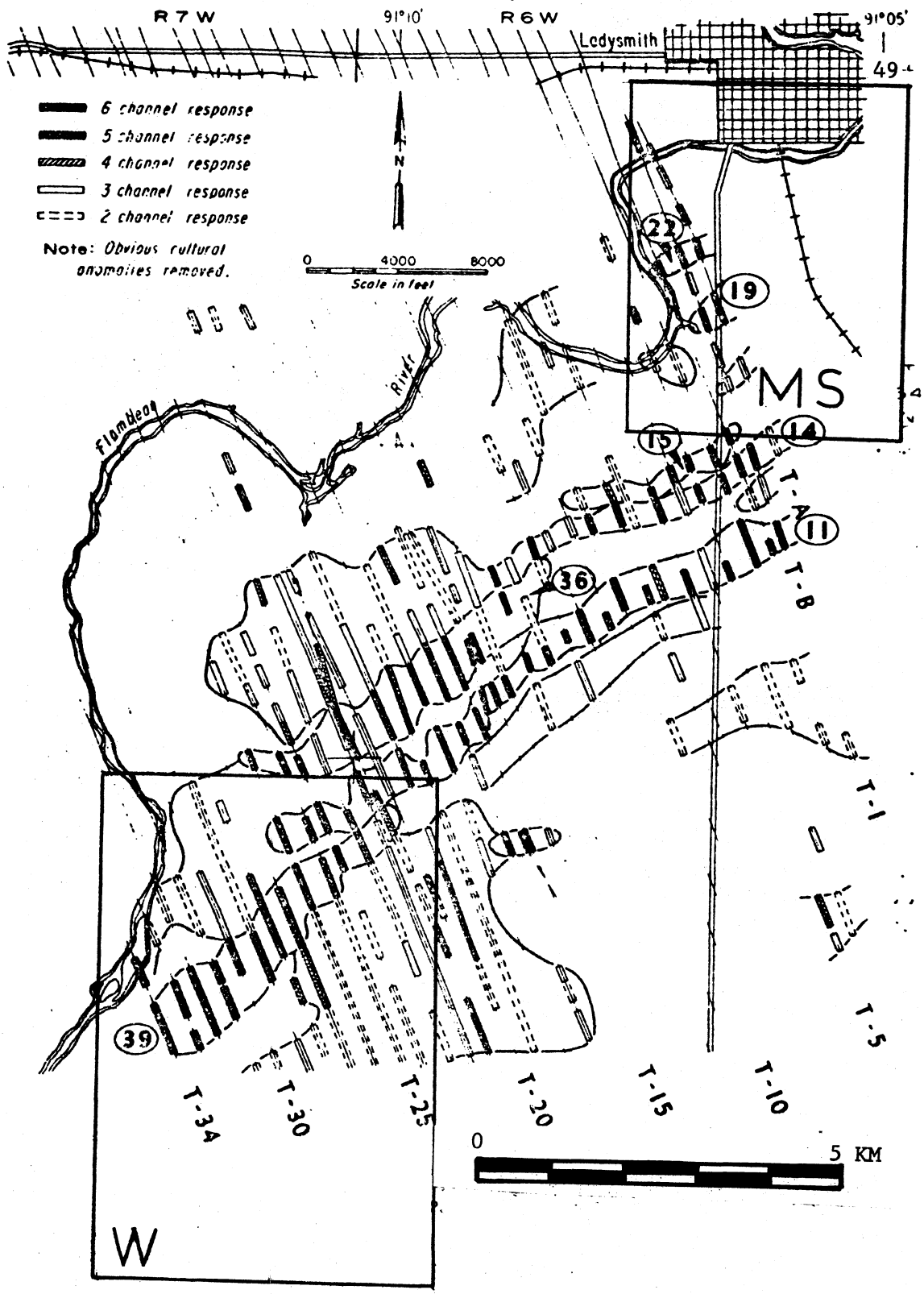

Figure 6.2.2. Airborne electromagnetic (INPUT) anomalies, from Schwenk, 1976. Boxes labelled MS and W locate approximate area of data sets from the minesite and Washington township, respectively.

Most sites were chosen along roads or in terrain accessible by truck. The size and weight of the coils and the need for a reasonably clear area to extend the electrode wires were basic limitations on station locations. The stations were at least one hundred meters away from powerlines to reduce interference.

At each station the coils and preamplifiers were set up 30 to 40 meters away from the recording truck. Usually the electrodes had separation of 50 meters. Smaller separations of 10 or 20 meters were used for detailed profiling or if the underbrush was too dense to extend the wires the usual 50 meters.

At each site the sensors were set out and data were recorded for five minutes. After the data sets were recorded, microvolt or millivolt calibration signals were recorded at three frequencies, 4, 10 and 40 Hz, for gain calibration.

To acquire dense profile data at the minesite and at Fireside Lakes, I moved only the electrode pairs along the traverse and transmitted the electrode signals through a 500-meter 4-conductor cable. This technique is adapted from Slankis, Becker and Telford (1972).

Chapter 7. Data Analysis

The data were digitized and analyzed with the programs described here and the Appendix.

7.1 Standard Analysis Procedure

The analog tape-recorded data were digitized by program NUDIG at the University of Wisconsin Geophysical Computing Facility. For each site I used 60 seconds of continuous data, then 10 seconds of the 10 Hz calibration tone on each channel. After NUDIG I used program HANDY to pick maxima and minima of the calibration tones and calculate the gains for that data set.

The digitizing rate of 128 samples per second, gave a Nyquist frequency of 64 Hz; thus the powerline fundamental was not folded into the band of interest. Powerline harmonics were highly attenuated in the amplifiers and did not appear to be a problem. Each digitized data set consisted of a 600-word header record of information entered from the teletype, followed by data in blocks of 600 words, each containing 150 data from each channel written in ASCII characters, on 800 bits per inch 9-track tape. NUDIG and HANDY run on the Geophysical Computing Center's Datacraft 6024 computer. The programs which follow run on the Madison Academic Computer Center's Univac 1110. Program CONVERT converts the NUDIG data tapes to Univac format, numbers the records consecutively, lists the headers and produces a new tape compatible with MAGTEL. After CONVERT, program MAGTEL performed frequency analysis, made system response corrections, computed auto- and cross-spectra, scalar and tensor resistivities, phases and coherencies, according to the equations in Chapter 4, and produced a printed output

and a data tape.

MAGTEL averaged results over adjacent frequencies to yield data in bands centered at frequencies 1, 2, 3, 4, 5, 6, 7, 8.5, 11, 14, 17.5, 22.5, 28.5, 35.5, 45, 57 and 64 Hz. The three highest bands, 45, 57 and 64 Hz were not used in my analysis. They were subject to power-line interference and the signals coming through the amplifiers were very weak.

Program AVETEL averaged MAGTEL outputs and calculated scalar apparent resistivities, tensor impedances and resistivities, rotation angles for R-max and R-min, rotated impedances and resistivities.

AVETEL used a slightly different subroutine to select frequencies, omitting MAGTEL output frequencies 7 and 28 Hz.

MAGTEL and AVETEL are part of a series of magnetotelluric analysis programs developed at the University of Wisconsin by F. Dowling, C.R. Bentley and T. Wolfe. I have modified these programs slightly to insert a filter response table, and to reduce computing costs.

The tests for data rejection, available in programs MAGTEL and AVETEL, were not used. I used all 60 seconds of data "as is". I inadvertantly left in the test to exclude data with skew greater than unity. Skew = $|Z_{XX} - Z_{YY}| / |Z_{XY} - Z_{YX}|$, defined for example, by Vozoff, 1972, if not about equal to zero, signifies that the structure appears to have variations in three dimensions at that site at that frequency range. Approximately 90 percent of my data passed this test. A few sites lost one or two low frequency data due to skew failure, but these points had low coherency too, and

were bad data simply due to low signal power. Data from three sites were totally rejected and were reprocessed with the test removed. Kurtz and Garland, 1976, suggest that high skew data signify local inhomogeneities and conclude that modelling the data with two-dimensional models "might be useful even at stations with high skew", p. 333.

The quality of data is indicated by coherency of orthogonal E, H pairs or by E - E predicted coherencies, defined in section 4.3, or by variances of tensor resistivities and phases calculated according to Bentley, 1973. The cutoff levels used for rejection of data are discussed in Chapter 8 on a case by case basis. Low coherency could usually be traced to the erratic behavior of some signal pair as shown by large fluctuations in complex coherency with frequency. Such problems could possibly be due to a malfunctioning amplifier or some local geologic disturbance.

Data away from anomalies can be interpreted as layered earth models, with resistivity a function of depth only. The simplest layered earth models fitting my resistivity and phase data generally consist of three layers. I used these models as host rock in which to model the conductors in two-dimensions.

The complete computer output for each site and a data summary consisting of scalar or apparent resistivities and phase for each site are stored in the University of Wisconsin Geophysical and Polar Research Center data archives.

7.2 Sources and Effects of Measurement Uncertainty

Measurement uncertainty can be expected from three basic sources:

1. Instrument noise, which will be uncorrelated between channels,
2. Fluctuations due to measurement of a random process,
3. Geologic noise, that is, local inhomogeneities in the subsurface near the receiver which alter the electric and magnetic fields in an almost unpredictable manner.

Collectively these fluctuations or noises cause scatter in the data at a particular site across the band of frequencies. They cause fluctuations in the apparent resistivity, phases, and the orientations. For example, for stations away from an anomaly, where the ratio of R-max to R-min is only slightly greater than unity, I would expect the orientations to be scattered over my band of frequencies. In contrast, where the ratio of R-max to R-min is greater, ten or more, I would expect the orientations to be more tightly grouped with frequency even though there is scatter in the resistivities. Geologic noise can affect all of the frequencies approximately equally at a particular site, possibly causing the orientation to be different at that site compared to the rest of the profile.

These effects are discussed on a case-by-case basis in Chapter 8.

Chapter 8. Results and Interpretation

The first parts of this chapter contain results and interpretation from my three field areas: 8.1, Washington township; 8.2, the minesite; 8.3, the Fireside Lakes area. The latter parts of the chapter contain data validating two assumptions important to my analysis: 8.4, that scalar resistivities are approximately equal to rotated tensor resistivities if the apparatus is aligned with the structure being investigated; 8.5, that a physical rotation of the apparatus is equivalent to mathematical rotation.

I first compared my data away from anomalies with flat-layered models. If the data do not fit flat-layered models, then the true conductivity structure is more complex, either two-dimensional or three-dimensional. I then attempted to approximate the actual three-dimensional variations by two-dimensional variations.

The two-dimensional model in Section 3.3 shows that the R-perpendicular data should behave as flat-layered data at a modest distance from a conductor. Thus R-perpendicular data can be interpreted with layered models to determine a host rock model in which to model the known conductors.

Program MDLMT which calculates apparent resistivity and phase curves for layered models uses formulas of Keller and Frischknecht, 1966, page 313 and is documented in Sternberg, 1977.

For two-dimensional modelling I used EPOL and HPOL, University of Wisconsin versions of programs of Jones and Pascoe, 1971, and Pascoe and Jones, 1972, which determine "the perturbation of alternating electric currents in a two-dimensional model of a region

of uniform conductivity with an embedded inhomogeneity". Pascoe and Jones use the finite-difference technique applied to evaluating boundary conditions and calculate fields over a 40 by 40 grid of conductivity values representing a cross section of the earth and atmosphere. EPOL calculates the fields for R-perpendicular, HPOL for R-parallel. The programs are listed in Pascoe and Jones article. Modifications and special run instructions are discussed in Sternberg, 1977.

Sternberg points out that, for accurate modelling with EPOL and HPOL, the changes in grid size must be gradual, the physical size of the model must be within certain limits, the grid size must be small compared to skin depths and embedded inhomogeneities must be distant from the grid edges. In applying this program to my problem I found that because I had a high resistivity middle layer, 25,000 ohm meters with an extremely long skin depth, 25 kilometers, I could not simultaneously keep inhomogeneities several skin depths away from the edge of the grid and have a desirable density of grid points near the anomalies. Trials showed that relaxing the requirement for several skin depths to the edge of the grid resulted in errors of about 20 to 40 percent for apparent resistivities near conductors and errors of a factor of two for apparent resistivities away from the conductor. Jones and Pascoe, 1971, report errors of about 10 percent over uniform regions of the grid. My apparent resistivity data range over four orders of magnitude; therefore I consider these amounts of error in my model to be acceptable.

To estimate phase error, I simplified a model and increased the distance from the conductor to the grid edge to 3 skin depths. At 10 Hz, EPOL calculated a phase 15 degrees different from the plane-layered model for points distant from the conductor and the grid edges. I expect that all my phases are in error by at least this much. Even so, the calculated phase should be useful to show regions of constant phase and general trends.

8.1 Washington Township

The location map, Figure 8.1.1, shows the Washington township sites in relation to airborne EM anomaly 39, Figure 6.2.2. The drill logs from holes 39-1 and 39-2, Table 8.1.1, show that the conductors are pyrite and graphitic phyllite, embedded in volcanics.

8.1.1 Sounding data and layered models

Figure 8.1.1.1 is a summary of layered models for sites 7, 9, and 10 R-max rotated tensor resistivities. The data and model sounding curves are given in Figures 8.1.1.2 and 8.1.1.3. I chose these sites for layered model solutions because they (1) were located away from the INPUT anomaly and (2) had amplitudes and phases reasonably consistant with one another and with flat-layered models. The R-max orientations for these sites, presented in the next section, are oriented approximately perpendicular to the axis of the INPUT anomaly. Data and models are also given for R-min at site 10, Figure 8.1.1.3 as an example of a layered model for R-parallel. It is inconsistant with the R-perpendicular models.

Figure 8.1.1. Washington township station location map. Ruled region is INPUT airborne EM anomaly 39 from Figure 6.2.2. Solid circles 1 through 14 are the MT stations. Open circles 39-1 and 39-2 are drill holes; the marks perpendicular to T-1200 indicate the turam anomalies (both are from Great Lakes Exploration, 1972). INPUT anomaly 39 and turam anomalies on T-1200 are plotted on my data profile in Figure 8.1.2.1d. Drill hole data are summarized in Table 8.1.1. Background map is from USGS map of Flambeau Ridge quadrangle.

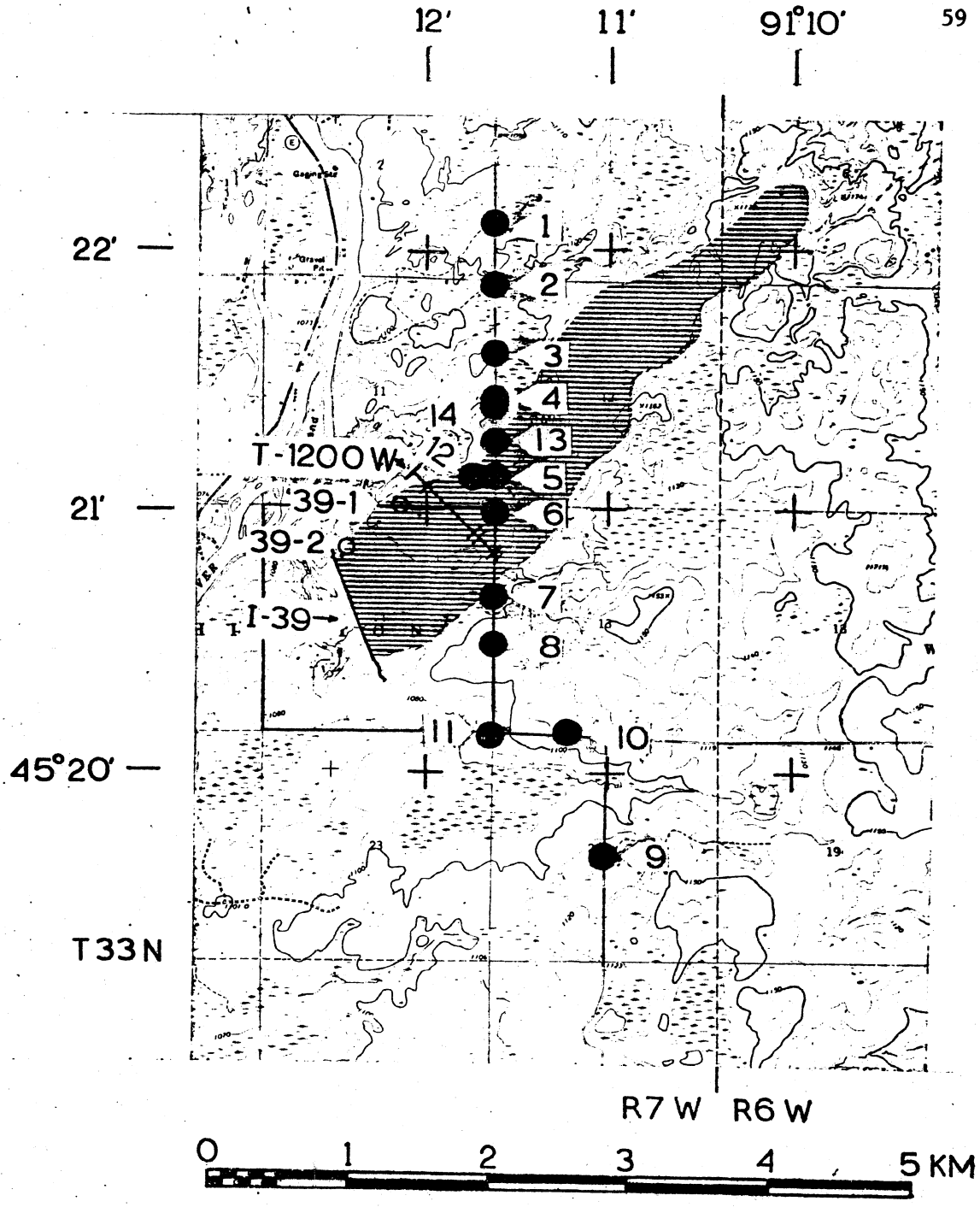
12'
11'
91°10'
22'
21'
45°20'
T33N
R7W
R6W
1
2
3
4
14
13
12
5
6
7
8
11
10
9
T-1200W
39-1
39-2
I-39
0
1
2
3
4
5 KM

Table 8.1.1.

DRILL HOLE 39-1	Drilled to SE, 50° from horizontal about 114 meters NW of turam anomaly.
0-51 meters	Overburden
51-132.6	Intermediate volcanics
132.6-193.3	Black carbonaceous pyrite (projection of surface turam anomaly)
193.3-213.4	Black graphitic pyrite phyllite with tuff interbeds; very contorted locally
DRILL HOLE 39-2	Drilled to SE, 50° from horizontal about 76 meters NW of turam anomaly.
0-54.9 meters	Overburden, bottom 10 m is Cambrian sandstone
54.9-72.6	Quartz-muscovite phyllite
72.6-73.8	Green hornfels
73.8-131.1	Black carboniferous phyllite with interbedded volcanics; 121 m is projection of turam anomaly
131.1-140.2	Black graphitic phyllite
140.2-166.	Porphyritic quartz andesite
166.-193.5	Black graphitic phyllite broken and distorted
193.5-223.8	(bottom) muscovite - chlorite phyllite

Table 8.1.1. Drill log and correlation with surface turam anomaly for drill holes 39-1 and 39-2, Figure 8.1.1. From Great Lakes Exploration Company, 1972.

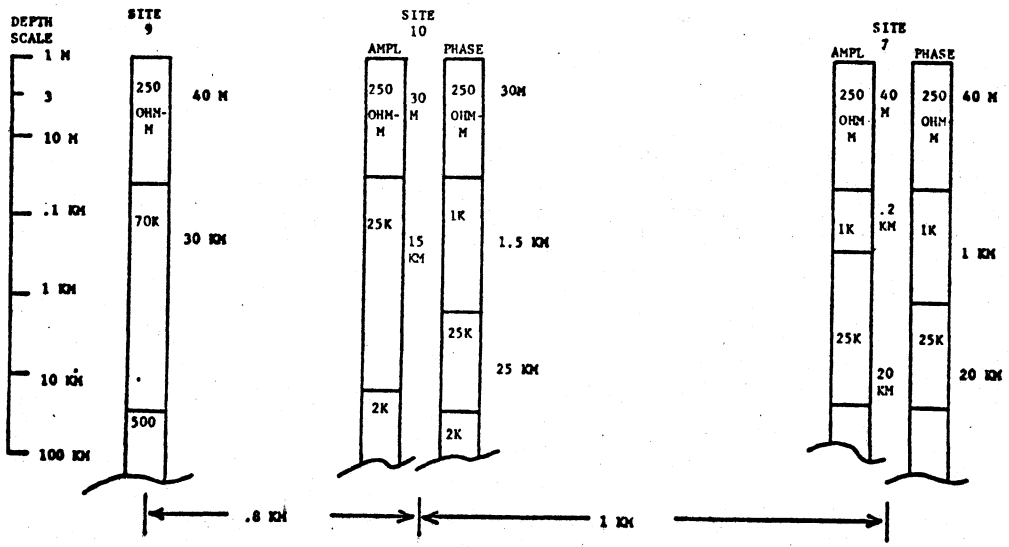

Figure 8.1.1.1. Washington township layered model summary. Logarithmic depth scale. Resistivity of layers indicated in the layer, thickness of layer outside. Distance between stations is not to scale.

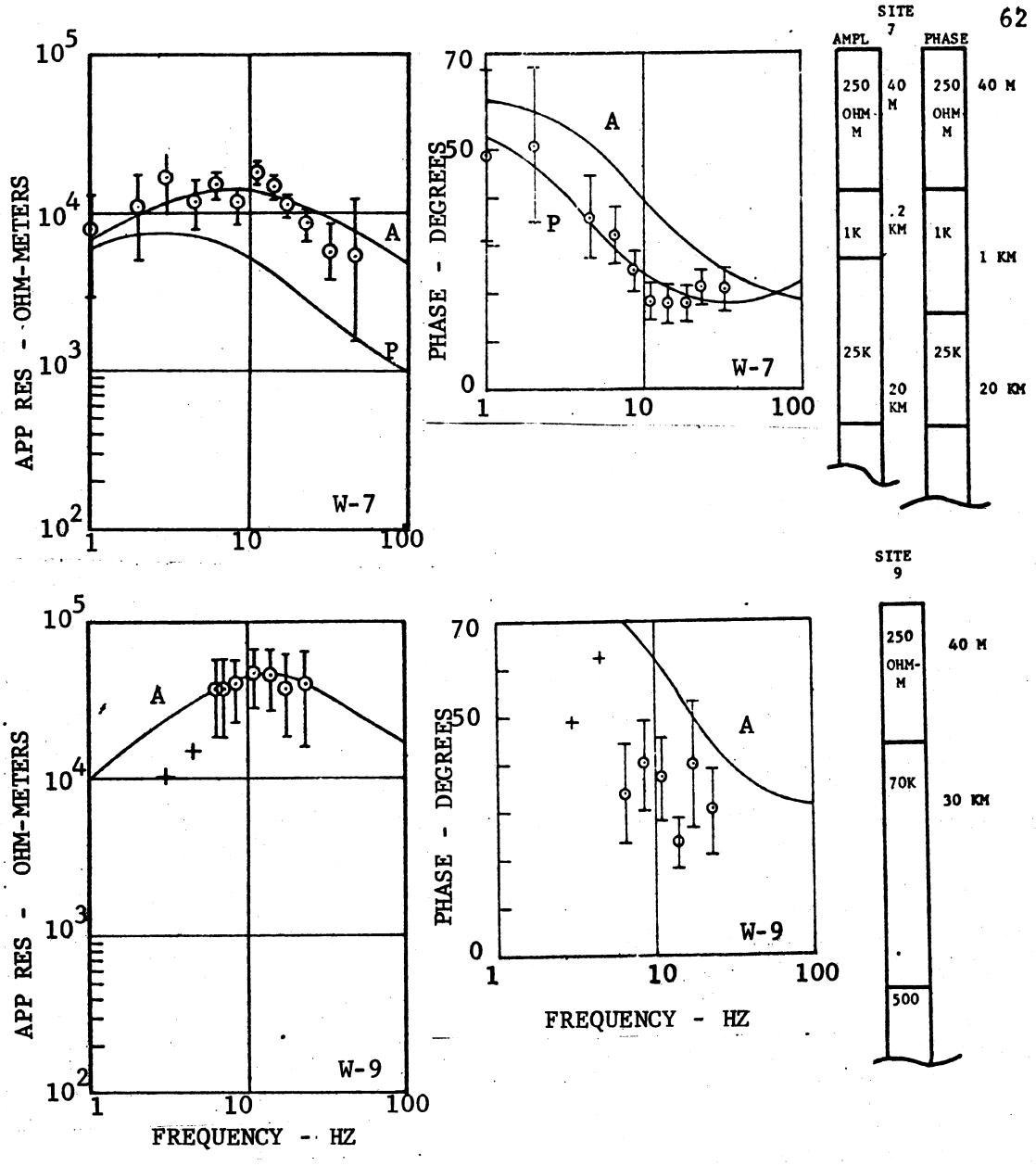

Figure 8.1.1.2. Washington township R-max apparent resistivity and phase.

a. Site 7. The data are shown as points on resistivity and phase diagrams. The solid line labelled A is calculated from the model, labelled AMPL that fits the amplitudes. The solid line labelled P is the model that fits the phases.

b. Site 9. The solid line is the model calculation based on the amplitude data. The two pluses are data that failed the skew test.

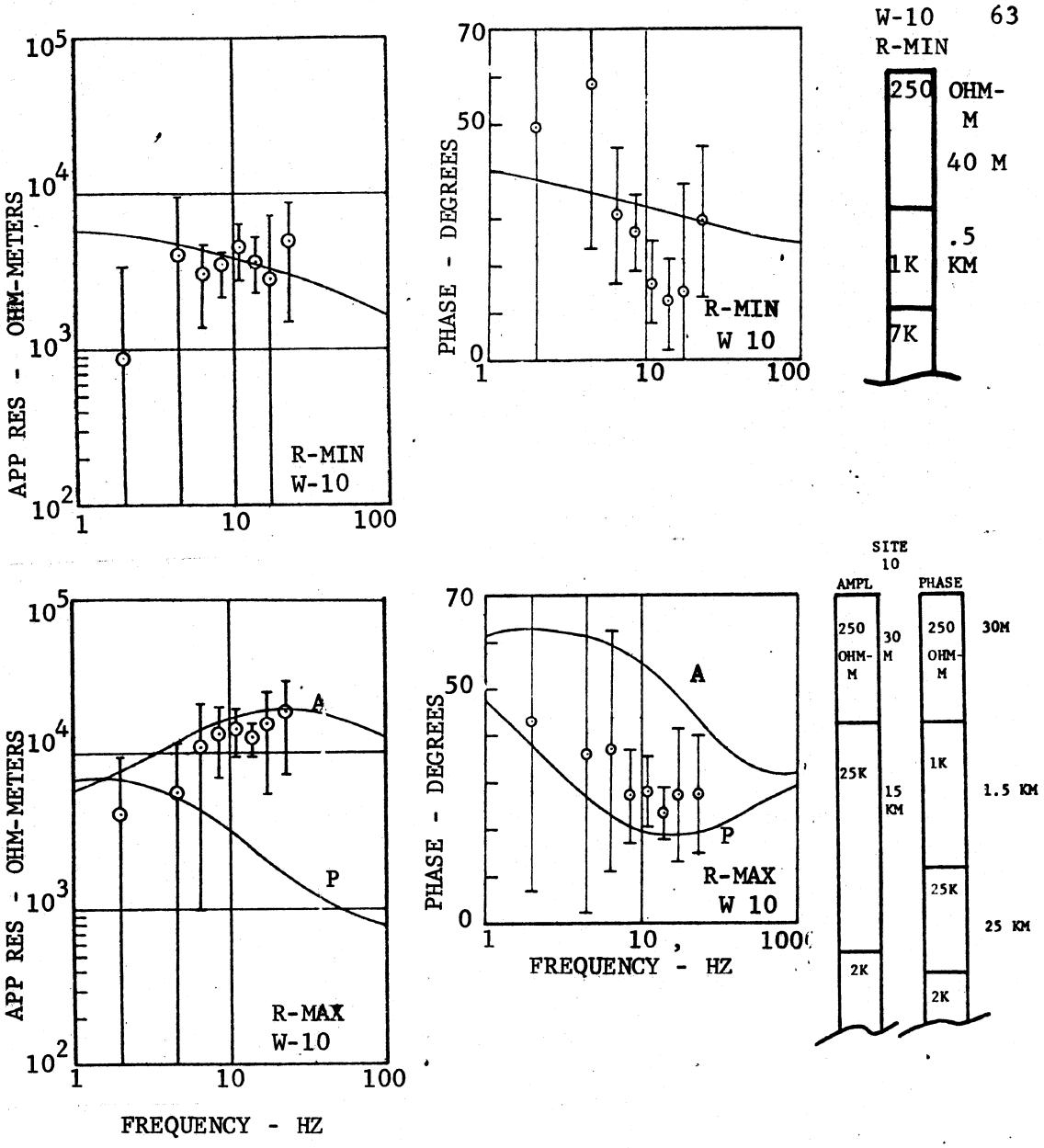

Figure 8.1.1.3 Washington township site 10 R-MAX and R-MIN resistivity and phase data and model. Same symbols as previous figure.

The R-max resistivity data from these sites display downward concavity, peaking at 5,000 to 20,000 ohm meters for frequencies from 5 to 15 Hz. Phases have high values at low frequencies, 45 to 60 degrees below 8 Hz, and have low values at high frequencies, 15 to 20 degrees above 25 Hz.

The models use four layers:

1. First layer of resistivity 250 ohm-meters and thickness 40 meters, probably glacial till. Thickness is from nearby drill holes 39-1 and 39-2, Figure 8.1.1 and Table 8.1.1. Resistivity is a typical value from dipole-dipole measurements near the minesite, Schwenk, 1976, Figure 8.2.1.4.

2. Second layer 1000 ohm-meters, zero to 1500 meters thick, probably Paleozoic sandstone or limestone, as observed in drill holes at the minesite, or a weathered layer of crystalline bedrock.

The model is sensitive to both the thicknesses and the conductivities of the first two layers. The model sounding curve is not invariant with constant thickness-conductivity product of these two layers.

3. Third layer 25,000 to 80,000 ohm meters and thickness 20 to 30 kilometers. The resistivity is a lower bound of values that could fit the data.

4. Bottom half space of resistivity 500 to 2000 ohm-meters. This layer is defined mainly by the data between 1 and 8.5 Hz, which generally have higher variances than the other data.

To fit the curves, I (1) assigned layer 1 to the above resistivity and thickness, layer 2 at 1000 ohm-meters, layer 3 at 25,000 ohm-meters, and layer 4 at 2000 ohm-meters; (2) found suitable thicknesses of layers 2 and 3; (3) when necessary, adjusted the resistivities of layers 2, 3, and 4 for better fit.

Given the uncertainty in resolving the bottom layer in this frequency range and the variations I expect due to near surface features, top layer thickness and conductors, I conclude that the R-max sounding data from sites 7, 9 and 10 show generally similar layered earth structure.

8.1.2 Profile data

The Washington township profile data are presented in Figure 8.1.2.1. The apparant resistivity values, Figure 8.1.2.1c, at each site have been averaged over 3 to 35 Hz. The phases, Figure 8.1.2.1e and g, in two dimensions: station location on the horizontal axis and frequency on the vertical axis. I drew contours where possible. Typically the variances of the phases were five to ten degrees, and I drew the contours as if the data were smoothed. At the south end of the profile, stations 7, 9, 10 and 11 show similar phases and resistivities. Station 11 R-perpendicular data was lost due to a dead H-parallel channel. Station 8 has distorted and higher phases than the others. High skew, above unity for most frequencies, indicates that station 8 is probably near an inhomogeneity. Station 7, near the INPUT anomaly, has low R-parallel apparent resistivity. At the low apparent resistivity zone near Kilometer 0 over the INPUT anomaly, the R-min phases for stations 5 and 12 increase with

Figure 8.1.2.1. Washington township data and model calculations. From top to bottom:

a. Ratio of absolute value of perpendicular (X-axis) to parallel (Y-axis) magnetic field, averaged at each site over frequencies which has H_X-E_Y or H_Y-E_X coherency greater than 0.5.

b. Orientation of R-max rotated tensor resistivities. Sectors or circle enclose orientations of eleven frequency bands from 1 to 33 Hz center frequency. There is a 180 degree ambiguity in these orientations. INPUT conductor 39, Figure 2, is parallel to the Y-axis, perpendicular to the line of stations (X-axis).

c. Scale in kilometers, station numbers, R-max and R-min resistivity data (points) and model calculations (continuous lines). Resistivities in ohm-meters. Data averaged at each station over 3 to 35 Hz. Circles represent data approximately perpendicular to conductor 39 and are inferred to represent R-perpendicular. Triangles represent data oriented approximately parallel to conductor 39 and are inferred to represent R-parallel. Stations plotted according to NW-SE distance from axis of conductor 39.

d. Location of INPUT airborne EM anomaly 39 across my line of stations (I-39) and turam anomalies from line 1200W, Great Lakes Exploration, 1972, from Figure 8.1.1.

e. R-min data phase contours and tabulation as function of frequency.

f. Model R-parallel phase contours and tabulation max at 3, 10, and 30 Hz.

g. R-max data phase contours and tabulation as function of frequency.

h. Model R-perpendicular phases. Phase was calculated at all cells indicated in e, but are tabulated only at edge of diagram and where they are different from adjacent phases.

i. Conductivity cross-section. True vertical scale except for depth to lower interface as shown.

There is a small scale change of about one millimeter per kilometer between the model and data plots. Both sets of plots are aligned on the main conductor.

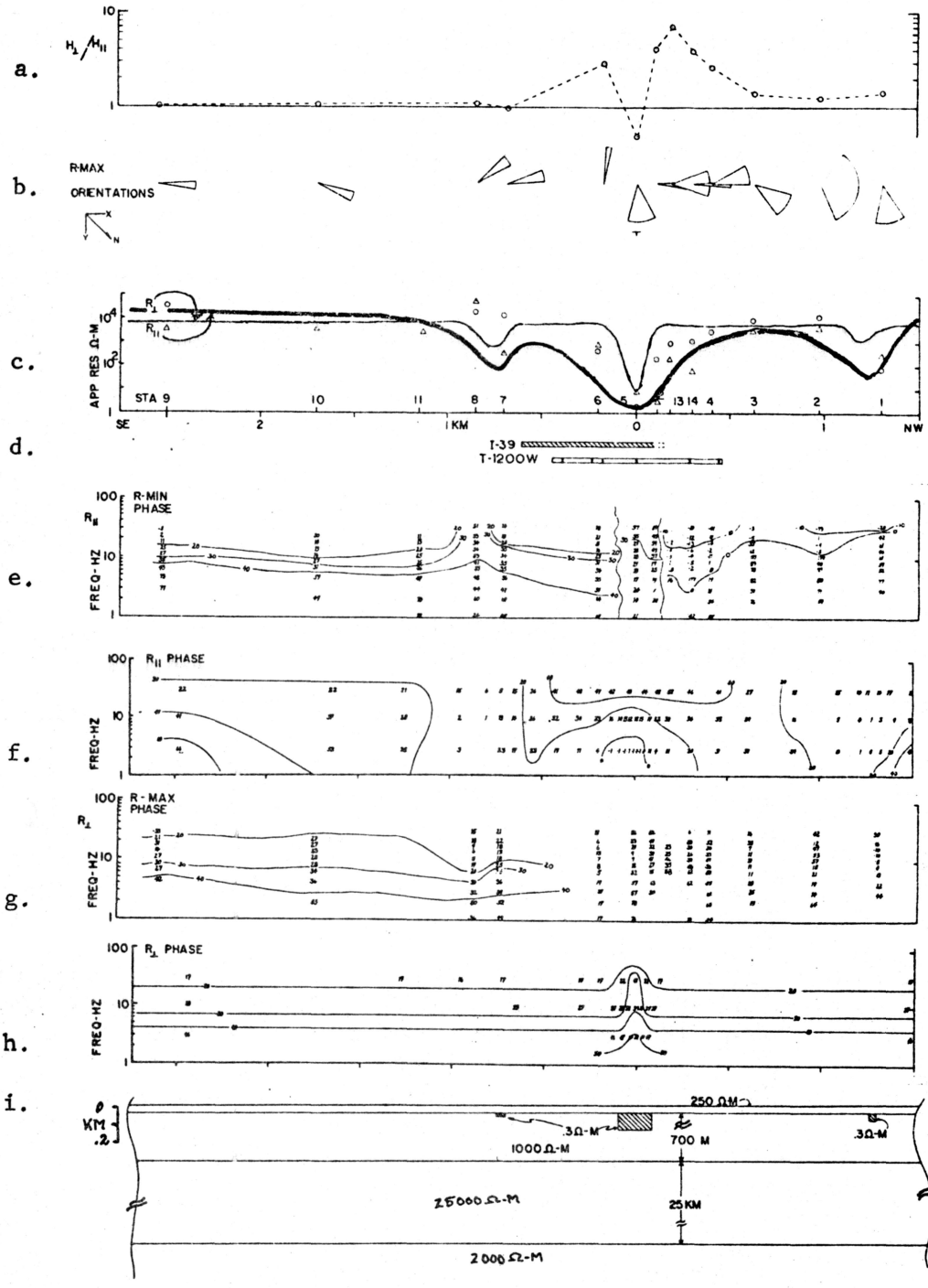
a.
10
$H_\perp / H_{II}$
1
b.
R-MAX
ORIENTATIONS
X
N
c.
$R_\perp$
R_{II}
APP RES Ω-M
10^4
10^2
1
STA 9
10
11
8
7
6
5
4
3
2
1
SE
2
1 KM
0
1
NW
d.
T-39
T-1200W
e.
100
R-MIN
PHASE
R_{II}
FREQ-HZ
10
1
f.
100
R_{II} PHASE
FREQ-HZ
10
1
g.
100
R-MAX
PHASE
$R_\perp$
FREQ-HZ
10
1
h.
100
$R_\perp$ PHASE
FREQ-HZ
10
1
i.
0
KM
.2
250 Ω-M
3Ω-M
1000 Ω-M
700 M
3Ω-M
25000 Ω-M
25 KM
2000 Ω-M

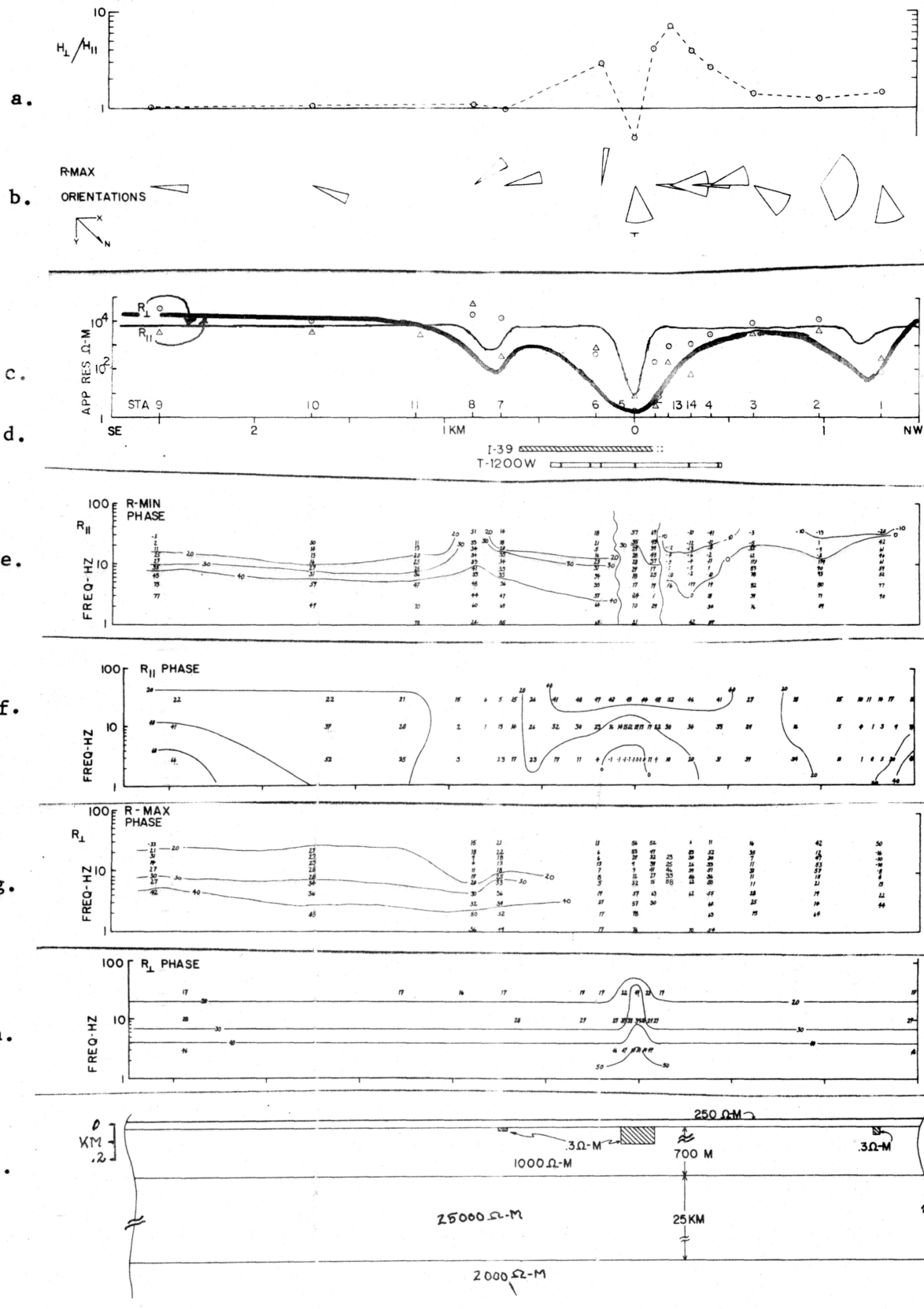
a.
$H_\perp / H_{II}$
10
1
b.
R-MAX
ORIENTATIONS
X
Y
N
c.
APP RES Ω-M
10^4
10^2
1
$R_\perp$
R_{II}
STA 9
10
11
8
7
6
5
4
3
2
1
d.
SE
2
1 KM
0
1
NW
I-39
T-1200W
e.
100
10
1
R-MIN PHASE
R_{II}
FREQ-HZ
f.
100
10
1
R_{II} PHASE
FREQ-HZ
g.
100
10
1
R-MAX PHASE
$R_\perp$
FREQ-HZ
h.
100
10
1
$R_\perp$ PHASE
FREQ-HZ
i.
0
KM
.2
250 Ω-M
.3Ω-M
700 M
.3Ω-M
1000 Ω-M
25000 Ω-M
25KM
2000 Ω-M

frequency; they decrease elsewhere. The R-max phases here are too irregular to contour. The turam data from Great Lakes Exploration Company, 1972, show 6 conductors here in a space of one kilometer, which could account for the complicated phases. To the northwest, the apparent resistivities rise to host rock values, and drop again at station 1, probably due to another conductor. The R-min phases have negative values at high frequency to the northwest, most pronounced near the INPUT anomaly. I could tell in the field that the northwest magnetic field, H_X, was stronger than the southeast magnetic field, H_Y, near the INPUT anomaly, by the difference in amplifier attenuator setting required for proper recording. The calculated ratios of H_X to H_Y, Figure 8.1.2.1a, show a peak of about 7 at station 13, probably due to currents induced in the conductor.

The Washington township R-max orientations are shown in Figure 8.1.2.1b plotted relative to the profile direction, northwest, which is the X-axis. Each pie segment in the figure represents the range of R-max orientations for the eleven frequency bands between 1 and 35 Hz. I would expect these segments to be narrow and aligned perpendicular to the INPUT anomaly near the anomaly. From the low apparent resistivity values, Figure 8.1.2.1c, I conclude that stations 5, 12, and 13 are over the conductor. Of these, 5 is not aligned perpendicular to the conductor, but is rotated about 30 degrees. Stations 4, 12, 13, and 14 have R-max perpendicular to the conductor. 6 has R-max parallel to the conductor. Away from the conductor, to the northwest, station 3 is rotated about 30 degrees clockwise from the X-axis and station 2 has scattered

orientations. For stations 2 and 3, R-max-R-min ratios are 2.2 and 2.8.

The scattered orientations at station 2 are probably the effect of random errors due to circuit noise, weak signals and the measurement of a random process. Rotations at station 3 may be caused by a local inflection of the main conductor. Further northwest, station 1 R-max is oriented at right angles to the X-axis, and has values of 73 and 168 ohm meters for R-min and R-max. This station is probably affected by some other nearby conductor.

To the southeast, station 7 has R-max oriented about ten degrees counter clockwise from the X-axis. Since the ratio of R-max to R-min is about 100 here, I suspect that there is a nearby conductor. Station 8 R-max is about 45 degrees counter clockwise from the X-axis, also probably due to some nearby conductor. Stations 9 and 10 have R-max aligned parallel to the X-axis. I suspect that this alignment is due to nearby conductors that my profile does not resolve.

8.1.3 Two-dimensional model

Figure 8.1.2.1 shows the model, i, apparent resistivities, c, and phases, f and h, for Washington township. Phases are flat if not tabulated. I compare the R-max data with the R-perpendicular model and the R-min data with the R-parallel model. The orientations show that R-max is perpendicular to the conductor except at stations 1, 5, and 6. At these stations, the R-max orientation has swung about 90 degrees, parallel to the conductor, that is R-max is R-parallel. Model apparent resistivities and data show the R-perpendicular anomaly narrower than the R-

parallel anomaly. The cross over of R-perpendicular and R-parallel model resistivities near station 11 to the southeast is an artifact of the computation also occurring in the sample run in Jones and Pascoe, 1971. R-perpendicular and R-parallel values should asymptotically approach each other away from the anomaly. The conductor responsible for airborne EM anomaly 39 of Figure 8.1.1 and for the low apparent resistivities near kilometer zero on the MT data profile is modelled with a width of 120 meters and a depth of 80 meters. A wide shallow conductor was needed to match R-parallel on the shoulders of the anomaly. This model treats the multiple conductors discovered by turam as a single conductor. In comparison, Sternberg and Clay's 1977 MT model for conductors in the Flambeau Anomaly is 20 to 30 meters wide and one kilometer or more deep. There are two additional small conductors to account for low apparent resistivities at stations 1 and 7. The R-parallel phases are in general agreement with the model at the southeast end of the profile. Model phases do not agree with data over the conductor nor over the northwest end of the profile. Denser data are probably needed to resolve the structures here, and a finer grid needed for modelling. It may be that I have reached the point where applying a two-dimensional model to a three-dimensional problem is no longer useful. The H-perpendicular/H-parallel results from this model, not shown, have a central anomaly that is wider and stronger than the data. Further model calculations showed that I needed a conductor of smaller cross-section buried at a shallower depth to match the H ratio data.

8.2 Minesite

The station location map, Figure 8.2.1, shows the minesite MT stations in relation to INPUT anomaly 22, the ore deposit and INPUT anomaly 19, a graphitic conductor.

Schwenk, 1976, used geophysics to investigate the copper deposit. Preliminary airborne EM (INPUT by Barringer Exploration) located many long conductors, Figure 6.2.2, striking approximately northeast, 45°, in a pattern similar to conductors reported by Sternberg and Clay, 1977. Ground geophysical followup utilized magnetics, Figures 8.2.2 and 8.2.3, gravity, Figures 8.2.4, 8.2.5 and 8.2.6, electromagnetics (slingram and turam, not shown), audio-magnetotellurics (AMT), Figure 8.2.7, induced polarization and spontaneous potential (not shown). Schwenk verified the location of the ore deposit with gravity measurements, Figure 8.2.5, and developed a cross-section model, Figure 8.2.6. He estimated the total mass of ore at 6.33×10^6 tons.

Figure 8.2.8 is a geologic cross-section of the orebody and surrounding rocks. These metamorphosed volcanic rocks, including the ore, have a dip of 75 degrees, a strike of 45 degrees (NW), and thicknesses of a few meters to hundreds of meters. The sulfide ore body, consisting mainly of pyrite and chalcopyrite, has a strike length of 170 meters at the bedrock surface, increasing to 800 meters at 200 meters depth, May, 1976.

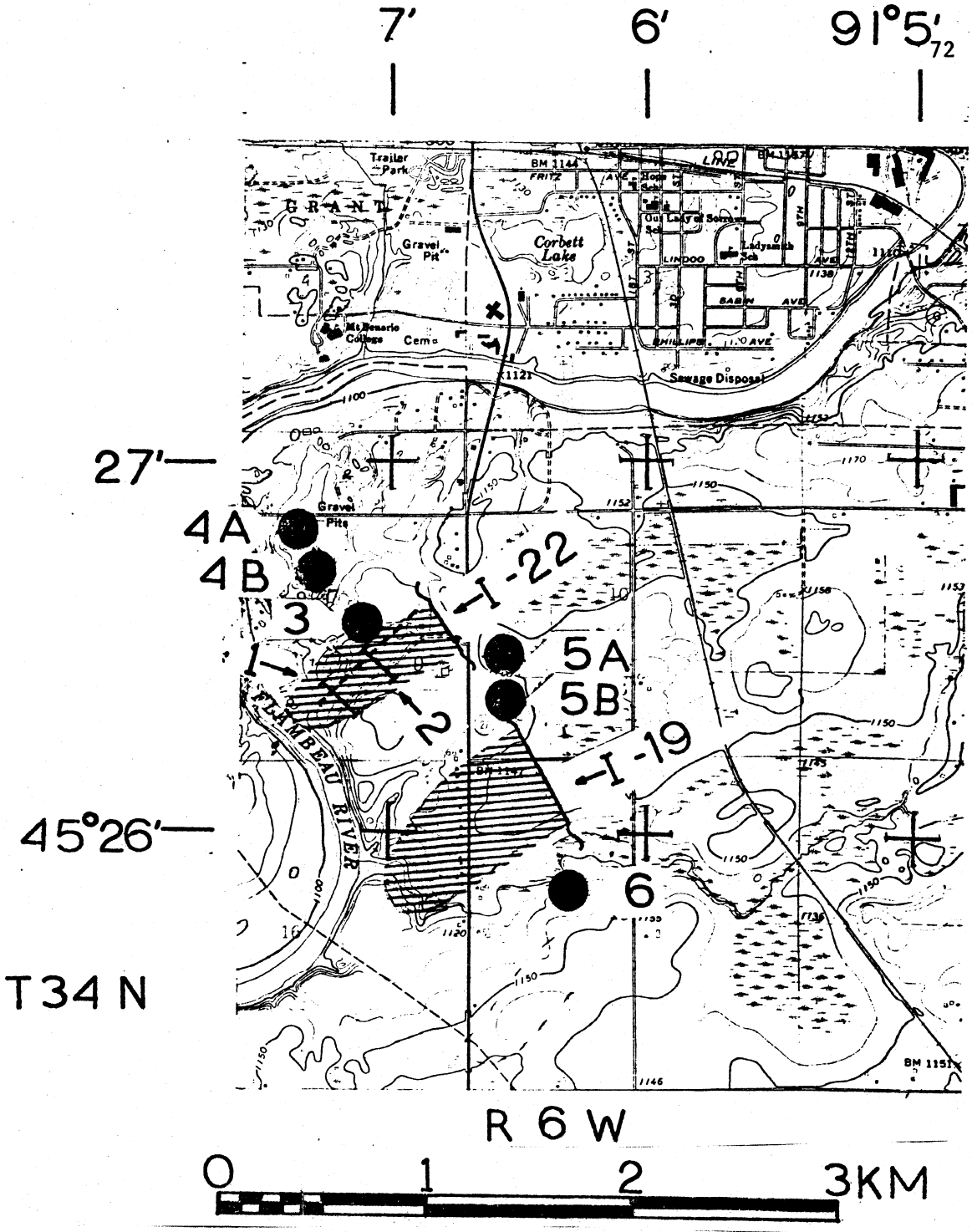

Figure 8.2.1. Minesite station map. Ruled areas are INPUT anomalies 19 and 22 from Figure 6.2.2. Anomaly 22 is the copper mine site, dashed line is approximate axis of ore body. Stations 1 and 2, solid lines in anomaly 22, are traverses across orebody. Stations 3 to 6 are indicated by large dots. Background map is USGS quadrangle of Ladysmith, Wisconsin.

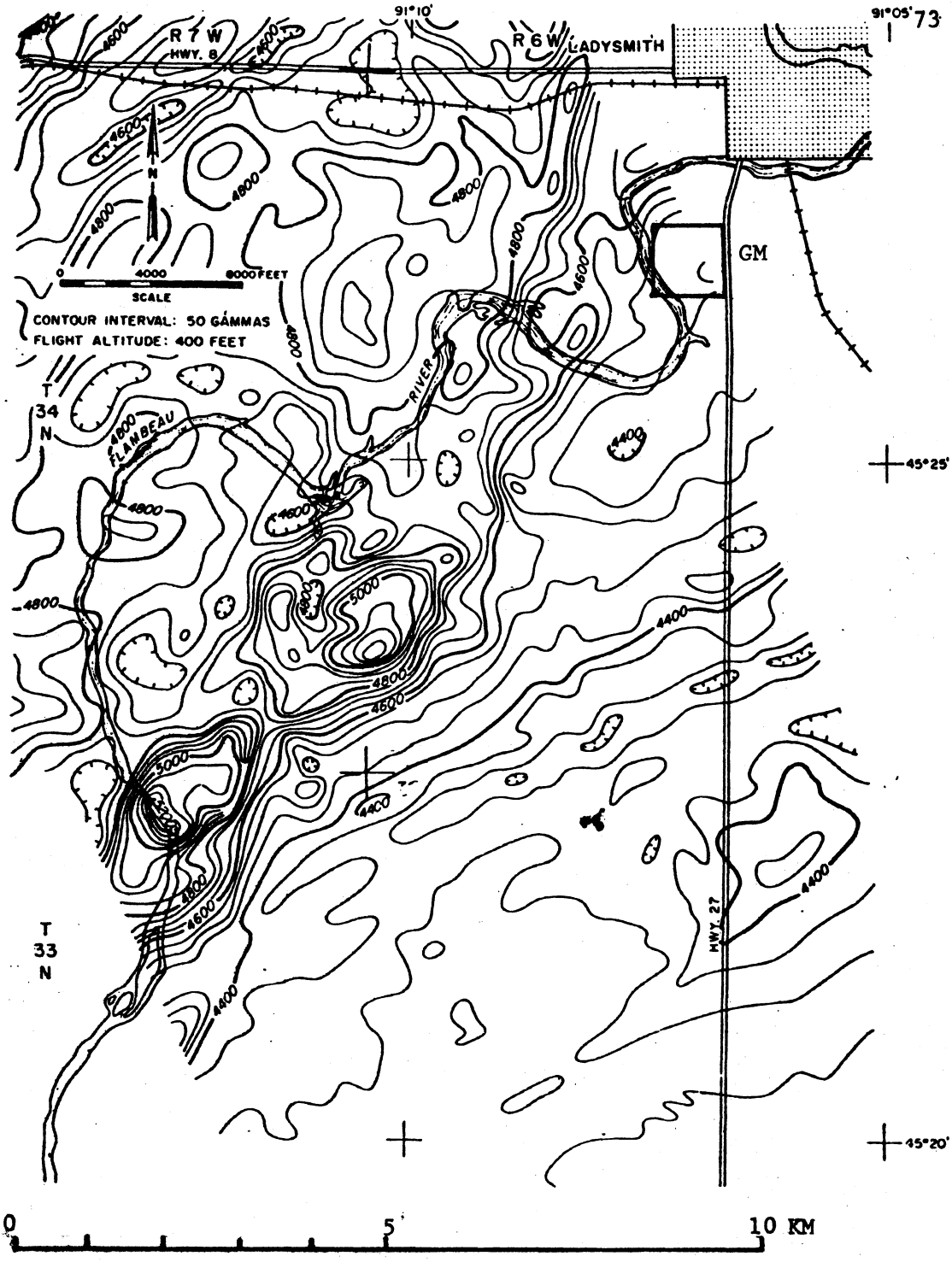

Figure 8.2.2. High Resolution aeromagnetic map of minesite and Washington township areas, from Schwenk, 1976. Box marked GM is location of ground magnetics map, Figure 8.2.3.

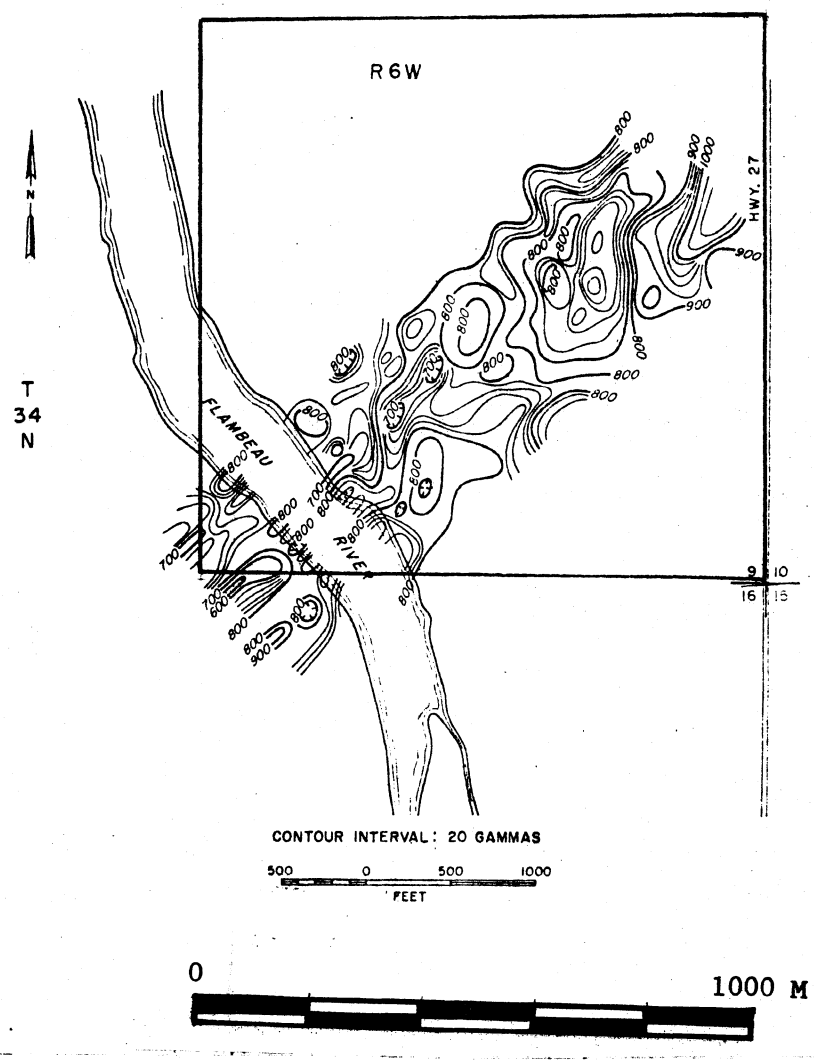

Figure 8.2.3 Minesite ground vertical magnetics map, from Schwenk, 1976. Square keys this map to Figure 8.2.2.

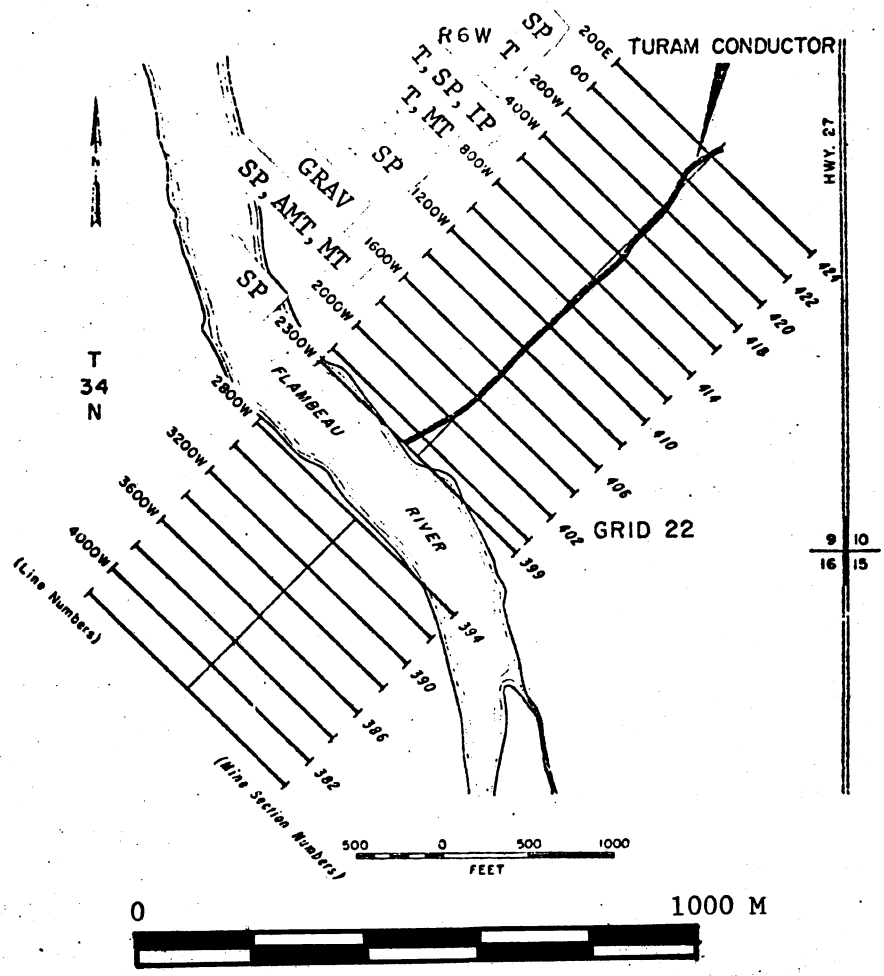

Figure 8.2.4. Plan map of conductor at minesite as determined by turam, active source EM, from Schwenk, 1976. The initials at the upper left end of traverse lines indicate type of data given in Schwenk and location of my MT traverses as follows: SP spontaneous potential, T turam, IP induced polarization, AMT audiomagnetotellurics (Kennecott), GRAV gravity (approximate location), MT magnetotellurics (University of Wisconsin).

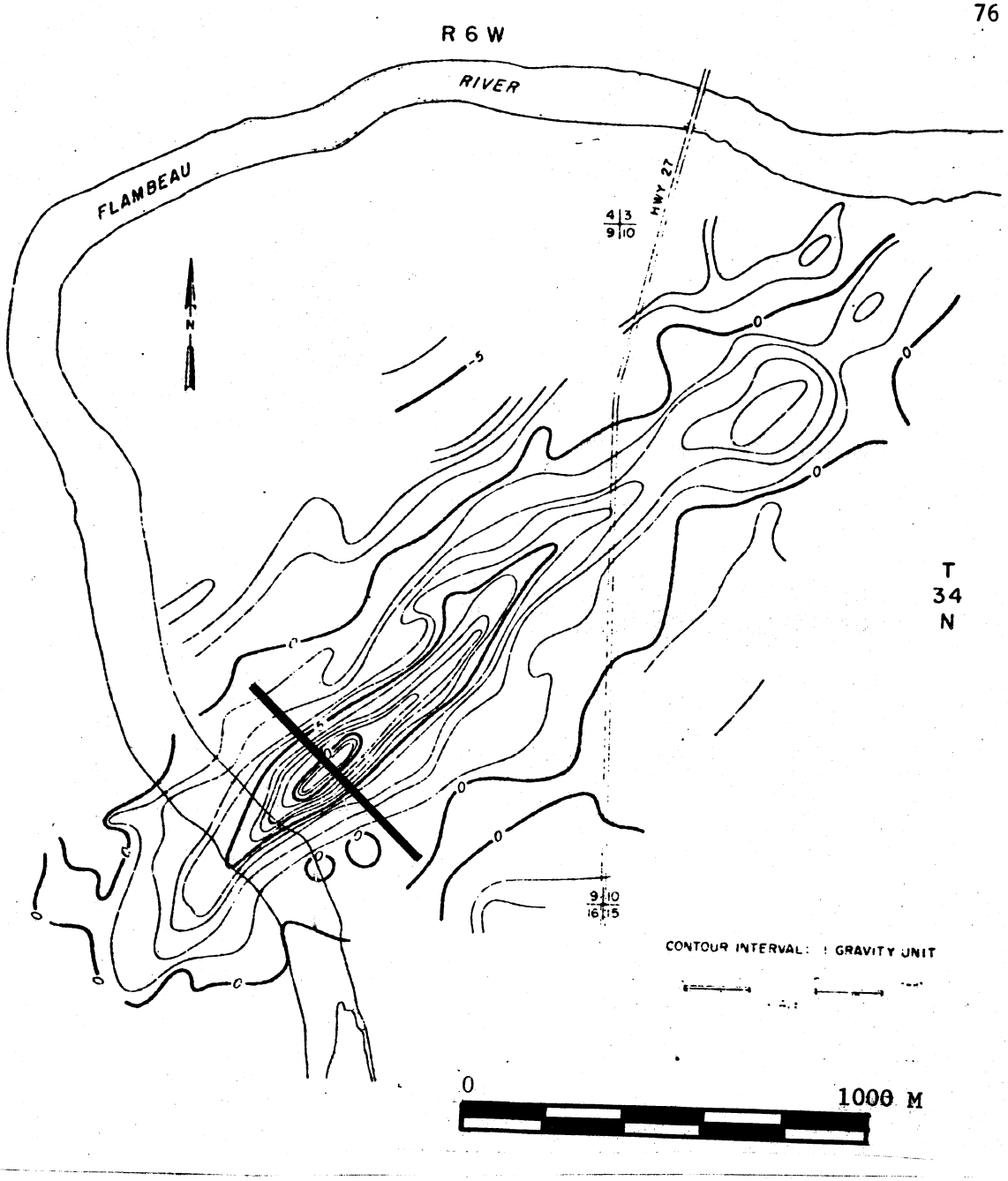

Figure 8.2.5. Minesite residual gravity map, from Schwenk, 1976, showing 10 gravity unit anomaly over orebody. Ten gravity units equal one milligal. Solid heavy line indicates profile which is modelled in the next figure.

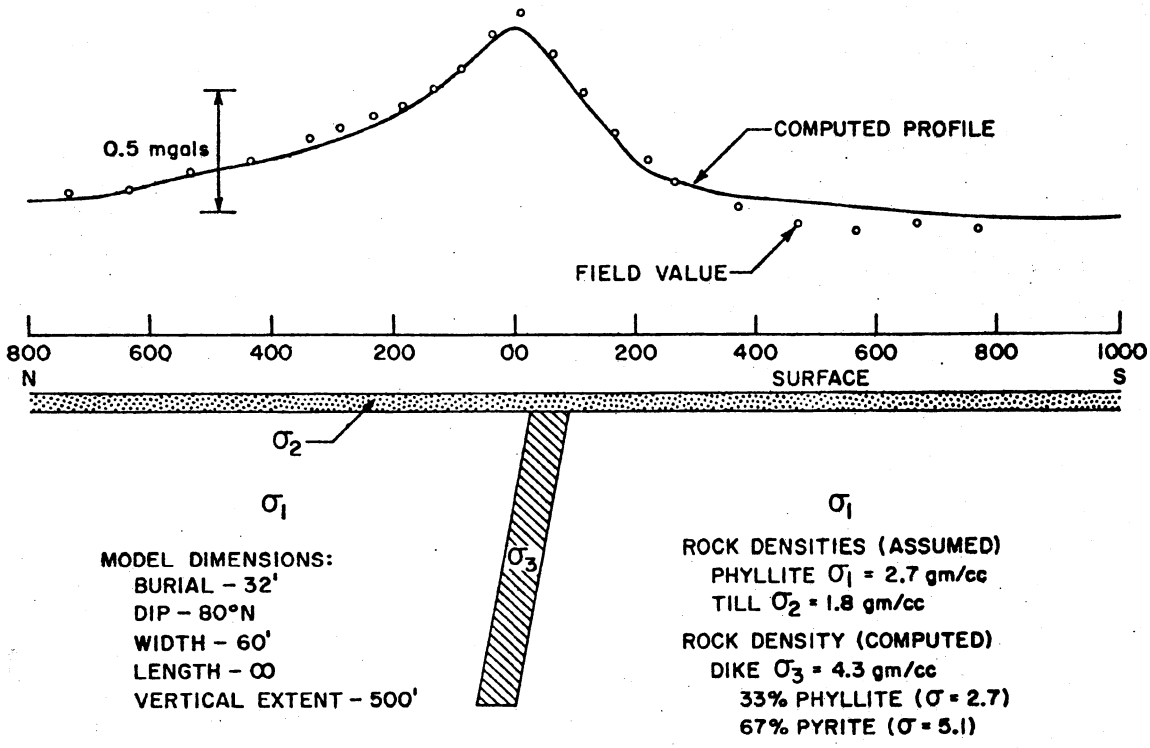

Figure 8.2.6. Gravity data and model across orebody, from Schwenk, 1976. Location of profile is shown as heavy line on map of Figure 8.2.5.

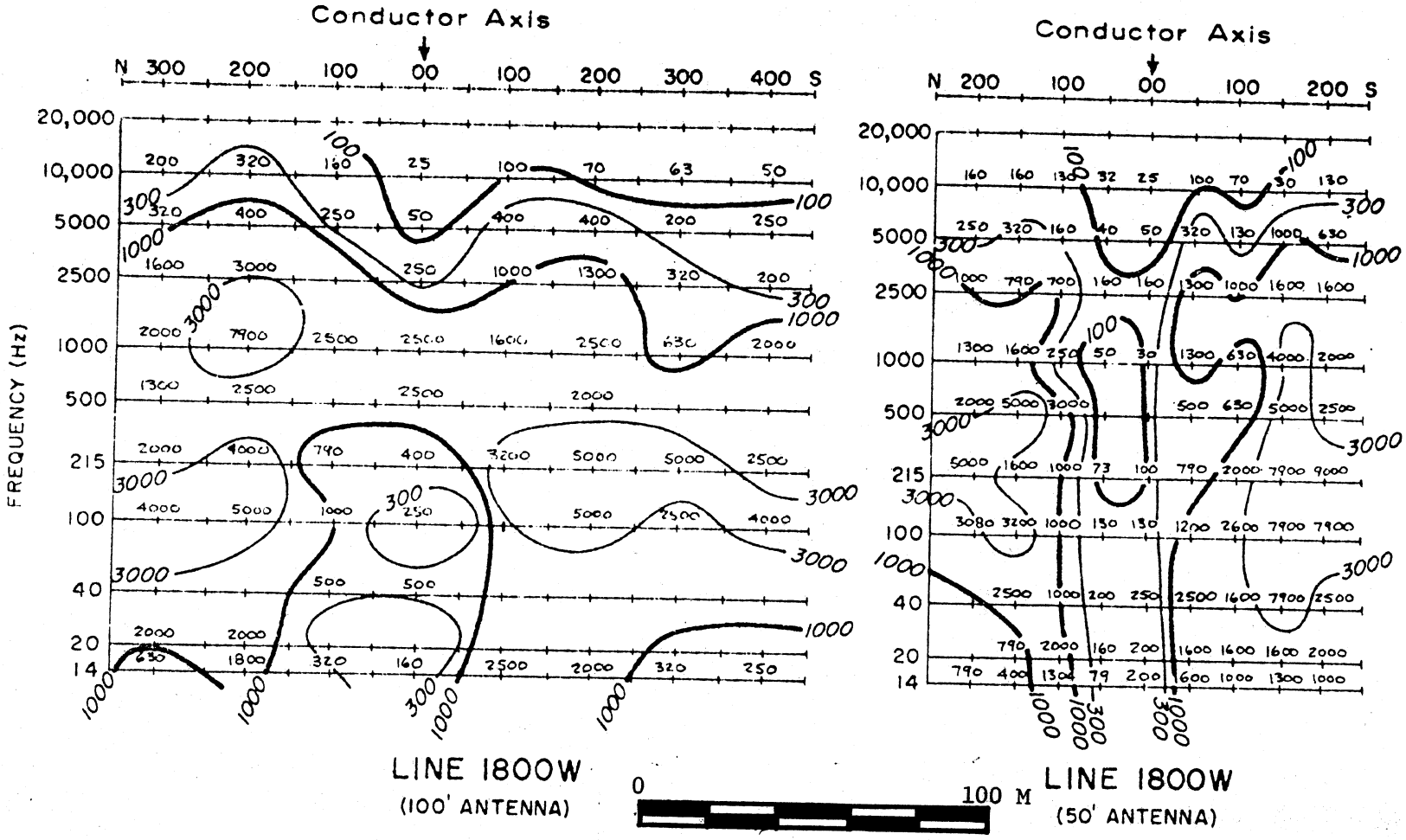

E FIELD ANTENNA DUE EAST. DATA PLOTTED AT COIL END OF DIPOLE IN OHM-METERS

Figure 8.2.7. Minesite audiomagnetotelluric (AMT) pseudosection from Schwenk, 1976. Location of profile is line number 1800W or mine-section 404 shown on Figure 8.2.4.

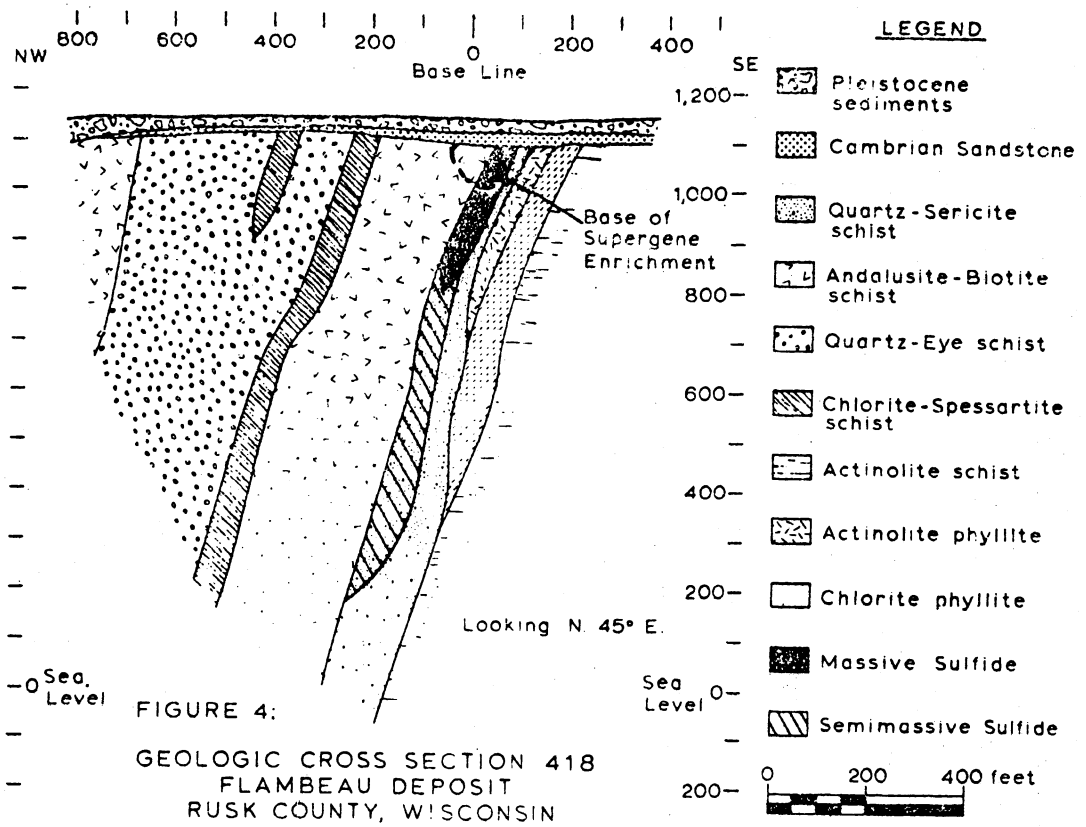

FIGURE 4:

GEOLOGIC CROSS SECTION 418
FLAMBEAU DEPOSIT
RUSK COUNTY, WISCONSIN

Figure 8.2.8. Geologic cross-section of copper deposit at minesite, across minesection 418, Figure 8.2.4, from May, 1976.

8.2.1 Sounding data and layered models

A layered model summary for sites 3, 5B, and 6 is shown in Figure 8.2.1.1; the data and model sounding curves are shown in Figures 8.2.1.2 and 8.2.1.3. These sites were chosen for layered model fitting because they exhibit resistivities and phases similar to each other, and appear to be far enough away that they are unaffected by the copper deposit. For sites 3 and 5B, R-max is approximately perpendicular to the ore body. For site 6, R-max is scattered with frequency and R-max values only a few percent greater than R-min, indicating that for this frequency range, the earth appears to be flat layers.

The layered models for the minesite, summarized on Figure 8.2.1.1, use (1) a top layer of 250 ohm-meters, a typical value of nearby resistivity measurements, Figure 8.2.1.3. The model is sensitive to both the thickness and resistivity of this layer. One normally expects a thin conductive surface layer to terminate at the bedrock surface, but both my data and the DC resistivity require a thicker layer. (2) A second layer of 25,000 ohm-meters resistivity and thickness 17 to 40 kilometers. This resistivity is a lower bound of values that fit the data. (3) A bottom half space of resistivity 500 or 2000 ohm meters. The bottom half-space is determined mainly by the low frequency data, below 8 Hz. These data have the highest variances, so the bottom half space resistivity is not resolved well. Given the uncertainty in resolving the bottom layer and the variations one expects due to near surface features from site to site, I conclude that the data from sites 3, 5B, and 6 show a generally

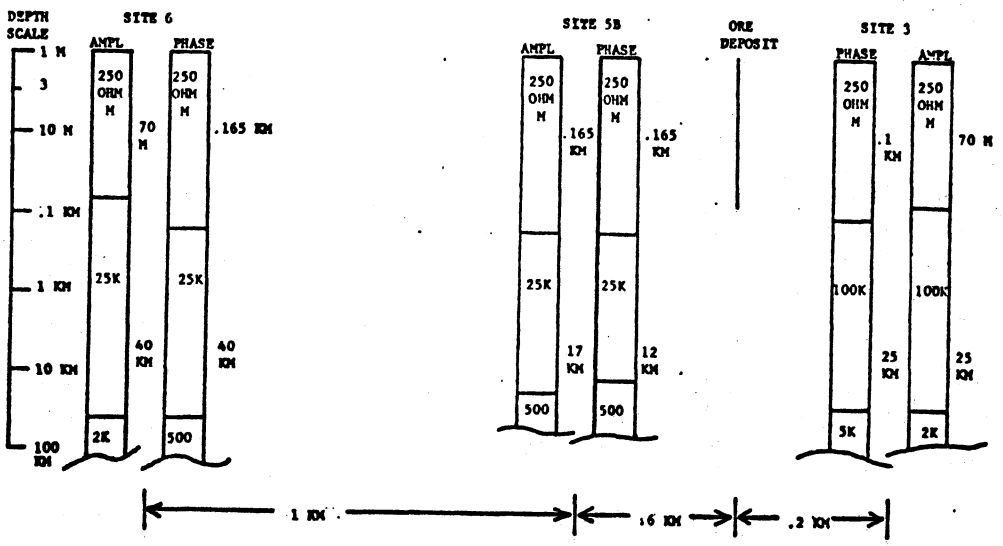

Figure 8.2.1.1. Minesite layered model summary. Logarithmic depth scale. Resistivity of layers tabulated inside layers, thickness of layers outside. Distance between stations is not to scale.

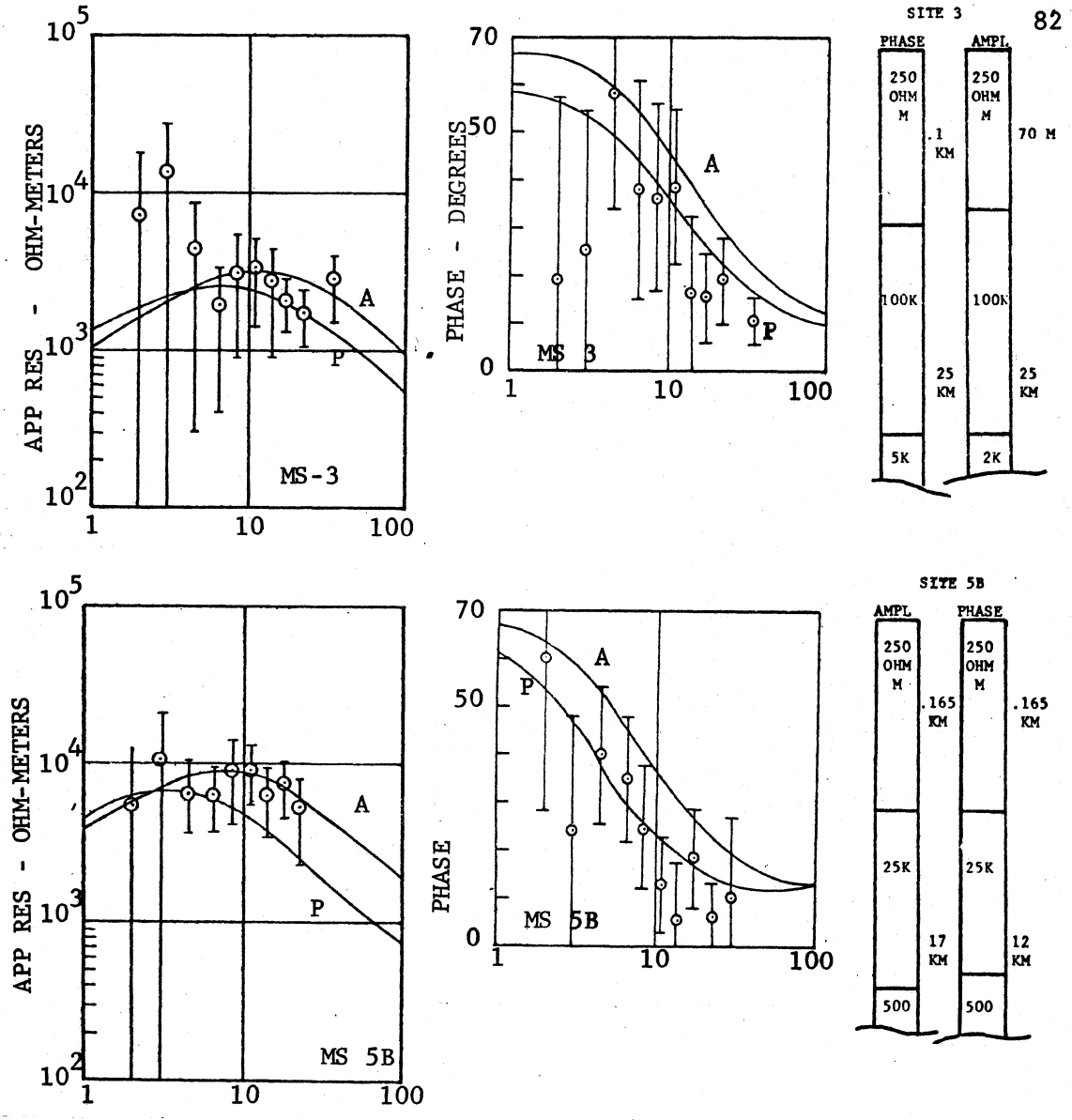

Figure 8.2.1.2 Minesite stations 3 and 5B R-MAX data (points) and models (solid curves). Error bars are one standard deviation. A is amplitude match model. P is phase match.

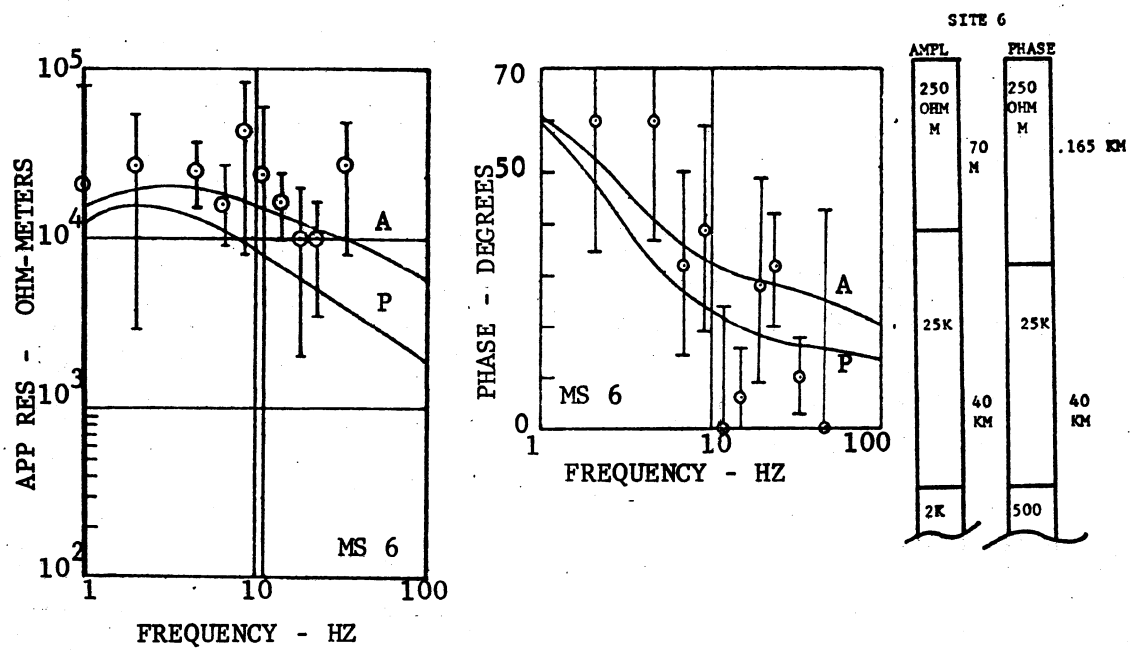

Figure 8.2.1.3 Minesite 6 R-MAX data and model. Same symbols as previous figure.

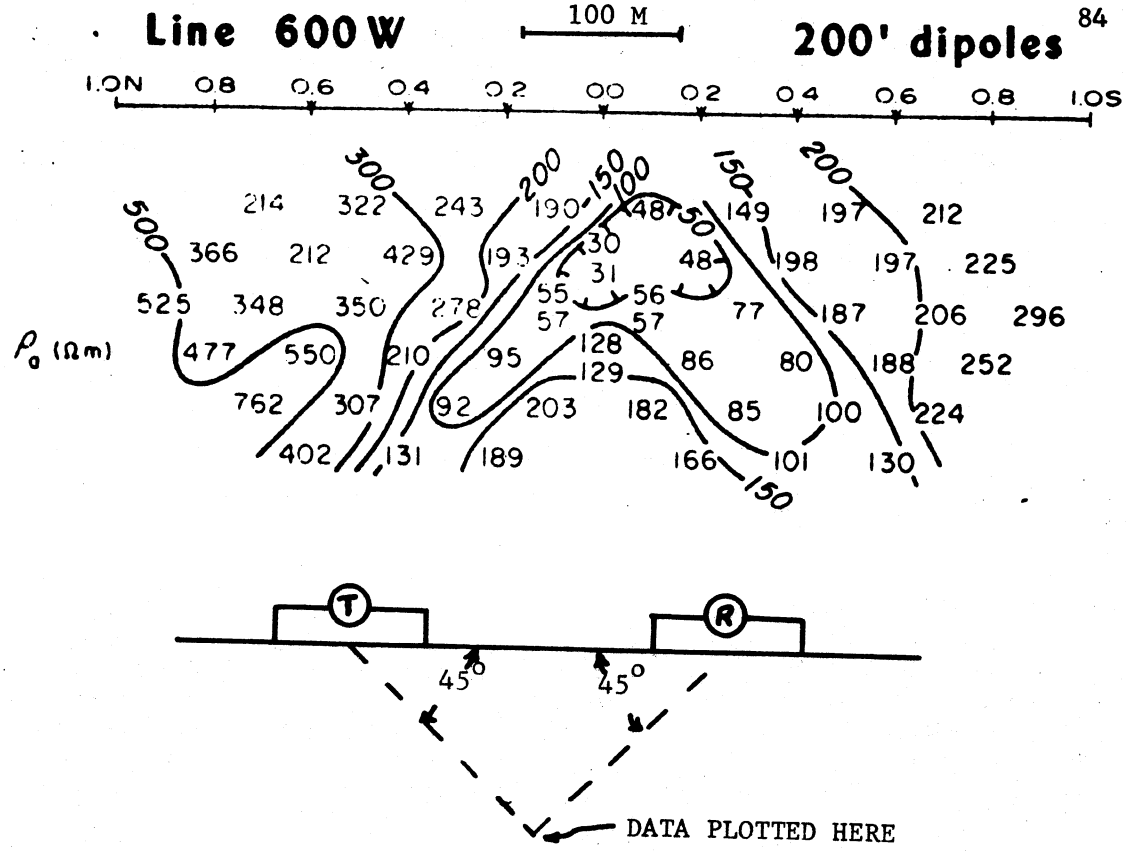

Figure 8.2.1.4. Minesite dipole-dipole d.c. resistivity profile across ore body, from Schwenk, 1976. Location is line number 600W, minesection 416 of Figure 8.2.4. Results are presented as a pseudo-section, that is, apparent resistivities are tabulated at points midway between transmitter and receiver location, at the intersection of lines drawn 45 degrees downward from transmitter and receiver, as shown in the inset diagram.

similar earth structure, similar to Washington township and generally similar to Sternberg and Clay, 1977, and Dowling, 1970, Figure 6.2.1. The fact that a single model does not fit both resistivity and phase means that the earth here is too complicated to be fit by layered models alone.

8.2.2 Profile data

I show profile data for the minesite in Figures 8.2.2.1, 8.2.2.2 and 8.2.2.3. The first figure covers about 3 kilometers, the next two figures are parallel telluric current profiles 304 meters (1000 ft) apart, taken directly over the conductor in ten meter station spacings, covering about 150 meters each. The detailed apparent resistivity data from Figure 8.2.2.3 are also plotted on Figure 8.2.2.1b, but the phase data are omitted.

The apparent resistivities, Figure 8.2.2.1b, show that three of the five stations more distant than 400 meters from the conductor, 6, 4A, and 4B, have R-max, R-min ratios of less than two, representing relatively laterally homogeneous earth. The other two distant stations, 5A and 5B, show R-max, R-min ratios greater than ten, probably influenced by INPUT conductor 19, within 300 meters of both stations.

Typically, the distant stations have phases that decrease with increasing frequency, and the R-min phases here have lower values than R-max, with negative values at high frequency. To the northwest stations 4A and 4B R-max phases are scattered with frequency and could not be contoured. The negative phases are remarkable because they are never seen on flat-layered models.

Figure 8.2.2.1. Minesite data profile and model calculations. Location map is Figure 8.2.1. Profile extends northwest (right) to southeast (left), stations measured from axis of ore deposit which runs northeast-southwest. From bottom to top:

a. Orientation of R-max rotated tensor resistivities. Sector of circle encloses all orientations from 1-35 Hz. INPUT conductor 22 is perpendicular to line of stations (X-axis).

b. R-max and R-min resistivity data (points) and model calculations at 10 Hz (continuous and dashed lines). Resistivities in ohm-meters, data averaged at each station over 3-33 Hz. Circles represent data approximately perpendicular to conductor 22, and are inferred to represent R-perpendicular. Triangles represent data oriented approximately parallel to conductor 22 and are inferred to represent R-parallel. Exceptions are scalar values within 150 meters of zero kilometers, from Traverse 2, Figure 10, and the unnumbered four telluric stations northwest of Station 3. These are unrotated scalar resistivities. These circles are R-perpendicular, triangles are R-parallel.

c. Location of airborne EM anomalies 19 and 22, Figure 6.2.2, along line of stations.

d. R-min data phase contours and tabulation with frequency. Data inside brackets are stations 1 and 2 base stations only.

e. R-perpendicular model phase contours calculated at 3, 10, and 30 Hz, tabulated at edge and where they are different from adjacent values.

f. R-max phase contours and tabulation with frequency. Data inside brackets are stations 1 and 2 base stations only.

g. R-parallel model phase contours calculated at 3, 10 and 30 Hz.

h. Model conductivity cross-section. True vertical scale except for depth to lower interface as shown. Note that the top conductive layer is deeper than the known till and sedimentary layers as discussed in section 8.2.1.

There is a small scale change of about one millimeter per kilometer between the model and data plots. Both sets of plots are lined up on the central conductor.

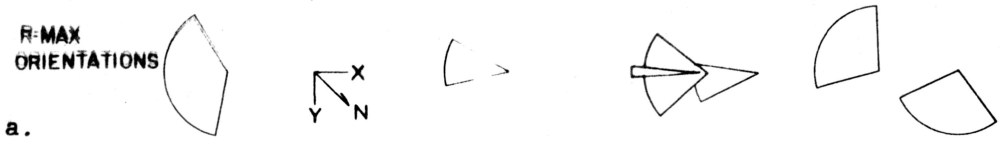
R-MAX
ORIENTATIONS
X
Y
N

a.

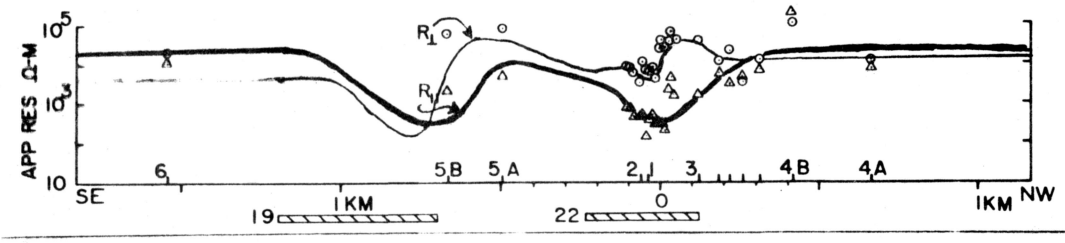
APP RES Ω-M
10^5
10^4
10
$R_\perp$
$R_\parallel$
6
5B
5A
2
1
3
4B
4A
SE
NW
1KM
19
22
0

b.

c.

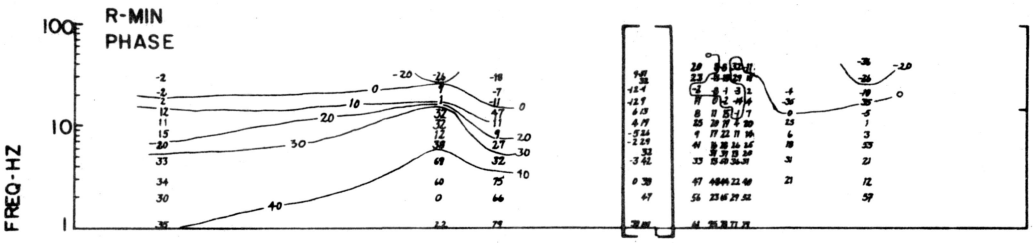
R-MIN
PHASE
FREQ-HZ
100
10
1

d.

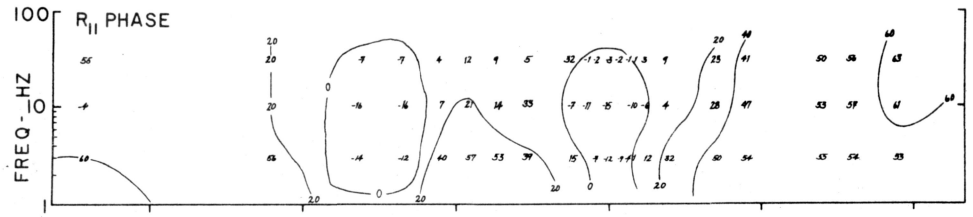
R_{II} PHASE
FREQ-HZ
100
10
1

e.

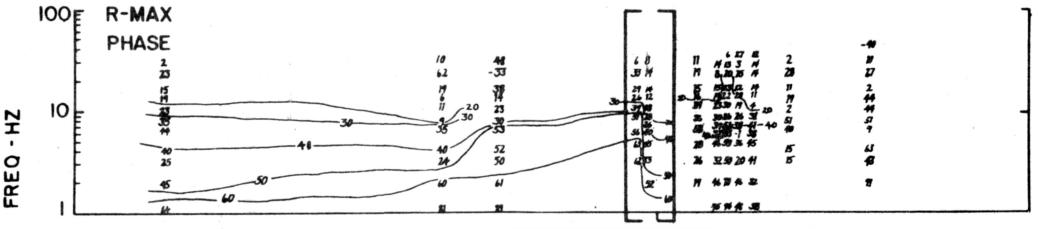
R-MAX
PHASE
FREQ-HZ
100
10
1

f.

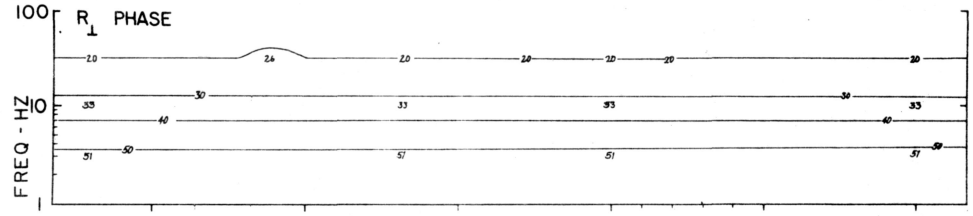
$R_\perp$ PHASE
FREQ-HZ
100
10
1

g.

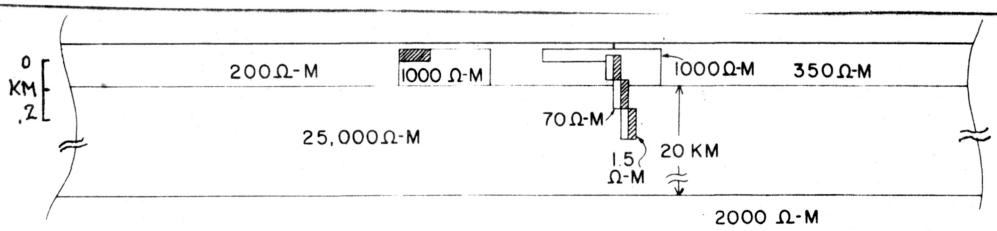
0
KM
.2
200Ω-M
1000 Ω-M
1000Ω-M
350Ω-M
70Ω-M
25,000Ω-M
1.5
Ω-M
20 KM
2000 Ω-M

h.

Figure 8.2.2.2. Minesite detailed data profile, Traverse 1, at 10 meter spacing across mine section 404, line number 1800W, map view in Figure 8.2.4. From bottom to top data are:

a. scale in meters and station location. Arrow at 40 meters marks approximate axis of turam conductor, from Figure 8.2.4.

b. scalar apparent resistivities averaged over 3-33 Hz, excluding frequencies with coherency less than 0.3. Triangles are R-parallel, circles are R-perpendicular. Data are for moving electrodes taken with 4 electrode "L" array, plotted at corner of L, with magnetic detectors stationary at base. Crosses, +, are 20 Hz AMT data and X's are 14 Hz AMT data from Schwenk, 1976.

c. R-perpendicular phase contours and tabulation vs. frequency. Boxes around data indicate coherency less than 0.3.

d. R-parallel contours and tabulations vs. frequency.

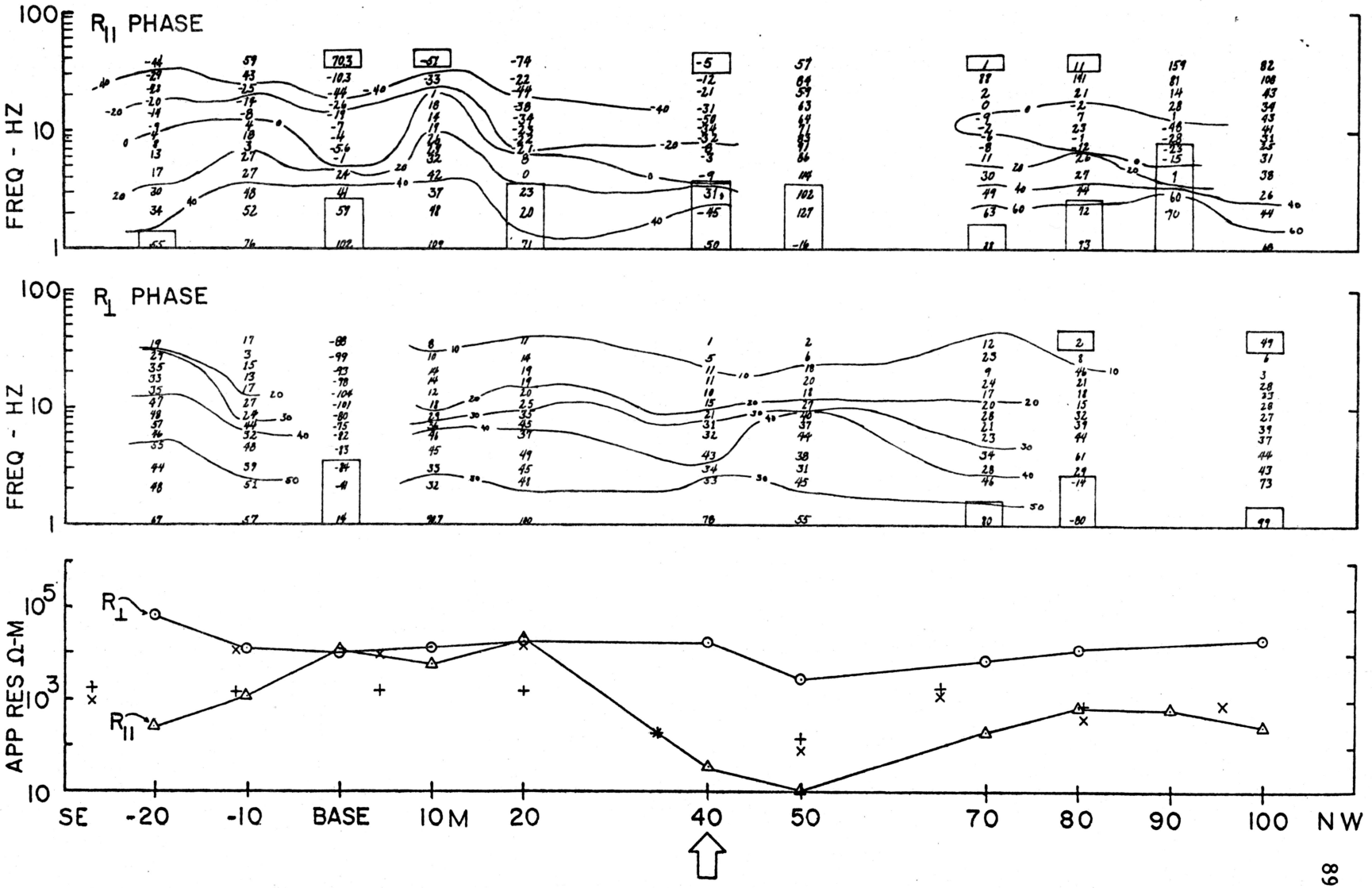
100
10
1
FREQ - HZ
R_{II} PHASE
$R_{\perp}$ PHASE
APP RES Ω-M
10^5
10^3
10
$R_{\perp}$
R_{II}
SE
-20
-10
BASE
10M
20
40
50
70
80
90
100
NW

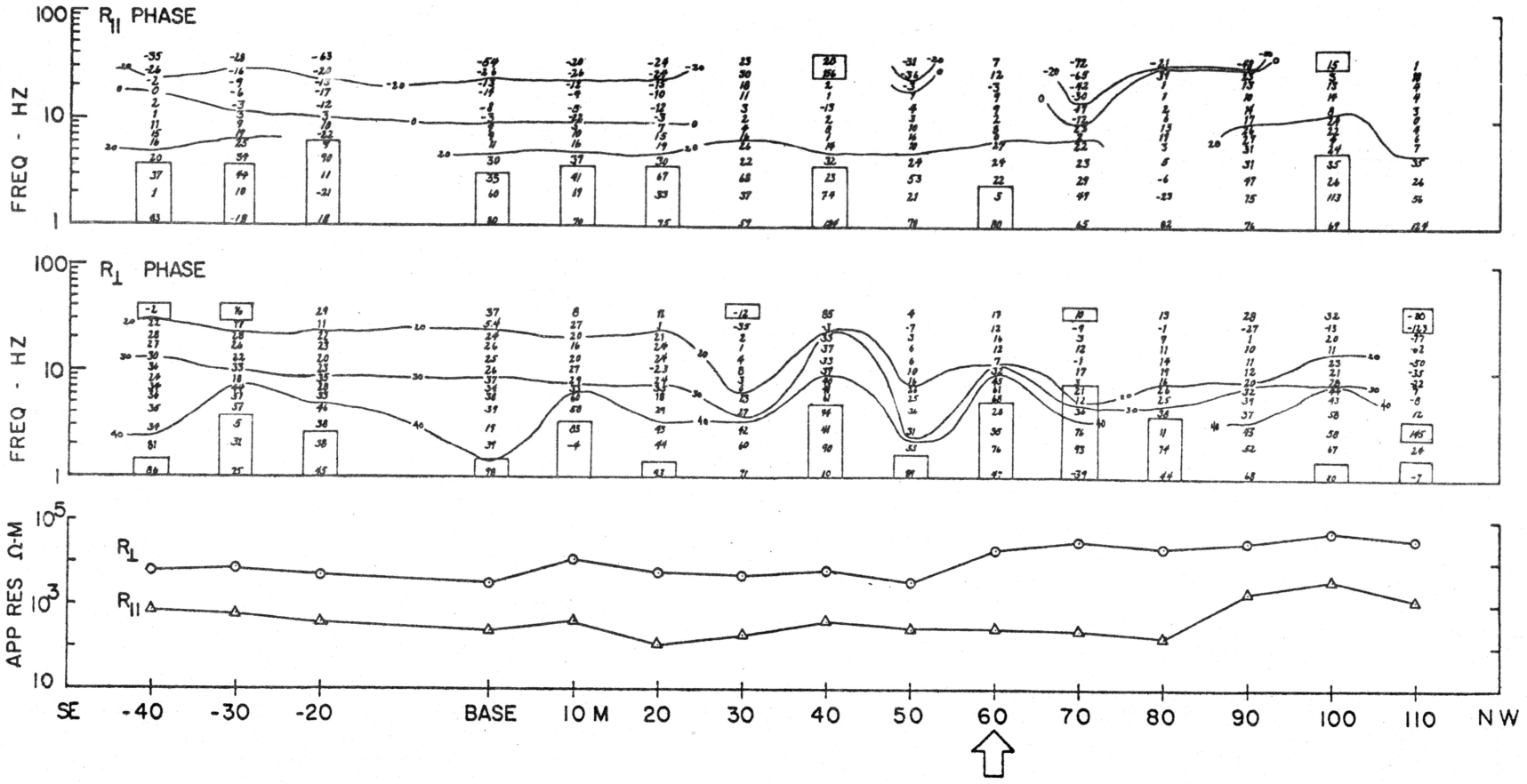

Figure 8.2.2.3. Minesite detailed Traverse 2 at 10 meter station spacing across mine section 414. line number 800W, Figure 8.2.4. Data from bottom to top are same as in previous figure.

Parallel traverses 1 and 2, Figures 8.2.2.2 and 8.2.2.3, are scalar apparent resistivity and phase taken with the coils stationary at the base and the electrode pairs moved along the traverse.

Traverse 1 is the same line as Schwenk's, 1976, AMT profile. His data from 14 to 20,000 Hz all show two low resistivity stations over the conductor in the center of the profile. Schwenk's electrode pair extended due east; and his coil was north-south. His results should be intermediate between my R-perpendicular and R-parallel; they are for 13 of his 16 data. My R-parallel apparent resistivity data are highest at the southeast end of Traverse 1, four of the five stations are above 10^3 ohm meters. The three stations at the northwest end have R-parallel apparent resistivities between 10^2 and 10^3 ohm meters, and the two stations nearest the conductor at 40 and 50 meters have values between 10 and 100 ohm meters. All R-perpendicular values are between 10^4 and 10^5 ohm-meters except for the two nearest the conductor at 40 and 50 meters, these two data are between 10^3 and 10^4 ohm-meters. I could not take data at 30 and 50 meters because there was heavy underbrush. The R-perpendicular data at 90 meters were rejected because of scalar coherency below 0.1.

The phases, once again, are generally decreasing with increasing frequency; the R-parallel phases have some negative values and are generally lower than R-perpendicular. For R-parallel, the station at 50 meters has higher phases than the adjacent stations, and also has the lowest apparent resistivity. The R-parallel phases for stations northwest of the central conductor are below zero at mid frequencies.

The R-parallel phases show an abrupt change over the conductor, and some distortion from station to station which must be due to local geologic changes. The R-perpendicular phase shows little, if any, change over the central conductor, but is apparently affected by other local inhomogeneities at the base station and at 100 meters.

There was no noticeable enhancement of the H-perpendicular/H-parallel ratio for the minesite, as observed in the Washington township data.

Traverse 2, Figure 8.2.2.3, is parallel to Traverse 1 and is displaced about 302 meters (1000 feet) northwest along mine section 414, line number 800 W, Figure 8.2.4. The R-parallel apparent resistivities are all less than R-perpendicular. No values are as low as they were in minesite Traverse 1; that is, below ten ohm-meters, but 12 of the 15 stations have resistivities between 100 and 1000 ohm meters. These higher values suggest that the conductor is more deeply buried here. There is no localized low over the axis of the conductor at 60 meters as there was in Traverse 1. Both R-parallel and R-perpendicular have higher values at the northwest end of the profile; the six northwest-most R-perpendicular data are all greater than 10,000 ohm-meters. The three most northwest R-parallel data are greater than 1000 ohm-meters. This asymmetry agrees with the nearby d.c. resistivity data along survey line 600, mine section 416, Figure 8.2.4, which shows higher values northwest of the conductor.

The phases, are generally decreasing with increasing frequency, with the R-parallel being generally lower than R-perpendicular. R-perpendicular contours bend over stations 30, 40, 50, and 60. Here, near the conductor, the phases become more positive than elsewhere. There are only 5 negative R-perpendicular phase data at these four stations, compared with 25 negative data at stations -10, 10, 20, and 30. The furthest R-perpendicular stations at 110 meters have phases inconsistant with the other stations.

The minesite R-max rotation directions are shown in Figure 8.2.2.1a. R-max is aligned perpendicular to the conductor at most sites but has scattered orientations at sites 6, 4A and 4B. Site 1, 40 meters southwest of the conductor, shows much more scatter than adjacent stations. I suspect that Site 1 data are of poor quality, but was not able to determine why. Site 5A rotations, not shown, had erratic orientations and high skew. It is physically unrealistic to expect the orientations to change as abruptly as they did. I have rejected Site 5A rotated tensor data from Figure 8.2.2.1 as obviously bad data.

R-max orientations perpendicular to the conductor agree with model resistivities over a narrow conductor in Section 3.3, that is, R-perpendicular is always greater than R-parallel. The scatter in R-max agrees with the arguments in Section 7.1: stations 2, 3, and 5B near the conductor show small scatter, stations 4A and 6 show a large amount of scatter, station 4B is intermediate between 3 and 4A.

The transition to highly scattered orientations occurs somewhere beyond 500 meters from the central conductor.

While conducting the fieldwork, I could tell which direction was going to be R-max by noting which electric channel needed the most attenuation for proper recording levels. This experience suggests that rotation directions could be determined in the field, and ratio of R-max to R-min determined by an analysis of these two data channels, using either analog or digital apparatus to rectify and integrate the signals.

8.2.3 Two-dimensional model

The two-dimensional model for the minesite is given in Figure 8.2.2.1h. The host rock structure is from Schwenk's dipole-dipole data and my layered models. The shape and resistivity of the 1.5 ohm-meter conductor and the 70 ohm-meter disseminated zone, approximated here by staggered rectangles, were determined by drill hole data (including a resistivity log), Schwenk, 1976, and May, 1976. The 1000 ohm-meter body around the conductor improves the fit with the data, and agrees with Schwenk's resistivity data which show high resistivities, up to 762 ohm-meters, on the northwest side of the conductor. This body causes R-perpendicular to be high within 100 meters northwest and to be relatively flat within 100 meters southeast of the conductor. Without this body, R-perpendicular would have a sharp low over the conductor, as in Figure 3.3.2.

The model contains another conductor and 1000 ohm-meter body to the southwest to satisfy the low apparent resistivity of site 5B R-parallel and the high resistivity at 5B and 5A R-perpendicular.

Data and model on Figure 8.2.2.1b illustrate the fit to the general shape of R-perpendicular and R-parallel apparent resistivities near the central anomaly. There are a few erratic data that do not match the model: high R-max and R-min at 4B and some R-parallel points to the immediate northwest of the conductor. The R-perpendicular model phases are generally similar to the data over the southwest end of the profile, but the R-parallel model phases do not fit the data very well except over the central anomaly where both model and data from Traverses 1 and 2 have negative phases. It may be that with a finer grid and considerable patience I could match these points as well, or it may be that the structures are too complicated to be modeled in two dimensions. It is not reasonable to attempt to match the phase data in cases where they can not be contoured from station to station: such data are probably dominated by geologic noise, structures too detailed or too small to be resolved by my measurements.

8.3 Fireside Lakes Reconnaissance

The site map for the Fireside Lakes area is shown in Figure 8.3.1. The bedrock in the central and northwestern parts of the map is known to be granite and rhyolite, determined by drill holes 202, 204, 205, 207 and 208, Figure 8.3.1 and Table 8.3.1, Hotchkiss and Bean, 1929. P.M. Wright of Kennecott Exploration said that there is an INPUT anomaly in the area, the approximate location is marked

Figure 8.3.1. Fireside Lakes station locations map. Heavy line between stations 4 and 5 is approximate location of INPUT anomaly. Open circles are drill holes, from Hotchkiss and Bean, 1929, discussed in text. KC is approximate location of a Kennecott Exploration hole drilled to investigate anomaly. Background map is USGS map of Fireside Lakes, Wisconsin quadrangle.

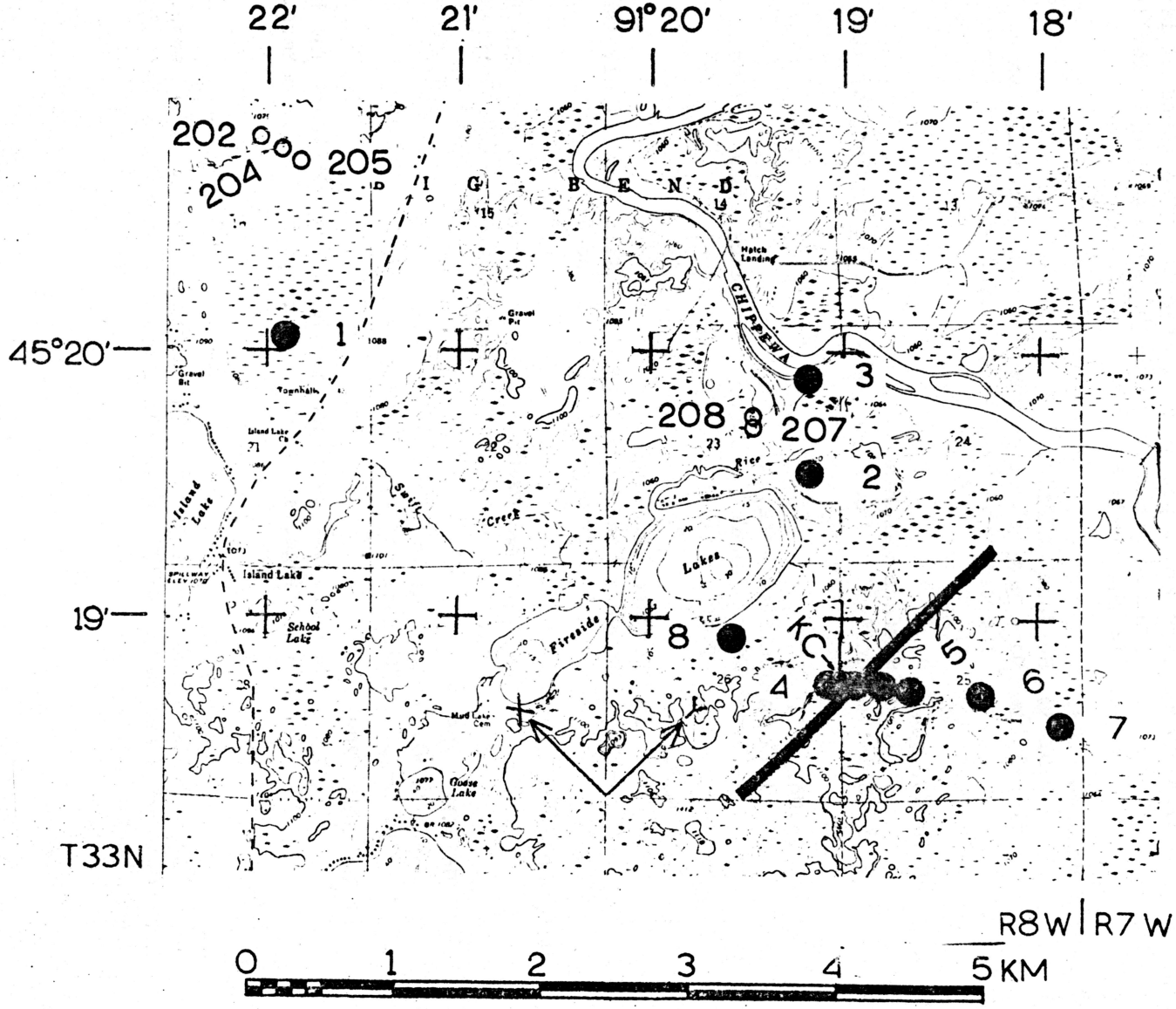
22'
21'
91°20'
19'
18'
45°20'
19'
T33N
R8W
R7W
202
204
205
208
207
1
2
3
4
5
6
7
8
KC
BEND
CHIPPEWA
Island Lake
Island Lake
School Lake
Fireside
Lakes
Rice
Creek
Hatch Landing
Gravel Pit
Mud Lake Cem
Goose Lake
0 1 2 3 4 5 KM

Hole No. 202.	
0-47.9m	Surface material.
47.9-50.3m	Dark gray, porphyritic rhyolite with abundant fine grained magnetite. Rough banding steeply inclined to the surface.
Hole No. 203.	
0-51.8m	Surface material.
51.8-53.3m	Dark gray rhyolite without doubt from the same formation as that encountered at 47.8m in hole No. 202.
Hole No. 204.	
0-51.8m	Surface material.
51.8-56.4m	Gneissic pink rhyolite with original porphyritic texture.
Hole No. 205.	
0-43.5m	Surface material.
43.5-47.3m	Finely banded dark gray to black, fine grained porphyritic rhyolite.
Hole No. 206.	
0-43.5m	Surface material.
43.5-59.4m	Roughly banded dark gray rhyolite very likely the same as that from holes No. 202 and 203.
Hole No. 207.	
	No core was examined in the Survey Office. The hole was ledged in granite at a depth of 33.5 meters.
Hole No. 208.	
0-30.1m	Surface material.
30.1-33.5m	Disintegrated pink granite.
Hole No. 209.	
	No core was examined in the Survey Office. The hole was ledged in granite at a depth of 31.7 meters.

Table 8.3.1. Drill hole and core data from Fireside Lakes area, from Hotchkiss and Bean, 1929. Hole locations are plotted on map of Figure 8.3.1.

by the heavy bar in Figure 8.3.1. The conductor was also detected by turam, drilled and found to be another graphitic schist.

I intended to make less detailed measurements here than at the other field areas, intending to obtain data sufficient only to determine the presence or absence of a conductive zone. My data are not dense enough to model the variations in two dimensions. I analyzed the data with MAGTEL, and present scalar resistivities as shown in Figure 8.3.2. At each station, R-parallel is lower than R-perpendicular. Stations 4, 5, 6, and 8, to the northwest over the granite and rhyolite intrusives, generally have the highest resistivities, above 1000 ohm-meters. Stations 4, 5, and 6, spanning 700 meters, are nearest to the reported INPUT anomaly. These stations have the lowest apparent resistivity values, 9 to 80 ohm-meters for R-parallel and 100 to 200 ohm-meters for R-perpendicular. R-parallel for station 4 and its three auxiliary telluric current stations shows low coherency, 0.2 to 0.4. With the exception of R-perpendicular at Site 8, noted on Figure 8.3.2, the other coherencies range from .57 to .77.

The E E-predicted coherencies for site 4 are above .5 so I know the low scalar coherency is not just due to low signal power. The remaining MAGTEL output for site 4 shows that there is coherency above 0.5 between E-parallel and H-parallel signal pairs, suggesting that locally the electric currents induced by H-parallel are diverted to run in the E-parallel direction rather than the E-perpendicular direction. This means that either (1) the apparatus is not aligned with the structure, or (2) the earth here cannot be thought of as two-

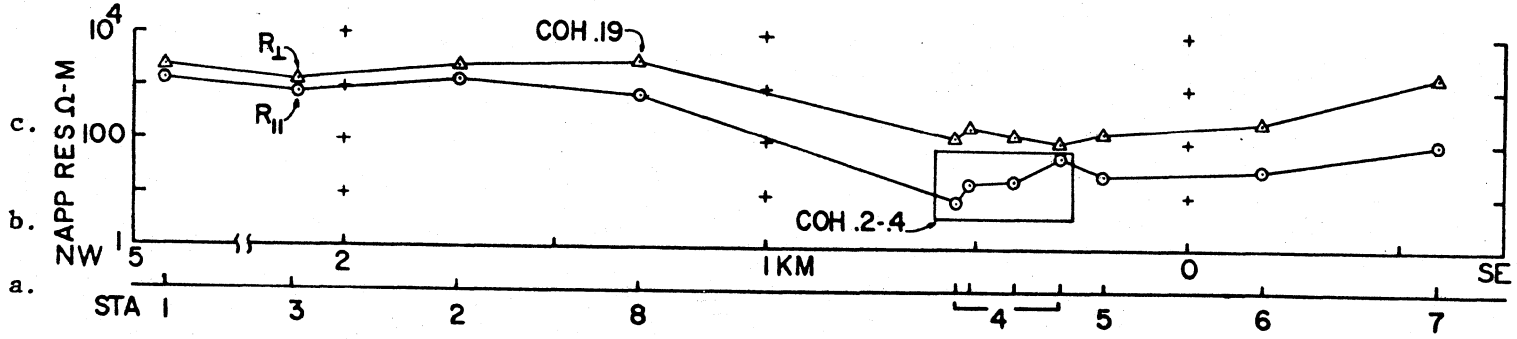

Figure 8.3.2. Fireside Lakes data profile. Stations projected to northwest-southeast line. Airborne EM anomaly is perpendicular to profile, approximately under station 4. From bottom to top:

a. station numbers and location. At station 4, northwest, left most mark is base station, others are remote telluric stations.

b. scale in kilometers.

c. scalar apparent resistivity data. R-perpendicular are triangles, R-parallel are circles.

dimensional. A similar phenomenon of losing coherence when working over a conductor is reported by Slankis, Telford and Becker, 1972, for their telluric current work at 8 Hz.

The Fireside Lakes data show that the magnetotelluric technique in this frequency range is sufficient to determine the presence or absence of conductors; however, I might have missed other conductors where my station spacing was large. For practical mapping it would probably be necessary to make measurements as close together as 200 to 500 meters.

8.4 Comparison of Scalar Resistivity, Tensor Resistivity and Rotated Tensor Resistivity for Washington Township Site 7

Here I compare scalar, tensor and rotated tensor resistivities and phases for a single site to see if they are all approximately equal for measurements taken when the apparatus was aligned with the known structure. This comparison is important for two practical reasons. First, in case one channel fails at a site, I would like to be able to use the scalar apparent resistivity calculated from the good E - H signal pair to compare with tensor resistivities at adjacent sites.

Second, I would like to use the scalar results for my detailed traverses over the minesite, saving the cost of computing the rotated tensor resistivities for these 25 stations.

The equations in the text defining the apparent resistivities discussed and tabulated are:

1. Scalar resistivity R_X and R_Y Equations 4.2.2, 4.2.3, and 4.2.4

2. Unrotated tensor resistivities R^{E}_{XY}, R^{H}_{XY}, R^{E}_{YX} and R^{H}_{YX}. Equations 4.1.8, 4.1.9, 4.1.13, and 4.1.11

3. Rotated tensor resistivities Equations 3.4.1 and 3.4.2.

As an example I present tabulated data summary, Tables 8.4.1 and 8.4.2, from Washington township site 7, Figure 8.1.1, located approximately 700 meters southeast of INPUT anomaly 39. The measurement axes were aligned so that the X-axis was perpendicular to the conductor, northwest, and the Y-axis was parallel to the conductor, northeast. These data have coherencies higher than 0.6 for 17 of the 24 orthogonal E-H data. The E E-predicted coherencies, defined in Equation 4.3.2, are mostly above 0.6.

Table 8.4.1a gives scalar resistivities R_X (R-perpendicular), tensor resistivities R^{E}_{XY} and R^{H}_{XY}, rotated tensor resistivity R-max (oriented approximately perpendicular, to the INPUT anomaly) for my eleven frequency bands. The table also lists angles of rotation for R-max and the variance of R-max, computed according to Bentley, 1971. The unrotated axes are northwest (315°). The table shows that the scalar resistivity values R_X are within one standard deviation of R-max.

Table 8.4.1b gives the phases of quantities above. The tensor phases for R^{H}_{XY}, R^{E}_{XY} and R-max all agree within one standard deviation. The scalar phases for R-X are higher than the tensor phases by five to ten degrees. R-max rotations range from 1 to -21 degrees.

Table 8.4.2 gives the same information for R_Y (R-parallel), R^{E}_{YX}, R^{H}_{XY} and R-min. R-min agrees with the scalar resistivity to within about one-fourth of one standard deviation. Nineteen of the

a. RESISTIVITIES

Frequency (Hz)	R_X ohm-m	R^H_{XY} ohm-m	R^E_{XY} ohm-m	R-max orientation	R-max ohm-m	Variance of R-max ohm-m
1	$.49 \times 10^4$	$.21 \times 10^4$	2.3×10^4	-17.°	$.8 \times 10^4$	$.5 \times 10^4$
2	.89	.37	2.7	-16.	1.1	.6
3	.12	.62	3.2	-21.	1.7	.8
4.5	.56	.62	1.7	-21.	1.2	.37
6.5	.95	.96	1.7	-14.	1.4	.30
8.5	1.3	1.4	1.9	-14.	1.7	.27
11.	1.2	1.4	1.9	-14.	1.8	.29
14.	.98	1.1	1.4	-14.	1.4	.20
17.5	1.0	.94	1.3	- 8.	1.1	.17
23.	.90	.61	1.2	- 3.	.89	.22
32.	.51	.21	1.3	1.	.53	.32

b. PHASES

Frequency (Hz)					
1	60.°	52.°	52.°	49.°	18.°
2	62.	55.	56.	52.	15.
3	47.	41.	41.	39.	12.
4.5	60.	45.	44.	36.	8.
6.5	43.	36.	36.	33.	6.
8.5	40.	28.	28.	25.	4.
11.	33.	22.	22.	18.	4.
14.	29.	17.	17.	13.	3.
17.5	29.	20.	20.	18.	3.
23.	29.	24.	21.	22.	5.
32.	24.	23.	18.	21.	10.

Table 8.4.1, Site 7. a. data frequency, are scalar R-perpendicular, (R_X), unrotated R^H and R^E R-parallel tensor resistivities (R^H_{XY} and R^E_{XY}), rotation angles, rotated tensor R-max resistivities and variances. b. phases of top table resistivities. Apparent resistivities in ohm-meters, phases in degrees, rotation in degrees clockwise from northwest (315°).

a. RESISTIVITIES

Frequency (Hz)	R_Y (scalar) ohm-m	R^H_{YX} ohm-m	R^E_{XY} ohm-m	R-max orientation	R-min ohm-m	Variance of R-min ohm-m
1	2.5×10^2	1.2×10^2	$10. \times 10^2$	73.°	2.2×10^2	4.1×10^2
2	5.9	3.1	13.	75.	4.4	5.4
3	9.4	7.6	16.	69.	3.7	6.0
4.5	5.7	6.2	13.	69.	3.5	3.7
6.5	4.3	5.1	7.2	76.	3.2	2.2
8.5	5.1	6.7	7.9	76.	4.3	2.1
11.	4.3	6.7	9.0	76.	4.8	2.7
14.	4.0	5.3	6.8	76.	4.6	2.0
17.5	3.0	4.0	5.6	82.	3.9	1.4
23.	2.8	3.0	5.4	87.	3.9	1.2
32.	1.6	4.6	4.1	-90.	1.6	1.2

b. PHASES

Frequency (Hz)					(Θ-180)	
1	-106.°	-115.°	-118.°	85.°	(-95°)	53.°
2	-126.	-130.	-131.	69.	(-111)	35.
3	-145.	-145.	-146.	47.	(-133)	46.
4.5	-154.	-159.	-159.	57.	(-123)	34.
6.5	-153.	-160.	-161.	35.	(-145)	19.
8.5	-162.	-164.	-165.	35.	(-145)	14.
11.	-158.	-167.	-167.	34.	(-146)	15.
14.	-154.	-166.	-167.	35.	(-145)	12.
17.5	-163.	-171.	-171.	20.	(-160)	9.
23.	-157.	-165.	-166.	18.	(-162)	7.
32.	-161.	-166.	-165.	14.	(-166)	10.

Table 8.4.2, Site 7. a. frequency, scalar R-parallel, (R_Y), unrotated R^H and R^E R-perpendicular tensor resistivities (R^H_{YX} and R^E_{XY}), rotation angles, rotated tensor R-min resistivities and variances. b. phases of top table resistivities. Same units as table 8.4.1

twenty-two unrotated tensor resistivities R^{E}_{YX} and R^{H}_{YX} are higher than the rotated values. The rotated phases for R-min are generally higher than unrotated tensor and scalar phases.

I conclude that scalar apparent resistivities and phases are approximately equal to rotated tensor apparent resistivities and phases for measurements that were taken with the apparatus aligned with structure.

8.5 Physical Rotation of Coordinates Compared to Mathematical Rotation

An assumption implicit in magnetotelluric work has been that the mathematical rotation of coordinates is equivalent to physical rotation of the apparatus. In order to verify this assumption I carried out tests at minesite station 3, about 200 meters northwest of the ore deposit. Figure 8.5.1 gives the orientations of R-max and the values of R-max and R-min at site 3 with the apparatus rotated 0, 30, 60, and 90 degrees and again at zero degrees. The data are tabulated in the data summary volume. Out of the five data sets, the 30, 60, and 90 degree rotations give the orientations of R-max at a compass heading of about 290 degrees, the last zero degree roation gives an orientation of about 270 degrees and the first zero degree orientation gives an inconsistent orientation of about 45 degrees. Three of the five R-max values are nearly equal to each other at 3.6, 3.5, and 3.6 x 10^4 ohm-meters. The other two R-max values are lower at 2.9 and 2.8 x 10^4 ohm-meters. The R-min values run from 1600 to 3800 ohm-meters. The R-max and the R-min resistivities for the five trials agree with each other within one

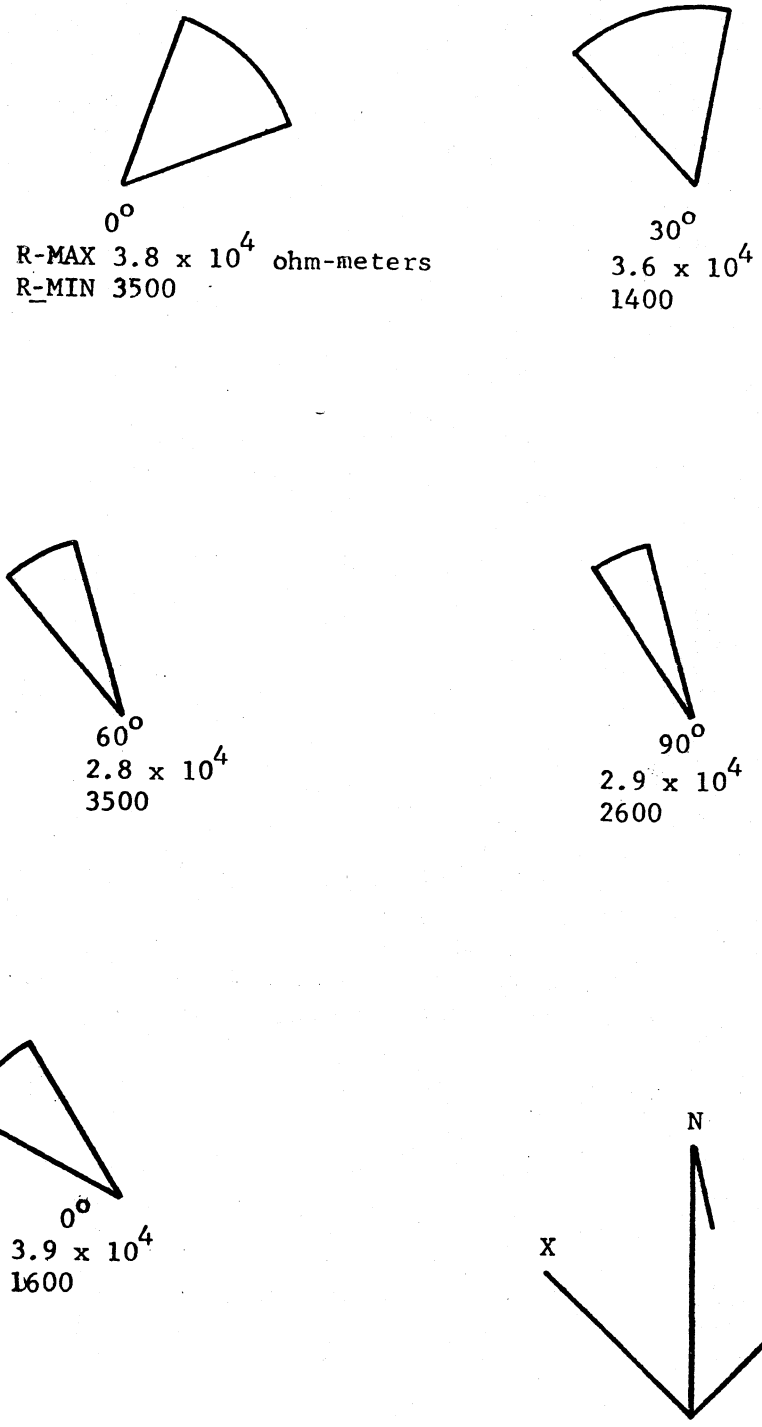

Figure 8.5.1. R-max orientations, R-max and R-min values for site 3 with apparatus rotated 0°, 30°, 60°, 90° and 0° (repeat run) from normal. Sector encloses orientation vectors of frequencies from 1 to 35 Hz. Rotation is clockwise from normal orientation of X axis positive northwest Y axis positive northeast. The nearby conductor is parallel to the Y axis.

standard deviation.

This test illustrates that mathematical rotation is equivalent to physical rotation of the axes. Out of the five trials, 4 orientations agree with each other. I am not able to account for the misalignment of the fifth trial.

Chapter 9. Conclusion

I have designed and constructed equipment for detection and recording of magnetotelluric signals at 1 to 35 Hz, and have established equipment sensitivity and noise level requirements for satisfactory operation.

I have used this equipment to acquire dense data of good quality over targets of scientific and economic interest. The data show that one must be much closer than one skin depth (=25 kilometers) to detect the presence of conductors. The practical detection limit is 100 to 300 meters.

The sounding data show three layers in the depth range 0.1 to 40 kilometers. This layering is in basic agreement with Sternberg and Clay, 1977, and Dowling, 1970, Figure 6.2.1. For most sites there was a difference between the models matching apparent resistivity and phase data, indicating that the earth is more complicated than can be expressed by flat layers.

The detailed data over the central anomalies taken with station spacing as small as ten meters enabled me to construct two-dimensional models. At the minesite and at Washington township, I observed negative phase values at high frequencies for R-parallel near the anomaly. Negative phases, never seen in flat-layered models, can be seen on the model R-parallel results as well, although there is disagreement between model and data as to the spectral and spatial distribution of the negative phases.

In addition to being able to calculate rotated tensor resistivities, the use of simultaneous H_X and H_Y measurements made it

possible to observe the anomalous behavior of H-perpendicular/H-parallel, the ratio of magnetic fields perpendicular and parallel to the structure. I calculated these ratios for each station on my traverse over the graphitic schist and found that they rose from a normal value of unity at distance to about seven for the station nearest the anomaly. Compared to the model that matched resistivities, a model to match these data required a conductor of smaller cross-section buried at a shallower depth. The minesite measurements did not exhibit anomalous behavior of H-perpendicular/H-parallel.

All the models are sensitive to the resistivity and thickness of the top layer. One can see how variable this layer is from Schwenk's dipole-dipole resistivity data in Figure 8.2.1.4, which is typical of his four pseudosections within 5 kilometers of the minesite. The profiles show fluctuations of near-surface resistivity; the shortest transmitter to receiver separations typically show apparent resistivities from 100 to 300 ohm meters. It would be very useful to know these near surface resistivities for interpretation of MT results. These resistivities could be found either with d.c. resistivity or by using MT with continuous wave signal sources such as the navigation stations broadcasting between 10 and 200 KHz. Assuming a top layer of 250 ohm-meter resistivity, these frequencies would give skin depths of 7.9 to 17.6 meters, which would be appropriate for near surface studies. Gineau, 1975, gives examples of survey techniques using these signal sources.

I conclude that magnetotellurics in this frequency range provides an effective tool for followup exploration of airborne electromagnetic work, for sounding into the crust and for indicating broad zones of anomalous conductivity. My field measurements show that I could not detect conductors from as far away as simple two-dimensional models would suggest, say at a distance of one skin depth. For the sort of geologic structure that I was working over, it appears that the response of a long narrow conductor such as the graphitic schist is masked at distances greater than about 1/10 of a skin depth by other inhomogeneities which may or may not be detected on the airborne e.m. This result leads to the recommendation that when using magnetotellurics for ground reconnaissance conductive zones, the stations should be dense, say every 200 to 500 meters. Whereas in the past, others have had to restrict themselves to a single frequency and calculate only scalar resistivities for this sort of survey, for example the 8 Hz work of Slankis, Becker and Telford, 1972, the current rapid growth of microprocessor-based instrumentation systems may make it possible to do broad-band magnetotelluric field work and obtain on-site spectral analysis, coherency, resistivity and phase.

Bibliography

References

Anderson, G. C., Finnie, B. W., Roberts, G. T., 1967, Pseudo-random and random test signals: Hewlett Packard Journal, September, p. 1-20.

Bannister, P. R., 1969, Source distance dependence of the surface-impedance conductivity measurement technique: Geophysics, v. 34, n. 5, p. 785-788.

Bentley, C. R., 1973, Error estimation in two-dimensional magneto-telluric analysis: Physics of the Earth and Planetary Interiors, v. 7, p. 423-430.

Berdichevskiy, M. N., 1965, Electrical prospecting with the telluric current method: Trans. Keller, G.; Quarterly of the Colorado School of Mines, v. 60, n. 1, p. 1-216.

Clerc, G., 1970, Prospection magnéto-tellurique superficielle à partir des variations électromagnetique de frequencies comprises entre 8 Hz, et 16 KHz: C.R. Acad. Sc. Paris, v. 270, Serie B, p. 645-648.

Dowling, F. L., 1968, A magnetotelluric investigation of the crust and upper mantle across the Wisconsin Arch. Ph.D. Thesis, University of Wisconsin, Madison.

Dowling, F., 1970, Magnetotelluric measurements across the Wisconsin Arch: J. of Geophys. Res., v. 75, n. 14, p. 2683-2698.

Dutton, C., and Bradley, R., 1970. Lithological, geophysical, and mineral commodity maps of pre-Cambrian rocks in Wisconsin: USGS, Misc. Geological Investigations, Map I-631.

Gineau, B., 1975, Exemples d'application de la méthode magnéto-tellurique de prospection géophysique à l'étude de structures ou de formation, géologiques situées sous un très faible recouvrement: Geophysical Prospecting, v. 23, p. 104-124.

Great Lakes Exploration Company Inc., 1972, Report to Owens Illinois, Inc. on mineral exploration performed on Owens Illinois land in T33N R7W Rusk County, Wisconsin. On file at Wisconsin State Geological and Natural History Survey, 1815 University Avenue, Madison, Wisconsin.

Grosskopf, B. M., Bostick, F. X., and Smith, H. W., 1974, Determination of electric dipole patterns using audio magnetotelluric techniques: Electrical Geoscience Laboratory, University of Texas at Austin.

Hermance, J. F., and Thayer, R. E., 1975, The telluric-magnetotelluric method: Geophysics, v. 40, n. 4, p. 664-668.

Hill, L. K., and Bostick, F. X., Jr., 1962, Micropulsation sensors with laminated mumetal cores: The University of Texas Electrical Engineering Res. Lab., Report 126, 25 May, 1962, 84 pp.

Hoover, D. B., and Long, C. L., 1975, Audio magnetotelluric methods in reconnaissance geothermal exploration, in U.N. symp. on dev. and use of geothermal resources, U.S. Govt. Pr. Off., p. 1059-1064.

Hotchkiss, W. O., and Bean, E. F., 1929, Mineral lands of part of northern Wisconsin: Wisconsin Geological and Natural History Survey, Bulletin n. 46, economic series n. 21, State of Wisconsin, 212 pp.

Kan, Tze-Kong, 1975, Ray theory approximation in geoelectric probing: Ph.D. Thesis, University of Wisconsin, Madison.

Jones, F. W., and Pascoe, L. J., 1971, A general computer program to determine the perturbation of alternating electric currents in a two-dimensional model of a region of uniform conductivity with an embedded inhomogeneity: Geophysical J. Roy. Ast. Soc., v. 24, p. 3-30.

Keller, G. V., and Frischknecht, F. C., 1966, Electrical Methods in Geophysical Prospecting: Pergamon Press, New York, 517 pp.

Kurtz, R. D., and Garland, G. D., 1976, Magnetotelluric measurements in eastern Canada: Geophysical J. Roy. Astr. Soc., v. 45, p. 321-347.

Lepley, L. K., and Adams, W. M., 1966, Audio-magnetotellurics: unpublished manuscript, University of Hawaii, 15 pp.

Madden, T., 1963, Cross spectral and bispectral analysis of low frequency electromagnetic data: technical report, Geophysics Laboratory, Massachusetts Institute of Technology, Cambridge, Mass. Project NR - 371-402, Office of Naval Research, 44 pp.

Madden, T., and Thompson, W., 1965, Low-frequency oscillations of the earth-ionosphere cavity: Rev. Geoph. v. 3, n. 2, May, p. 211-254.

Maxwell, E. L., 1966, Atmospheric noise from 20 Hz to 30 KHz: DECO Electronics, Inc., Boulder, Colorado, 39 pp.

May, E. R., 1976, Flambeau, a pre-Cambrian supergene enriched massive sulfide deposit: AIME preprint number 76-I-55, 30 pp.

Pascoe, L. J., and Jones, F. W., 1972, Boundary conditions and calculation of surface values for the general two-dimensional electromagnetic induction problem: Geophys. J. Roy. Astr. Soc., v. 27, p. 179-193.

Schlumberger, M., 1939, The application of telluric currents to surface prospecting: Trans. Am. Geophys. Union, v. 20, p. 271-277.

Schwenk, C. G., 1976, Discovery of the Flambeau deposit, Wisconsin, a geophysical case history, AIME preprint number 76-I-63, 30 pp.

Sims, P. K., 1976, Pre-Cambrian tectonics and mineral deposits, Lake Superior region: Econ. Geology, v. 71, p. 1092-1118.

Sims, W. E., 1960, Methods of magnetotelluric analysis: Ph.D. Thesis, University of Texas at Austin, 86 pp.

Slankis, J. A., and Becker, A., 1969, Telluric and magnetotelluric measurements at 8 Hz: Trans. Soc. Mining Engineers, AIME, v. 244, p. 237-244.

Slankis, J. A., Telford, W. M., and Becker, A., 1972, 8 Hz telluric and magnetotelluric prospecting: Geophysics, v. 37, n. 5, p. 862-878.

Sternberg, B. K., and Clay, C. S., 1977, Flambeau anomaly, a high-conductivity anomaly in the southern extension of the Canadian Shield: in AGU Monogr. 20, in press.

Sternberg, B. K., 1977, Electrical resistivity structure of the crust in the southern extension of the Canadian Shield: Ph.D. Thesis, University of Wisconsin, Madison.

Strangway, D. W., Swift, C. M., and Holmer, R., 1973, The application of audio-frequency magnetotellurics (AMT) to mineral exploration: Geophysics, v. 38, n. 6, p. 1159-1175.

Strangway, D. W., and Vozoff, K., 1967, Mining exploration with natural electromagnetic fields, in mining and groundwater geophysics, 1967: Geological Soc. of Canada, Economic Geology Report n. 26, Ottawa, p. 109-122.

Swift, C. M., 1967, A magnetotelluric investigation of an electrical conductivity anomaly in the southwestern United States: Ph.D. dissertation, Massachusetts Institute of Technology, 211 pp.

Swift, C. M., 1971, Theoretical magnetotelluric and turam response from two-dimensional inhomogeneities: Geophysics, v. 36, n. 1, p. 38-52.

Vozoff, K., 1972, The magnetotelluric method in the exploration of sedimentary basins: Geophysics, v. 37, n. 1, p. 98-141.

Ward, S. H., Ryu, J., Glenn, W. E., Hohmann, G. W., Dey, A., and Smith, B. D., 1974, Electromagnetic methods in conductive terrains: Geoexploration, v. 12, p. 121-183.

Word, D. R., Smith, H. W., and Bostick, F. X., 1970, An investigation of the magnetotelluric tensor impedance method: Technical report, Electrical Geophysics Research Laboratory, University of Texas at Austin, 264 pp.

Yungul, S. H., 1966, Telluric sounding, a magnetotelluric method without magnetic measurements: Geophysics, v. 31, n. 1, p. 185-191.

References for General Reading

Becker, A., 1967a, Design formulas for electromagnetic sensing coils: Geoexploration, v. 5, p. 81-88.

Becker, A., and Flint, T. R., 1967b, A portable microvoltmeter for the measurement of 8 c/s telluric currents; inhouse document, EEMTIC 67, 2-3, Geological Survey of Canada, 37 pp.

Bliel, D. E., (editor), 1964, Natural Electromagnetic Phenomena Below 30 Kc/s: Plenum Press, New York, 470 pp.

Cormy, G., and Muse, L., 1975, Utilization of MT-5-EX in geothermal exploration, in Proc 2nd. U.N. symp. on dev. and use of geothermal resources, U.S. Govt. Pr. Off., p. 933-935.

DECO Electronics Inc., 1963, Resistivity measurements by the audio-magnetotelluric method, Report 30-5-2, for Office of Naval Research, 36 pp.

Department of Natural Resources, State of Wisconsin, 1976, Environmental Impact Statement for the Flambeau Mining Corporation proposed copper mine, Rusk County, Wisconsin, 201 pp.

d'Erceville, L., and Kunetz, G., 1962, The effect of a fault on the earth's natural electromagnetic field: Geophysics, v. 37, n. 5, p. 651-665.

Grillot, L. R., 1975, Calculation of the magnetotelluric tensor impedance: analysis of band-limited MT signal pairs: Geophysics, v. 40, n. 5, p. 790-797.

Hotchkiss, W. O., 1915, Mineral land classification: Wisconsin Geological and Natural History Survey, Bulletin n. 44, Economic Series n. 19, State of Wisconsin, 378 pp.

Kunetz, G., 1972, Processing and interpretation of magnetotelluric soundings: Geophysics, v. 37, n. 6, Dec., p. 1005-1021.

Muse, L., 1973, A five-component magnetotelluric method in geothermal exploration; the MT-5-EX: Geothermics, v. 2, n. 2, June, p. 41-50.

Rankin, D., and Reddy, I. K., 1972, Effect of geoelectric structure on the polarization characteristics of geomagnetic micro-pulsations: J. Geophys. Res., v. 77, n. 7, pp. 1286-1291.

Reddy, I. K., and Rankin, D., 1971, Magnetotelluric measurements in central Alberta: Geophysics, v. 36, n. 4, p. 739-753.

Srivastava, S. P., 1967, Application of the magnetotelluric method to anisotropic and inhomogeneous bodies: Journal Geophys. Res., v. 68, n. 20, Oct. 15, p. 5857-5868.

Srivastava, S. P., 1965, Method of interpretation of magnetotelluric data when source field is considered: J. Geophys. Res., v. 70, n. 4, p. 945-954.

Sternberg, B. K., 1974, Controlled source electromagnetic soundings of the crust in northern Wisconsin. M.S. Thesis, University of Wisconsin, 50 pp.

Sternberg, B. K., 1975a, Compilation and interpretation of DC resistivity surveys in northern Wisconsin. Preliminary Technical Report, University of Wisconsin, Department of Geology and Geophysics, 15 pp.

Sternberg, B. K., 1975b, Surveys and models of electrical conductivity anomalies in Wisconsin: Trans., Am. Geophys. Union, (EOS), v. 56, n. 9, September (abstract), p. 604.

Trigg, D., 1972, An amplifier and filter system for telluric signals: Department of Energy, Mines and Resources, Ottawa, Canada, Pub., 5 pp.

Wait, J. R., and Spies, K. P., 1974, Magnetotelluric field for a segmented overburden: Technical report no. 7, Project No. NR-081-270, Dept. of the Navy, Office of Naval Research, Arlington, Va., 74 pp.

Ward, S. H., 1967, The electromagnetic method, in Hansen et al., eds.: Mining Geophysics, v. II, Theory, Society of Exploration Geophysicists, Tulsa, p. 224-372.

Appendix Computer Programs and Run Directions

Programs NUDIG, HANDY, CONVERT, MAGTEL and AVETEL, described here, are used to digitize analog MT data and determine scalar and rotated tensor resistivities according to Chapter 3 and 4.

NUDIG and HANDY run on the University of Wisconsin Geophysical Computing Facility Datacraft 6024 computer, performing digitizing and utility file handling, respectively. CONVERT, MAGTEL and AVETEL run on the Madison Academic Computer Center Univac 1110 computer. CONVERT rewrites the NUDIG output tapes in MAGTEL input tape format. MAGTEL performs frequency analysis, and computes scalar and unrotated tensor resistivities for each set of data. AVETEL averages several sets of data and calculates rotated tensor resistivities. MAGTEL and AVETEL are modified versions of programs developed by University of Wisconsin Geophysical and Polar Research Center personnel. The original program listings and run directions are on file in the archives of the University of Wisconsin, Madison, Geophysical and Polar Research Center.

A.1 NUDIG Description and Directions

The basic functions of NUDIG are to digitize four channels of analog data and to record the data on the upper tape deck, unit 14. In addition, after a preset length of record is digitized, the digitized data are displayed on the cathode ray tube (CRT), one block at a time.

The program communicates interactively with the operator by first printing:

MOVE PAST N EOF N = (I2)

The operator should respond by typing the appropriate one or two digit number. The end-of-tape mark is ten ends-of-file which are generated by the termination of the previous use of the digitizing program.

The next request is

ENTER LENGTH IN SECONDS, INTEGER

The response controls the number of blocks of data digitized. Each block is 600 words, 150 samples of each channel. The sample rate is controlled by an external oscillator which should be connected to the cable which normally goes to the phase-lock oscillator in the middle rack of equipment. The connector to which the cable usually goes is labelled "100 PPS". For digitizing AMT records the external oscillator runs at 128 Hz, which will be the digitizing rate. There is a 150 microsecond delay for each successive channel digitized.

NUDIG then requests:

ENTER UP TO 25 LINES FOR HEADER RECORD, FIN

The operator may type in any identifying information to be recorded ahead of the data. The last line should begin with "FIN". When the last line is entered by a carriage return, the digitizer begins operating. There are two other possible responses to the above request. No characters, just a carriage return, causes the program to re-ask "LENGTH IN SECONDS". A "NO" terminates the program.

In programs involving tapes files, one may write records, that is, blocks of data on tape or ends-of-file (EOF's) hardware-controlled marks used to mark the end of a group of records. When a data handling program "skip files" it counts forward on the tape for a given number of EOF's. This may or may not be the number of multiple-block records on the tape, depending on whether some records have extra EOF's at the end. In the case of the NUDIG output tape, there is an extra EOF at the tape beginning, so that to skip over, say, 20 data records, the program should be directed to skip 21 files (EOF's).

The tape format is as follows:

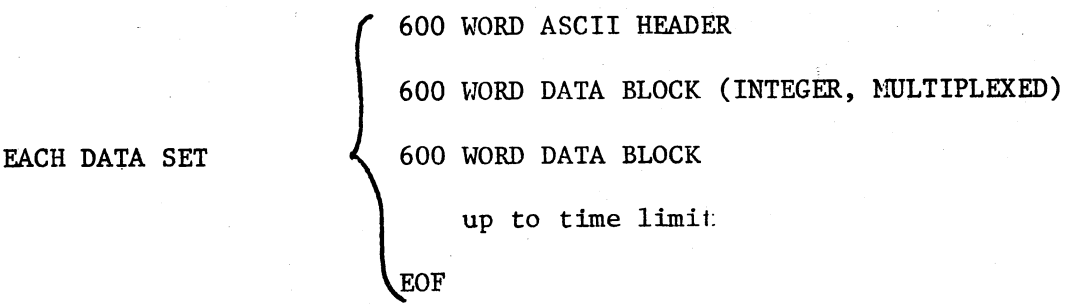

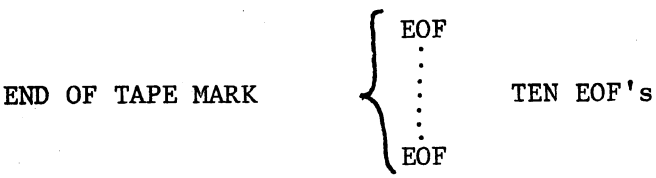

After each data set a double EOF is written. This happens before the playback-display routine, so if for some reason the program crashes, there is still a unique end of tape mark. The second EOF is then obliterated when another data set is digitized.

A count is kept of the number of files on the tape and listed on the TTY when the program terminates. Each header is also numbered on the TTY before the operator types in the information. After each data set, the tape rewinds to the beginning of the data just digitized and each block is displayed on the CRT. The display of recorded blocks is advanced by pushing switch 12 of the control box.

NUDIG was written to use a digitizer which has been replaced with a more modern unit. Before attempting to run NUDIG, the digitizing subroutines calls should be checked to determine whether they are obsolete. For future MT digitizing I recommend using program FLIGIT, written by the Geophysical Computing Facility staff. This program is kept up-to-date with the existing hardware and has useful options such as file editing and plotting. Program CONVERT would have to be rewritten to accommodate FLIGIT's output tapes.

A.1.1 NUDIG listing

```
$JOB CHUCK U82  D6
$OPTIONS ,21,8
$FORTRAN

  05-05-77                                                          PAGE     1
  61516-01 EXTENDED NON-SAU FORTRAN COMPILER   REVISION LEVEL 24.083076

 1:    C SUPER DIGITIZER
 2:    C PROGRAM NEW DIG REVIZED OCT 30 1974
 3:    C SET UP TO RUN ON DOS MAY 20,1976
 4:    C
 5:    C DIGITIZING PROGRAN 4- CHANNELS
 6:          COMMON/DATA/IX(600),IY(600),IZ(600)
 7:           INTEGER TIM
 8:          INTEGER OUT
 9:           DATA IN,OUT,JOUT/2,2,'14/
10:           DATA IFIN/3HFIN/
11:          DATA IGO/2HGO/
12:          DATA NO/2HNO/
13:          DATA IBLK/3H   /
14:    C
15:          CALL IC76
16:          OPEN '14
17:          REWIND '14
18:          CALL BUFMK(JOUT)
19:          DO 500 I=1,600
20:          IY(I)=0
21:          IX(I)=0
22:      500 CONTINUE
23:          WRITE(OUT,202)
24:    202   FORMAT(' MOVE PAST N EOF,  N=(I2)')
25:          READ(IN,102) IAL
26:      102 FORMAT(I2)
27:          JF=IAL+1
28:          IF (IAL.EQ.0) GO TO 44
29:          DO 3 I=1,IAL
30:        3 CALL BUFSF(JOUT)
31:       44 CONTINUE
32:          IF(IAL.LT.0) CALL SKIP(JOUT,3)
33:    199   CONTINUE
34:          WRITE(OUT,201)
35:      201 FORMAT(' ENTER LENGTH IN SECONDS,  INTEGER')
36:        5 READ(IN,101) TIM
37:          TIM=TIM*5/2
38:      101 FORMAT(I5)
39:        4 CONTINUE
40:          WRITE(OUT,200)
41:      200 FORMAT(' ENTER UP TO 25 LINES FOR HEADER RECORD,FIN')
42:          WRITE(OUT,205) JF
43:    205   FORMAT(' FILE ',I4)
44:          JMIN=1
45:        1 JMAX=JMIN+23
46:          READ(IN,100) (IY(J),J=JMIN,JMAX)
47:      100 FORMAT(24A3)
48:    C TYPING THREE BLANKS WILL ALLOW YOU TO RESPECIFY THE RECORD LENGTH
49:    C TYPE NO TO QUIT
50:          IF(IY(JMIN).EQ.IBLK) GO TO 199
51:          IF(IY(JMIN).EQ.NO) GO TO 351
52:          IF(IY(JMIN).EQ.IFIN) GO TO 2
```

```
53:           JMIN=JMAX+1
54:           GO TO 1
55:     C  NOTE - HEADER IS A 600 WORD BLOCK TOO
56:          2 BUFFEROUT(JOUT,IY,B,600,JSTAT)
57:           NTIM=TIM
58:           NSEC=3
59:     C
60:     C MINIMUM POSSIBLE LENGTH OF DIGITIZING IS TWO BUFFERS FULL
61:     C
62:       501 CALL STATUS(JOUT)
63:     C STATUS CHECTS THE TAPE TRANSPORT AND RETURNS A VALUE
64:     C 1,2, OR 3 WHICH MEANS BUSY,READT,ERROR, RESPECTFULY
65:           GO TO (501,502,503),JSTAT
66:       502 CONTINUE
67:           NCHAN=4
68:           KNN=600
69:           KPNT=KNN/NCHAN
70:           CALL INTER
71:           CALL DIGSET(NCHAN,KPNT,0,ISTAT)
72:           CALL DIGER(IY)
73:        21 CONTINUE
74:           GO TO (21,22,903,904),ISTAT
75:        22 CALL DIGER(IX)
76:        23 CALL STATUS(JOUT)
77:           GO TO (23,24,905),JSTAT
78:        24 BUFFEROUT(JOUT,IY,B,KNN,JSTAT)
79:           NSEC=NSEC+3
80:           IF(NSEC.GE.NTIM) GO TO 20
81:        25 CONTINUE
82:           GO TO (25,26,903,904),ISTAT
83:        26 CALL DIGER(IY)
84:        27 CALL STATUS(JOUT)
85:           GO TO (27,28,905),JSTAT
86:        28 BUFFEROUT(JOUT,IX,B,KNN,JSTAT)
87:           NSEC=NSEC+3
88:           IF(NSEC.GE.NTIM) GO TO 20
89:           GO TO 21
90:        20 CALL ENDDIG
91:           CALL BUFMK(JOUT)
92:           CALL BUFMK(JOUT)
93:           JF=JF+1
94:           CALL DEMUX(IX,IZ)
95:       340 CONTINUE
96:     C THE FOLLOWING TWO CARDS CONTROL DISPLAY RIGHT AFTER DIGITIZING
97:     C      CALL DIS(IZ)
98:     C      IF(ISENSE(1).EQ.0) GO TO 340
99:           CALL DATVU(IX,IZ)
100:          WRITE(OUT,345)
101:    345   FORMAT(' TO SCRATCH THIS RECORD TYPE N')
102:    346   FORMAT(1A1)
103:          READ(IN,346) IS
104:          IF(IS.NE.1HN) GO TO 350
```

```
105:          DO 348 J=1,2
106:    347   CALL BUFBR(JOUT,$348)
107:          GO TO 347
108:    348   CONTINUE
109:          CALL BUFSR(JOUT,$349)
110:    349   JF=JF-1
111:    350   CONTINUE
112:          GO TO 4
113:    351   CONTINUE
114:          DO 8888  KKK=1,10
115:          CALL BUFMK(JOUT)
116:    8888  CONTINUE
117:          CALL BUFRW(JOUT)
118:          WRITE(OUT,352) JF
119:     352  FORMAT(1X,I3,' FILES ON OUTPUT TAPE')
120:          STOP FIN
121:     503  CONTINUE
122:     506  WRITE(OUT,509)
123:     509  FORMAT(' TAPE STATUS ERROR...CRASH')
124:          STOP
125:     902  CONTINUE
126:    903   CONTINUE
127:    904   CONTINUE
128:     905  WRITE(OUT,1000)
129:    1000  FORMAT(' DIGITIZER ERROR...TRY AGAIN')
130:          CALL ENDDIG
131:          GO TO 4
132:          END
```

SIZE 438 00666


```
133:          SUBROUTINE SKIP(LUN,M)
134:          ASSIGN 1 TO JUMP
135:           IF(M.LT.0) ASSIGN 2 TO JUMP
136:          N=IABS(M)
137:          L=0
138:          GO TO JUMP
139:        1 CALL BUFSR(LUN,$4)
140:          GO TO 3
141:        2 CALL BUFBR(LUN,$4)
142:        3 L=0
143:          GO TO JUMP
144:        4 L=L+1
145:          IF(L.LT.N) GO TO JUMP
146:          RETURN
147:          END
```

SIZE 42 00052

```
148:          SUBROUTINE DIS( IZ )
149:          DIMENSION IZ( 1 )
150:           CALL INITCR
151:          ITSF=4096/600
152:          ITSF=4096/150
153:       50 CONTINUE
154:          DO 60 J=0,3
155:          NOF=( J+1 )*600
156:          N=J*150+1
157:          CALL CRTP( IZ( N ),150,ITSF,NOF,1 )
158:       60 CALL CRTP( 0,-1,0,0,1 )
159:          RETURN
160:          END
```

SIZE 56 00070


```
162:          SUBROUTINE DEMUX( IX,IZ )
163:     C IX IS ORIGINAL ARRAY   5
164:     C IZ IS DEMUXED OUTPUT
165:     C DIFFERENT CONSTANTS ARE ADDED TO EACH TRACE
166:     C SO THEY WILL SEPARATE WHEN DISPLAYED
167:          DIMENSION IX( 1 ),IZ( 1 )
168:          DO 100 J=0,3
169:          DO 100 K=0,149
170:          KK=K*4+J+1
171:          L=J*150+1+K
172:          IZ( L )=IX( KK )
173:      100 CONTINUE
174:      200 CONTINUE
175:          RETURN
176:          END
```

SIZE 50 00062

```
177:          SUBROUTINE DATVU( IX, IZ )
178:          DIMENSION IX( 1 ), IZ( 1 ), IB( 16 )
179:     C SEARCH BACKWARDS FOR EOF
180:          IT='14
181:          M=0
182:     C MUST BACK SPACE PAST THREE ENDS OF FILE
183:          DO 15 J=1, 3
184:     C BACKSPACE TILL  1 EOF
185:       10 CALL BUFBR( IT, $50 )
186:          GO TO 10
187:       50 CONTINUE
188:       15 CONTINUE
189:     C SKIP EOF
190:     C SPACE FORWARD OVER 1 EOF
191:          CALL  BUFSR( IT, $60 )
192:       60 CONTINUE
193:          IFLG=0
194:          GO TO 20
195:        1 CALL DIS( IZ )
196:     C INTERROGATE PUSH SWITCH 13
197:          CALL INFO1( IB )
198:          IF( IB( 12 ). LT. 250 ) IFLG=1
199:          IF( IB( 12 ). LT. 250. OR. IFLG. EQ. 0 ) GO TO 1
200:          IFLG=0
201:       20 CALL BUFIN( IT, 1, IX, 600, M, $100 )
202:      300 FORMAT( 'SURPRISE. . . NWORDS=', I5, 'CRASH' )
203:          CALL DEMUX( IX, IZ )
204:          GO TO 1
205:      100 RETURN
206:          END
```

SIZE 99 00143


```
207:          SUBROUTINE ONPR
208:          RETURN
209:          END
```

SIZE 4 00004


```
210:          SUBROUTINE OFFPR
211:          RETURN
212:          END$
```

SIZE 4 00004

```
$ASSIGN 7=DIGERT
$ASSEMB
BAKGND: ABT 23 @ 017310
$EOJ

CHUCK  TIME 00HRS 00MIN 06.176SEC
```

A.2 HANDY Description and Directions

This utility program searches the tape for a given file, lists the header record on the teletype, and either lists the data on the line printer or calculates the gain from a sine wave it expects to find on one channel. HANDY could be expanded by adding subroutines to plot the data or display it on the CRT.

HANDY first prints on the operator's terminal:

WHICH FILE TO USE.. QUIT = -1

The program advances the tape the requested number of EOF's. If the operator responds with ϕ, the first record is read, if the response is 1, the tape advances one file and reads a record. After finding the file the program prints

WHAT TO DO.. DUMP = 1, CALIBRATE = 2

DUMP, causes the data to be transferred to a disk file, which in turn will be listed on the line printer after the program terminates. CALIBRATE, causes the program to ask WHICH CHANNEL. The response should be 1, 2, 3 or 4. The program prints out maxima, minima and peak to peak excursion values for the sine wave calibration signal found on that channel, and the average value of the peak-to-peak excursion.

The program then asks

WHICH EXCURSION TO USE (I4)

The operator may type in the average excursion from above. Then

SPECIFY DIGITIZER FACTOR, VOLTS FULL SCALE F7.2

This factor is found by digitizing a square wave of known amplitude and, using DUMP option above, and calculating the voltage required for digitized excursion of 1024, the channel gain is then calculated according to the formula

$$\text{GAIN} = \frac{1000000. \ *\text{DIGITIZER FACTOR} \ *\text{EXCURSION}}{(\text{CAL SIGNAL IN MICROVOLTS}) \ * \ 1024}$$

The calculated gain is printed on the operators terminal.

A.2.1. HANDY listing

```
$JOB CHUCK U82  D6
$OPTION 7
$OPTIONS ,20,8
$OPTIONS ,21,8
$FORTRAN

   05-05-77                                                    PAGE     1
   61516-01 EXTENDED NON-SAU FORTRAN COMPILER   REVISION LEVEL 24.083076

 1:    C PROGRAM HANDY
 2:    C THIS PROGRAM FINDS THE RIGHT FILE AND DOES SOMETHING WITH IT
 3:           DIMENSION IDATA(600)
 4:          COMMON ID(600)
 5:          INTEGER T
 6:          T=2
 7:          IT='14
 8:           OPEN IT
 9:          REWIND IT
10:           IF(LINKME(0,T).LT.0) STOP LINKME
11:       50  WRITE(T,100)
12:    100   FORMAT(' WHICH FILE TO USE..  QUIT=-1')
13:           READ(T,101) JSF
14:          IF(JSF.EQ.0) GO TO 110
15:          IF(JSF.EQ.-1) GO TO 300
16:     101  FORMAT(I2)
17:           JSF=JSF-1
18:          IF(JSF.EQ.0) GO TO 105
19:           REWIND IT
20:           DO 105 J=1,JSF
21:     105  CALL BUFSF(IT)
22:          MWORDS=0
23:          ISTAT=0
24:     110  CALL BUFIN(IT,1,ID,600,MWORDS,$120)
25:          CALL TITLE(T)
26:     111  WRITE(T,112)
27:    C DISPLAY AND PLOT ARE NOT OPERATIONAL
28:    112   FORMAT(1X,' WHAT TO DO...  DUMP=1,CALIBRATE =2')
29:           CALL BUFIN(IT,1,IDATA,600,MWORDS,$120)
30:           READ(T,113) IDO
31:     113  FORMAT(I1)
32:           IF(IDO.EQ.1) CALL DUMP(IDATA)
33:          IF(IDO.EQ.2) CALL CALPT(IDATA)
34:           IF(IDO.EQ.3) CALL DIS(IDATA)
35:           GO TO 50
36:     120  WRITE(T,121)
37:     121  FORMAT(' ENCOUNTERED EOF INSTEAD OF DATA - TRY AGAIN')
38:          GO TO 50
39:    300   REWIND IT
40:          CALL EXIT
41:           END

                                    SIZE      766     01376
```

```
42:           SUBROUTINE CALPT( IDMX )
43:    C WHEN THIS SUBROUTINE IS PUT IN WITH THE DIGITIZER
44:    C PROGRAM IT PE  PICKS THE PEAKS AND CALCULATES
45:    C THE  CHANNEL GAINS
46:    C THIS SUBROUTINE FINDS MAX AND MIN OF CALIBRATION SIGNAL AND
47:    C GAIN FOR THAT CHANNEL
48:    C                                                          CALCULATES
49:          DIMENSION MINA( 10 ), MAXA( 10 ), IDIFF( 10 )
50:            DIMENSION IDMX( 4, 150 )
51:          INTEGER T
52:          DATA IFLG/0/
53:          T=2
54:          WRITE( T, 200 )
55:    200   FORMAT( ' WHAT CHANNEL AND , HOW MANY MICROVOLTS' )
56:          READ( T, - ) N, UV
57:            IF( N. LT. 0 ) CALL DUMP( IDMX )
58:            IF( N. LT. 1 ) RETURN
59:     201  FORMAT( I2 )
60:          K=0
61:          N2=N+150
62:          DO 300 NN=N, N2, 14
63:          K=K+1
64:          N3=NN+14
65:            LO=IDMX( N, NN )
66:            IHI=LO
67:          DO 69 J=NN, N3
68:            IF( IDMX( N, J ). LT. LO ) LO=IDMX( N, J )
69:            IF( IDMX( N, J ). GT. IHI ) IHI=IDMX( N, J )
70:       69 CONTINUE
71:          MINA( K )=LO
72:          MAXA( K )=IHI
73:     300  CONTINUE
74:    C                                          )01, 2=J, )J( ANIM(  )103, T( ETIRW
75:     301  FORMAT( ' MINIMA = ', 10( 2X, I4 ))
76:     302  FORMAT( ' MAXIMA= ',  10( 2X, I4 ))
77:    C                                          )01, 2=J, )J( AXAM(  )203, T( ETIRW
78:          ITOT=0
79:            DO 50 I=2, 10
80:          IDIFF( I )=MAXA( I )-MINA( I )
81:       50 ITOT=IDIFF( I )+ITOT
82:          WRITE( T, 303 ) ( IDIFF( I ), I=2, 10 )
83:     303  FORMAT( ' DIFFS= ', 10( 2X, I4 ))
84:            IAVG=ITOT/9
85:          WRITE( T, 304 ) IAVG
86:     304  FORMAT( ' AVERAGE EXCURSION = ', I4 )
87:          WRITE( T, 500 )
88:     500  FORMAT( ' WHAT EXCURSION TO USE ( I4 )' )
89:          READ( T, 501 ) IX
90:     501  FORMAT( I4 )
91:          IF( IFLG. NE. 0 ) GO TO 510
92:          WRITE( T, 600 )
93:    600   FORMAT( ' SPECIFY DIGITIZER FACTOR, VOLTS FULL SCALE, F7. 2' )
```

```
 94:          READ( T, 601 ) DF
 95:    601   FORMAT( F7.3 )
 96:          IFLG=1
 97:    510   CONTINUE
 98:          GAIN=1000000. *( DF*IX )/( UV*1024 )
 99:           WRITE( T, 502 ) N, GAIN
100:     502 FORMAT( ' CHAN ', 1X, I1, 5X, 'GAIN = ', F 15.1 )
101:         RETURN
102:         END
```

SIZE 337 00521


```
103:           SUBROUTINE DUMP( IDATA )
104:           DIMENSION IDATA( 600 )
105:         CALL TITLE( 6 )
106:         DO 5 J1=1, 600, 4
107:         J4=J1+3
108:       5 WRITE( 6, 10 ) ( IDATA( J ), J=J1, J4 )
109:      10 FORMAT( 1X, 4( I6, 2X ) )
110:         RETURN
111:           END
```

SIZE 48 00060


```
112:           SUBROUTINE TITLE( LUN )
113:           COMMON ID( 600 )
114:          IFIN=3HFIN
115:           JMIN=1
116:           DO 140 J=1, 10
117:           JMAX=JMIN+23
118:         WRITE( LUN, 130 ) ( ID( K ), K=JMIN, JMAX )
119:     130   FORMAT( 1X, 24A3 )
120:           IF( ID( JMIN ). EQ. IFIN ) GO TO 145
121:           JMIN=JMIN+24
122:     140 CONTINUE
123:     145 CONTINUE
124:         RETURN
125:         END
```

SIZE 57 00071


```
126:         END$
```

A.3 CONVERT Description

The data tapes produced by NUDIG on the Geophysical Computing Facility Datacraft 6024 are converted from 24-bit ASCII to 36 bit Fielddata by CONVERT, which also rewrites the data into block lengths compatible with MAGTEL, described in section A.4.

CONVERT uses the input tape format shown in Figure A.3.1. CONVERT requires one data card containing the following information:

Columns 1-6 name of input tape FORMAT A6, six alpha-numeric characters.

Columns 10-16 name of output tape FORMAT A6

Columns 25-30 maximum number of data sets to read in FORMAT (I6)

Columns 35-40 maximum number of EOF's to read FORMAT (I6)

The job will terminate if any of the following occur.

1. Number of headers exceeds that specified.
2. Number of EOF's exceeds that specified.
3. Number of EOF's in a row exceeds a number (1EOF) set in the program. Presently 1EOF = 2.

DIGITIZER TAPE FROM DATACRAFT (9 TRACK)

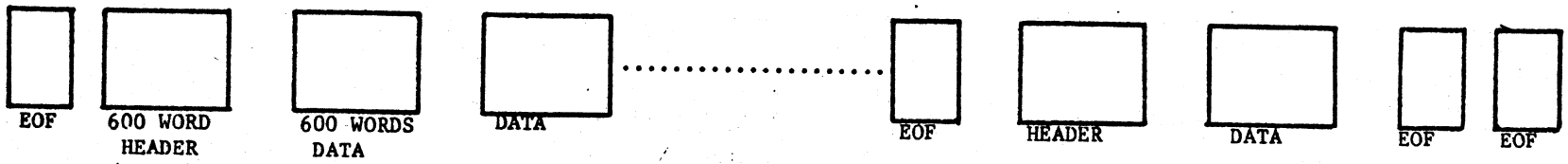

EOT INDICATED BY MORE THAN 2 EOFS

OUTPUT TAPE FROM CONVERT (7 TRACK)

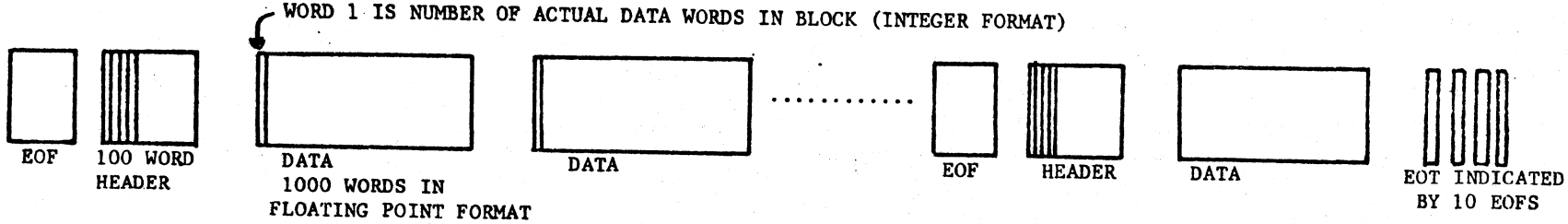

HEADER IDENTIFICATION WORDS

H(1) 'CONTRL'
H(2) LOGICAL RECORD NUMBER, I.E. FILE NUMBER
H(3) PHYSICAL RECORD NUMBER = 1
H(4) STRING = 1
H(5) AND FOLLOWING IS THE ASCII HEADER FROM THE DATACRAFT TAPE

Figure A.3.1. Format of digitizer output tape and MAGTEL input tape.

A.3.1 CONVERT listing

```
                                                                    1

'PRINT
'RUN YOUNG,40069,77od,55.00,100
'ASG,U CYAVE.
'SAVE,S CYAVE.,052075
'FOR,I CONVERT
C
C  PROGRAM CONVERT
C LATEST UPDATE  MAY 13,1975
C THIS PROGRAM CONVERTS DIGITIZED DATA  FROM THE DATA_CRAFT IN
C YOUNG'S FORMAT TO  DATA TAPES FOR  1110 IN VAGTEL INPUT
C MAKES ONE  7 TRACK 1110 TAPE FROM ONE 9 TRACK DATACCRAFT TAPE
C INTEGERS ONLY EXCEPT FOR ASCII HEADER
C EXPECTS INPUT FORMAT AS FOLLOWS ASCII HEADER(600 FRAMES),
C DATA(600),DATA(600)....,EOF,HEADER,DATA..... 3 EOFS
C THIS WRITES OUT THE ACCUMULATED FILE ONTO TAPE
C IOUT HAS AN EXTRA DATA POINT IN FRONT TO TELL HOW MANY POINTS
C PROGRAMMED BY C YOUNG, J GETTRUST AND PROBABLY T. WOLF.
      DIMENSION IOUT(1001)
      DIMENSION IDOUT(600)
       DIMENSION IN(6000),ID(600),IID(600)
      INTEGER PREC,STRNG
      REAL IOUT
      EQUIVALENCE (IOUT(1),NPTS)
      DATA IFIN/6HFIN
C  FUNA IS THE  ASCII TO FIELD DATA  TRANSLATOR
      EXTERNAL FUNA
      NREC=0
      NEOF=0
      LREC=0
      PREC=1
      STRNG=1
      KOUNT=0
      IFLG=0
      NCHAR=600
C     INPUT TAPE=LU
      LU=20
C     OUTPUT TAPE=LO
      LO=25
C FILL IN  IN WITH 512'S WHICH WILL BE ZEROS LATER
       DO 40 KK=1,6000
   40 IN(KK)=512
      KARD=5
      READ(KARD,50) INTAPE,OUTP,IEOF,IREC
        WRITE(6,49)
   49  FORMAT(//)
   50 FORMAT(2(A6,4X),2I10)
      WRITE(6,5*) INTAPE,OUTP,IEOF,IREC
   51 FORMAT(' INPUT TAPE ',A6,', OUTPUT TAPE  ',A6,3X,I3,
     S'EOFS EXPECTED,  ',I3,'  RECORDS EXPECTED' )
      DO 21 I=1,600
      IID(I)=0
   21 IN(I)=0
      K=600
```

```
 101  CONTINUE
   30 CONTINUE

C
C READ HEADER
C
      CALL INDATI(LO,ID,1800,$99,$8)
      LREC=LREC+1
C MVCHAR TRANSLATES DATACRAFTESE (STANDARD ASCII) TO FIELD DATA
C (ESPERANTO OF THE COMPUTERWORLD).
       CALL MVCHAR(ID,1,8,IID,1,6,NCHAR,FUNA)
      CALL XPND(ID,600)
      CALL SWAP(IID,IDOUT(3),95)
      IDOUT(1)='CNTRL'
      IDOUT(2)=LREC
      IDOUT(3)=PREC
      IDOUT(4)=STRNG
      DO 5000 J=1,120,12
      MIN=J
      MAX=J+11
      WRITE(6,2*02) (IID(K),K=MIN,MAX)
      IF(IID(MIN).EQ.IFIN) GO TO 5001
 2002 FORMAT(1X,12A6)
 5000 CONTINUE
 5001 CONTINUE
 2000 FORMAT(50X,'WROTE EOF MARK')
      IID(100)=IFIN
CTRUNCATE HEADER TO CONFORCONFORM TO MAGTEL FORMAT
C IF NOT THE FIRST TIME THROUGH, BACKSPACE OVER 2 EOFS
      IF(KOUNT.EQ.0) GO TO 5004
      DO 5003 II=1,2
      CALL IOTPBS(LO,$5003)
      WRITE(6,5005)
 5003 CONTINUE
 5004 CONTINUE
 5005 FORMAT(' BACKSPACED OVER FILE INSTEAD OF EOF')
C
C WRITE HEADER ON TAPE
C
      CALL IOTPOT(LO,1,IDOUT,100,$323)
      K=100
      WRITE(6,2001) K
 2001 FORMAT(1X,' WROTE RECORD OF ',I6,' WORDS.')
      KOUNT=0
 41   CONTINUE
       JREC=0
C
C READ DATA
C
C IBK = 1 IS A FLAG SIGNIFYING THAT THE INPUT RECORD IS GOING TO FILL
C THE ARRAY SO IT IS TIME TO BRANCH TO THE OUTPUT ROUTINE
C
C IBK IS A FLAG SIGNIFYING THAT THE INPUT RECORD IS GOING TO
C OVERFLOW THE ARRAY
C THIS SECTION READS RECORDS, EXPANDS THEM, AND REWRITES
C THEM SEQUENTIALLY INTO IN, THEN JUMPS OUT OF THE LOOP WHEN IT HITS
```

```
C AN EOF
  32    K=-599
 320    K=K+600
C K IS POINT IN ARRAY IN() WHERE DATA WILL BE TRANSFERRED.
C K MUST BE LT 5402 FOR EXACTLY TEN FULL BLOCKS
C SET IBK=1 AND JUMP OUT IF ARRAY IS FULL
C 5401=NUMBER OF BLOCKS DESIRED MINUS ONE TIMES 600 PLUS ONE
        IF(K.GT.5401) IBK=1
        IF(K.GT.5401) GO TO 3230
C IERET=1 MEANS THAT THE EOF RETURN HAS BEEN TAKEN FROM INDATA
      IERET=0
      CALL INDAT(LU,IN(K),1800,$99,$322)
        IBK=0
        JREC=JREC+1
      IFLG=0
      CALL XPND(IN(K),600)
      KL=K+599
      DO 321 I=K,KL
      IF(IFLD(12,1,IN(I)).EQ.1) IN(I)=IN(I)-16777216
  321 CONTINUE
 3210  CONTINUE
      GO TO 320
C
C IF INDATA READS AN EOF IT RETURNS HERE
  322  CONTINUE
C IF THE LAST BLOCK OF THIS FILE HAS ALREADY BEEN
C WRITTEN OUT DUE TO IBK=1, JUMP OUT OF THE LOOP
      IF(IBK.EQ.1) GO TO 3250
        IERET=1
 3230  CONTINUE
        K=K-1
      IF(K.EQ.0) GO TO 8
C
C NOTE K IS THE NUMBER OF WORDS READ IN WHEN AN EOF WAS ENCOUNTERED
C ROUND OFF STRING LENGTH TO NEXT GREATER MULTIPLE OF 1000
       KND=((K+995)/1000)*1000
C IF BUFFER IS FULL AND EOF NOT ENCOUNTERED PAD TO 6000 ONLY
        IF(IBK.EQ.1) KND=6000
      IXTRA=KND-K
        WRITE(6,3211) JREC
 3211   FORMAT(1X,'READ',I6,'  RECORDS OF STANDARD LENGTH')
      WRITE(6,324) K,IXTRA,KND
  324 FORMAT(' PADDED STRING OF LENGTH',I10,' WITH',I10,
     $'  ZEROES TO MAKE STRING OF LENGTH',I10)
      KP1=K
      KP1=K+1
      DO 4000 JJ=KP1,KND
 4000 IN(JJ)=0
C
C WRITE DATA ON TAPE
C
      DO 325 KK=1,KND,1000
      CALL SWAPP(IN(KK),IOUT(2),1000)
C LABEL IOUT(1)= 1000UNLESS WE ARE ON THE LAST PHYS REC OF THE STRING
C ARE IN THAT BLOCK.
C THEN IT TELLS THE NUMBER OF REAL DATA POINTS IN THAT STRING
```

```
      NPTS=1000
      IF((KND-KK).LT.1000) NPTS=K-KK+1
      CALL IOTPOT(LU,1,IOUT,1001,5323)
      III=1001
C     WRITE(6,2*01) III
      KOUNT=KOUNT+1
  325 CONTINUE
C RESET IBK IF EOF RETURN WAS TAKEN
      IF(IBK.EQ.1.AND.IERET.EQ.0) GO TO 41
 3250 CONTINUE
      WRITE(6,326) LREC,  KOUNT
      KOUNT=1
  326 FORMAT(' LOGICAL RECORD ',I5,' CONSISTS OF ',I5,
     5 '  BLOCKS OF  1001 WORDS .'//)
C
      DO 2005 II=1,3
 2005 CALL IOTPMK(LU)
      WRITE(6,2000)
      GO TO 8
C
  323 WRITE(6,9*00)
 900n FORMAT(50X,'ERROR = EOT')
      GO TO 99
C
C EOT DETECTOR
C
    8 CONTINUE
C M IS NO. OF EOFS SIGNIFYING EOT
      M=2
      M=3
      M=4
      NEOF=NEOF+1
      IFLG=IFLG+1
   80 IF(NEOF.LT.IEOF.AND.NREC.LT.IREC.AND.IFLG.LT.M) GO TO 30
C PROGRAM QUITS IF 1. IEOEOFS IS HAVE BEEN ENCOUNTERED, 2) IREC
C RECORDS HAVE BEEN ENCOUNTERED 3) 3 CONSECUTIVE EOFS ARE
C ENCOUNTERED
C TEN EOFS MARKS END OF OUPUT TAPE
      DO 81 I=1,10
      CALL IOTPMK(LU)
   81 WRITE(6,2 00)
   99 CONTINUE
      CALL IOTPCL(LU)
      CALL IOTPCL(LU)
      END
'FOR,I  XPND
      SUBROUTINE XPND(L,N)
      DIMENSION L(2)
      K=(2*N+2)*3
      JJ=MOD(N,3)+1
      DO 3 II=1,N
      I=N+1-II
      IF(I-2) 32,31,30
   30 L(I)=0
      GO TO (21,22,231),JJ
   21 L(I)=FLD(12,24,L(K))
```

```
      GO TO 29
 22   FLD(24,12,L(I))=FLD(0,12,L(K))
      K=K-1
      FLD(12,12,L(I))=FLD(24,12,L(K))
      GO TO 29
 31   ITM=L(I)
      L(I)=0
      FLD(24,12,L(I))=FLD(0,12,ITM)
      FLD(12,12,L(I))=FLD(24,12,L(I-1))
      GO TO 3
 32   ITM=L(I)
      L(I)=0
      FLD(12,24,L(I))=FLD(0,24,ITM)
      GO TO 3
 23   L(I)=FLD(0,24,L(K))
      K=K-1
 29   JJ=JJ+1
      IF(JJ.GT.3) JJ=1
 3    CONTINUE
      RETURN
      END
*FOR,I  SWAP
      SUBROUTINE SWAP(IN,IOUT,N)
C THIS SR PUTS THE STUFF IN IN INTO OUT
      DIMENSION IN(1),IOUT(1)
      DO 1 I=1,N
    1 IOUT(I)=IN(I)
      RETURN
      END
*FOR,I SWAPR
      SUBROUTINE SWAPR(IN,OUT,N)
C THIS SR PUTS THE STUFF IN IN (INTEGER) INTO OUT( REAL).
      DIMENSION IN(1),OUT(1)
      DO 1 I=1,N
    1 OUT(I)=IN(I)
      RETURN
      END
*FOR,I INDAT
      SUBROUTINE INDAT(LU,IA,NC,$,$)
C        RETURNS TO ALTERNATE 1 IF WRRNG DATA LENGTH
C        RETURNS TO ALTERNATE 2 IF EOF READ
      DIMENSION IA(1)
      N=(NC*2+8)/9
      CALL IOTPIN(LU,1,IA,N,L,$21,$22)
C     WRITE(6,2*00) L
 2000 FORMAT(' READ RECORD OF',I7,' CHARACTERS')
 20   IF(L.EQ.NC) RETURN
      WRITE(6,9*00) NC
 9000 FORMAT(' *****ERROR - SHOULD HAVE BEEN',I7,' CHARACTERS')
      RETURN 4
 21   WRITE(6,9001)
 9001 FORMAT(' READ EOF')
      RETURN 5
 22   WRITE(6,2000) L
      WRITE(6,9002)
 9002 FORMAT(' *****ERROR - PARITY ERROR')
```

```
      GO TO 20
      END
*MAP,INX  ,TPF5.CONV
*COPY,A TPF5.,CYAVE.
*FIN
*ENDP
```

A.4 MAGTEL Description

This program reads digitized data from tape, converts the time series to the frequency domain by fast Fourier transform, makes system response corrections, computes powers and coherencies, apparent resistivities and impedance elements according to the formulas outlined in Chapter 4. These data are printed out and written on magnetic tape.

A.4.1 MAGTEL modifications

MAG 2 corrects for a single present 4-channel system response, set for the instrumentation system of Chapter V. Old MAGTEL has several tables, perpared for the variable-bandpass instrumentation system described in Dowling's 1968 dissertation.

In modified MAGTEL, a table of frequencies that will require filter correction is set up, then subroutine FILTER is called, which contains the filter response table. Required responses are calculated by interpolation between the entries in the table, using subroutine INTERP. To compile this modified version of MAGTEL, old MAGTEL is called from a program tape, subroutines FILTER and FILTCN are deleted and new subroutines FILTER and INTERP are added, as in the listing below.

Other modifications include modifying the printer-plotter subroutine to separate the t-axis of the 4 channels being plotted and to plot one point per line instead of two, and a change to the page titling to use less paper by eliminating blanks.

We illustrate how to run data without the tests built into the program. In some cases the tests are skipped by leaving a blank in the card, in some cases the tests are skipped by specifying test level such that all the data passes, in other cases, the program has been modified to skip the tests.

Other information about the data cards and programs may be found in in-house University of Wisconsin Geophysical and Polar Research Center documents entitled: (1) complete listing of MAGTEL and AVETEL; (2) MT control cards and program descriptions.

The changes affecting MAGTEL control and data cards involve:

(1) Use of 9 track, ultra high density tape for MAGTEL input,

(2) Use of 7 track high density tape for MAGTEL output,

(3) Elimination of filter setting card,

(4) Change of gain specification card,

(5) Storage of absolute element of MAGTEL (compiled, ready to execute) on disk file.

A.4.2 MAGTEL executive control cards

Statements in the following set of cards preceeded by a @ sign are Executive Control statements from the Madison Academic Computing Center Univac 1110. Detailed instructions for their use are found in the MACC Computing Handbook.

MAGTEL runstream deck:

1. @ RUN user name, project number, user ID number, $ dollar limit, page limit
2. @ ASG,AX FILENAME. File containing compiled version of MAGTEL

3. @ ASG,VT 20.,U9V, Reel ID of CONVERT output tape to be used (ultra high density, 9-track)
4. @ ASG,HT 29.,T, Reel ID of old MAGTEL carryover output tape to be updated (the above card is required for UPDATE carryover selection only) (high density, 7-track)
5. @ ASG,HT 30., T, $reel ID of new MAGTEL output carryover tape to be made (the above card is required unless NOTAPE carryover selection) (high density, 7-track)
6. @ XQT FILENAME.MAG2 This modified version of MAGTEL is named MAG2
7. CARRYOVER SELECTION CARD defined below
8. @ EOF
9. Sets of seven MAGTEL control cards for each data set, defined below. Seventh card is @ EOF
10. @ FIN

Cards with first character "@" are executive control statements recognized by the EXEC operating system of the MACC Univac 1110. Use of these statements is discussed in the MACC 1110 Computing Handbook. Other cards are those read by the program MAGTEL.

A sample deck might be:

```
@RUN,/R YOUNG,40693,7768,$10.00,200
@ASG,AX CYAVE.
@ASG,VT 20.,U9V,TTS644
@ASG,HT 30.,T,$TTS742
@XQT CYAVE.MAG2
```

NEWTAP MINESITE

@EOF

MAGTEL CONTROL CARDS

@FIN

A @HDG (heading) card with a message may be inserted before the @ XQT card, causing the message to be printed on each page of output.

A.4.3 MAGTEL data deck

Carryover selection card is the first of the MAGTEL data cards and it appears only once. Following it are the packs of 7 cards specifying MAGTEL data sets.

COLS 1-6	NOTAPE	means no carryover tape is to be created
	NEWTAP	means no tape is to be updated but a new tape is to be written on logical unit 30.
	UPDATE	means the MAGTEL carryover tape on logical unit 29 is to be copied onto unit 30. New carryover output from this run is written onto unit 30 after the copied data.
COLS 11-20		Site and set numbers (Alphabetic; left justified for best printing)

If NOTAPE is specified, neither units 29 or 30 need be assigned. Unit 30 will need to be assigned to an output tape if either NEWTAP or UPDATE is specified and unit 29 will need to be assigned to an input tape if UPDATE is specified.

I state, underline, at the end of each specification what value I used, and in parenthesis I give the FORTRAN format by which the data are read, abbreviated by:

(1) I format for integer data, for example, I10 means that a field 10 columns wide is read, in which the data must be right justified. No decimal point.

(2) F.P. floating point. Decimal point must be punched.

(3) H format, alphabetic or numeric information, all characters may be used.

Card 1: (locate file)

Cols 1-10: Logical record number, (I10) the file number assigned by program CONVERT

Cols 11-20: Physical Record Number (I10), 1

Cols 21-30: String Number (I10), 1

Card 2: (Identification information)

Cols 1-10 Site and Set numbers (10H)

Cols 11-20: Location (10H)

Cols 21-30: Box (10H)

Cols 31-40: Pages (10H)

Cols 41-50: Field Record Number (10H)

The above alphanumeric data are not used in computation, but just reprinted on the MAGTEL output. Box, pages and field record number are meaningful in Dowlings, 1968, system of data storage. They may be left blank or used for any desired information.

Cols 51-60: Sampling Rate (F.P.) 128.

Card 3: (Smooth, decimate, segment)

Cols 1010: First point to use (I10), 1

Cols 11-20: Last point to use (I10), number of points in the string, 2048

Cols 21-30: Decimation number, "d" I10 1
(uses every d^{th}) pt.)

Cols 31-35: First Boxcar Width, (I10), blank equivalent to 1 1

Cols 36-40: Second Boxcar Width, (I10), blank equivalent to 1 1

Cols 41-45: Third Boxcar Width, (I10), blank equivalent to 1 1

Cols 46-50: Fourth Boxcar Width, (I10), blank equivalent to 1 1

Cols 51-60: Number of segments*, (I10) 16

Cols 61-70: Number of points* in, (I10), blank see note 1

*only one need be punched

MAGTEL has provisions for numerical anti-aliasing and low-pass filtering by decimating the time series and smoothing with a polynomial consisting of convolved boxcars. This feature is not used; the decimation number and boxcar widths are set to unity.

Card 4: (Trend removal, taper and appending)

Cols 1-10: Trend Removal Code (I10) 2

0 or blank - data unaltered

1 - mean removed

2 - linear least squares fit removed

other - error

Cols 11-20: % of segment to taper each end, (F.P.) such that ≤ 400 points tapered, 5.

Cols 21-30: min. % increase when zeros appended (F.P. ≥ 0; < 100.) 0.

Cols 31-34: 'PLOT', (4H), will produce a printer plot of the four time series, which should be used only when necessary, since the page changes are significant. PLOT option would be cheaper if it were placed with a call to Calcomp plotter routine.

Card 5: (Gains, coil factor, electrode separations, sign of phase correction and option for determining system response)

Cols 1-10: H_X system voltage gain (F.P.) negative sign for proper correction

Cols 11-20: H_Y system voltage gain (F.P.) negative sign for proper correction

Cols 21-30: E_X system voltage gain (F.P.) positive sign for proper correction

Cols 31-40: E_Y system voltage gain (F.P.)

Cols 41-50: H_X coil factor, sensitivity in microvolts per gamma at 10 Hz (F.P.) 2300.

Cols 51-60: H_Y coil factor, (F.P.) 2300.

Cols 61-65: E_X electrode separation meters (F.P.) usually 50.

Cols 66-70: E_Y electrode separation meters (F.P.) usually 50.

Col 71: Any character to set phase corrections to zero and gain correction to unity. See Note 1.

Cols 72-75: Any character to change sign of phase correction. XXXX

Card 6: (Data rejection tests and frequency averaging)

Cols 6-10: Number of frequency bands per decade (I), 10

Col 80: X, (H) to supress a phase test

Other columns are blank to suppress other tests

Card 7: @ EOF

Note 1: For obtaining the systems response with the pseudorandom test signals, I wanted densely spaced frequency data. I used 256 point strings, and specified 20 frequency bands per decade.

A.4.4. MAGTEL modification listing

```
*** PAGE  1   FILE W1        DATE 05-05-77     TIME 13:35:  0   ***************

  1  @RUN,/R YOUNG,40693,7768,$5.00,100
  2  @ASG,UX CYAVE.
  3  @SAVE,S CYAVE.,091076
  4  @ASG,MT 1.,T,5275
  5  @MOVF T.,1
  6  @COPY,G T.,TPF$.
  7  @DELETE,A TPF$.MAGTEL
  8  @DELETE,S TPF$.FILTCN
  9  @DELETE,S TPF$.FILTER
 10  @FOR,IX FILTER
 11        SUBROUTINE FILTER(F,LL,CHX,CHY,CEX,CEY)
 12  C THIS SR PROVIDES FILTER FACTORS CHY ETC AT FREQUENCIES F
 13         DIMENSION F(1),CHX(1),CHY(1),CEX(1),CEY(1),CF(21,9)
 14        DIMENSION SR(21,9)
 15          DIMENSION PHFAC(4)
 16          COMPLEX PHFAC
 17        COMPLEX CHY,CHX,CEX,CEY,B
 18        COMPLEX A1,A2,A3,A4
 19  C SYSTEM RESPONSE DETERMINED WITH PSEUDO RANDOM NOISE
 20  C JULY 9,1976
 21  C
 22  C COLUMN 1 FREQUENCIES
 23        DATA IBLK/1H /
 24        DATA SR/.5,1.,2.,3.,4.125,5.37,7.5,10.5,11.8,13.3,
 25       $15.0,16.8,18.9,21.1,26.6,33.5,37.6,42.25,47.3,59.6,70.0,
 26  C
 27  COLUMN 2 CHANNEL C AMPLITUDES
 28       $.031,.044,.118,.184,.258,.364,.563,1.,1.004,.887,.674,
 29       $.479,.359,.260,.130,.044,.031,.001,.001,.001 ,.001,
 30  C
 31  COLUMN 3 CHANNEL C PHASES
 32       $-157.,-124.,-96.,-75.,-56.,-39.,-9.6,49.9,88.8,118.5,
 33       $150.,175.,-165.,-144.,-104.,-58.,-32.9,-11.1,15.1,128.,0.,
 34  C
 35  CHANNEL D AMPLITUDES
 36       $.03,.054,.122,.187,.244,.364,.544,.998,1.06,.902,
 37       $.695,.544,.391,.279,.137,.054,.063,.004,.001,.001,.001,
 38  C
 39  C CHANNEL D PHASES
 40       $-88.,-129.,-99.,-76.,-68.,-42.,-13.,44.,80.7,119.3,
 41       $146.,170.8,-165.,-146.,-102.,-62.,-22.9,.8,41.4,-25.4,0.,
 42  C
 43  COLUMN 6 CHANNEL A AMPLITUDES
 44       $.55,1.,1.28,1.22,1.20,1.61,1.14,1.,.928,.880,.813,
 45       $.748,.667,.585,.403,.225,.151,.089,.001,.001,.001,
 46  C
 47  COLUMN 7 CHANNEL A PHASES
 48       $-65.,-34.,-10.,.2,19.0,30.5,50.9,76.0,86.,97.2,
 49       $111.2,123.,138.,152.6,-169.2,-127.2,-117.6,-97.,-75.9,-40.,0.,
 50  C
 51  COLUMN 8 CHANNEL B GAINS
 52       $.55,1.,1.28,1.22,1.20,1.61,1.14,1.,.908,.828,
```

```
      $.782,.761,.664,.573,.382,.228,.151,.070,.001,.001,.001,
C
COLUMN 9 CHANNEL R PHASES
      $-65.,-34.,-10.,5.1,19.5,32.7,51.,74.,85.,94.8,
      $106.,118.8,132.,147.3,-178.9,-139.9,-119.9,-101.,-83.,-78.,0./
C DF IS DIGITIZER FACTOR IN UNITS OF VOLTS PER NUMBER
C THE TRUE VALUE DEPENDS ON THE DIGITIZER ATTENUATOR SETTING BUT
C BUT IS  THE SAME FOR ALL CHANNELS ANYWAY.
      DF=2.5/1024
C ELSP IS ELECTRODE SPACING IN METERS
      LAST=LL
      SEX=1.
      SEY=1.
      SHX=1.
      SHY=1.
      READ(5,100) HXG,HYG,EXG,EYG,XCF,YCF,XELSP,YELSP,
     $ITST,IHX,IHY,IEX,IEY,I2HX,I2HY,I2EX,I2EY
100   FORMAT(6F10.3,2F5.0,10A1)
      WRITE(6,101) HXG,HYG,EXG,EYG,XCF,YCF,XELSP,YELSP
 101  FORMAT(' GAIN FACTORS...',/,' HX',T13,'HY',T23,'EX',T33,'EY',
     $T45,' X COIL',T55,'Y COIL',T65,'X-EL SP',T75,'Y EL SP',
     $//,6(1X,F10.2),2F5.0)
      DO 138 J=1,21
      CF(J,1)=SR(J,1)
138   CONTINUE
C FOR SPECIAL TEST SET AMPLITUDES TO UNITY, PHASES TO ZERO
      IF(ITST.EQ.IBLK) GO TO 150
      WRITE(6,141)
141    FORMAT(' GAIN SET TO UNITY AND PHASES SET TO ZERO')
      DO 140 J=1,21
      DO 140 K=2,8,2
      CF(J,K)=1.
      KK=K+1
140   CF(J,KK)=0.
      GO TO 172
150   CONTINUE
      WRITE(6,151) IHX,IHY,IEX,IEY
151   FORMAT(' ',4(9X,1A1))
      WRITE(6,152)
152   FORMAT(T8,'HX',T18,'HY',T28,'EX',T38,'EY',5X,
     $' SIGNS OF PHASE CORRECTION REVERSED AS MARKED')
      WRITE(6,151) I2HX,I2HY,I2EX,I2EY
C IF DESIRED , SET PHASE CORRECTIONS NEGATIVE
      IF(IHX.NE.IBLK) SHX=-1.
      IF(IHY.NE.IBLK) SHY=-1.
      IF(IEX.NE.IBLK) SEX=-1.
      IF(IEY.NE.IBLK) SEY=-1.
       DO 160 J=1,21
      CF(J,2)=SR(J,2)
      CF(J,3)=SHX*SR(J,3)
      CF(J,4)=SR(J,4)
      CF(J,5)=SHY*SR(J,5)
```

```
105          CF( J, 6 )=SR( J, 6 )
106          CF( J, 7 )=SEX*SR( J, 7 )
107          CF( J, 8 )=SR( J, 8 )
108          CF( J, 9 )=SEY*SR( J, 9 )
109   160    CONTINUE
110   172    CONTINUE
111   C CARDS PRINTED BACKWARDS CAN BE REVERSED
112   C TO PRINT OUT INTERMAEDIATE RESULTS SUCH AS
113   C CORRECTION FACTORS
114   C                                                                    )402, 6( ETIRW
115     204 FORMAT( ' CF S' )
116     203 FORMAT( / )
117   C                                                                    )202, 6( ETIRW
118          DO 10 J=1, LAST
119   C QUIT AT 79 HZ
120          IF( F( J ). GT. 79 ) WRITE( 6, 1000 )
121          IF( F( J ). GT. 79 ) GO TO 10
122    1000 FORMAT( ' FREQUENCY REQUESTED TOO HI FOR TABLE' )
123   C ARGS OF INTERP ARE( 1. FREQ 2. COLUMN OF CF TO USE 3. CORRECTION
124   C FACTOR MATRIX 4. RETURNED CORRECTION FACTOR
125   C THE DIGITIZER SKEW PHASE FACTORS , PHFAC,
126   C ARE SET UP ON THE ASSUMPTION THAT
127   C THE DIGITIZER CHANNEL ASSIGNMENT IS  CH1-HX  CH2-HY  CH3-EX  CH4-EY
128            PHFAC( 1 )=CMPLX( 1. , 0. )
129            P=. 00015*6. 2831*F( J )
130          DO 5 JJ=1, 3
131          JJP1=JJ+1
132          P=JJ*P
133            C=COS( P )
134            S=SIN( P )
135          PHFAC( JJP1 )=CMPLX( C, S )
136       5  CONTINUE
137     200  FORMAT( ' PHASE FACTORS' )
138     201  FORMAT( 1X, 4( F10. 5, F10. 5, 2X ) )
139     202  FORMAT( ' FREQ , CORRECT. FAC. , CEX, CEY, CHX, CHY' )
140          CALL INTERP( F( J ), 6, CF, B )
141          ELSP=XELSP
142           CEX( J )=DF*( 1. /( ELSP*EXG*PHFAC( 3 ) ) )*1000000. *( 1. /B )
143          A1=B
144            CALL. INTERP( F( J ), 8, CF, B )
145          A2=B
146          ELSP=YELSP
147            CEY( J )=DF*( 1. /( ELSP*EYG*PHFAC( 4 ) ) )*1000000. *( 1. /B )
148          CALL INTERP( F( J ), 2, CF, B )
149          A3=B
150            CHX( J )=DF*( 1000000. /( XCF*HXG*PHFAC( 1 ) ) )*( 1. /B )
151          CALL. INTERP( F( J ), 4, CF, B )
152          A4=B
153            CHY( J )=DF*( 1000000. /( YCF*HYG*PHFAC( 2 ) ) )*( 1. /B )
154   C                                                  4A, 3A, 2A, 1A, )J( F  )401, 6( ETIRW
155   C                                        )J( YEC, )J( XEC, )J( YHC, )J( XHC  )501, 6( ETIRW
156   C                                                                       )302, 6( ETIRW
```

```
157  C                                                                )302,6(ETIRW
158     105 FORMAT(16X,4(E10.3,2X,E10.3,4X))
159      10 CONTINUE
160      20 CONTINUE
161     104 FORMAT(1X,F10.3,6X,4(F10.3,2X,F10.3,4X))
162         RETURN
163         END
164  @FOR, I INTERP
165         SUBROUTINE INTERP(F,J,CF,B)
166  C J IS WHICH COLUMN OF CF TO WORK ON
167         DIMENSION CF(21,9)
168         COMPLEX B
169  C FIND FREQUENCY IN TABLE JUST LOWER THAN INPUT  FREQUENCY
170         NFREQ=21
171  C STAR OUT ASSUMING THAT F IS GREATER THAN CF(JJ,1) THEN
172  C INCREMENT TILL IT ISN'T SO
173          DO 10 JJ=1,NFREQ
174     10 IF(F.LT.CF(JJ,1)) GO TO 20
175     20 CONTINUE
176         IF(JJ.GT.1) JJ=JJ-1
177  C
178  C LINEAR INTERPOLATION
179  C
180  C FIGURE OUT THE INTERPOLATION FACTOR
181         FACT=(F-CF(JJ,1))/(CF(JJ+1,1)-CF(JJ,1))
182  C MAGNITUDE FROM TABLE
183         D1=CF(JJ+1,J)-CF(JJ,J)
184         B1=FACT*D1+CF(JJ,J)
185  C PHASE FROM TABLE
186         D2=CF(JJ+1,J+1)-CF(JJ  ,J+1)
187  C THIS MAKES THE  INTERPOLATOR REALIZE THAT THE PHASE DIFFERENCES
188  C SHOULD LIE BETWEEN  PLUS AND MINUS 180.
189         IF(D2.LT.180.) D2=D2+360.
190         IF(D2.GT.180.) D2=D2-360.
191         B2=FACT*D2+CF(JJ,J+1)
192  C CONVERT FROM POLARFORM TO RE IMAG
193  C REMEMBER  FORTRAN WANTS PHASE IN RADIANS
194         RE=B1*COS(B2/57.)
195         ZMAG=B1*SIN(B2/57.)
196         B=CMPLX(RE,ZMAG)
197         RETURN
198         END
199  @FOR,U  PLDATA,PLDATA
200  -2
201         REAL DHX,DHY,DEX,DEY,SC,SH
202  -5,5
203  C SOME IMPROVEMENTS INCLUDE; AN ADDITIVE CONSTANT TO SEPARATE
204  C TRACES, SC A CONSTANT SCALING FACTOR,
205  C AFTER ALL THAT CLIP AT 1024 AND ZERO
206         NPLINE=1
207         SC=1.
208  -25,28
```

```
209         SH=400.
210         DHX=( HX( IJ )-500 )*SC-1. 5*SH
211         DHY=( HY( IJ )-500 )*SC-. 5*SH
212         DEX=( EX( IJ )-500 )*SC+. 5*SH
213         DEY=( EY( IJ )-500 )*SC+1. 5*SH
214         CALL COL( DHX, 1H1 )
215         CALL COL( DHY, 1H2 )
216         CALL COL( DEX, 1H3 )
217         CALL COL( DEY, 1H4 )
218   @FOR, U MTITLE, MTITLE
219   -24, 24
220      60 FORMAT( ' ', 48X, '**********************', 24X, 'YOUNGS MOD MAGTEL'/
221   @FOR, UCX MAGTEL, MAGTEL
222   -153, 153
223         CALL FILTER( F, NFR, HXC, HYC, EXC, EYC )
224   -209, 209
225   210    FORMAT( ' SEGMENT NO. ', I3 )
226   -213, 213
227   C DATA FROM YOUNGS TAPES ARE ORDERED EX, EY, HX, HY
228   C RATHER THAN HX, HY, EX, EY AS IN OLD MAGTEL
229         CALL NXTSEG( EX, EY, HX, HY, IERR )
230   C THE FOLLOWING DELECTIONS STOP CERTAIN 'TIMER' CALLS, THUS SAVING PAPER
231   -234, 234
232   -243, 243
233   -264
234         SFR( I )=1.
235   -355, 355
236   420    FORMAT( '+', T20, ' POWERS PASSED ALL LEVEL TESTS AT ALL FREQUENCIES
237        $' )
238   -356, 356
239   450    CONTINUE
240   @FOR, UX READDT
241   -50, 50
242   C CHECK FOR IMPROPER BLOCK LENGTH FOR SEVEN TRACK AND NINE
243   C TRACK TAPE
244         IF( LEN. NE. 6006. AND. LEN. NE. 4505 ) GO TO 520
245   -71, 72
246         PRINT 525, LEN
247   525    FORMAT( 30X, 'LENGTH ERROR.  WORDS READ EQUALS ', I10 )
248   @MAP, IN   , TPF$. MAG2
249   @COPY, A TPF$. , CYAVE.
250   @PACK, C CYAVE.
251   @FIN
```

A.5 AVETEL Description

This program reads one or more data sets from the MAGTEL output tape, averages over successive data sets, calculates scalar apparent resistivities, tensor impedances and resistivities, rotation angles for R-max and R-min and rotated impedances and resistivities. These quantities are printed out and written on computer tape.

The modifications to AVETEL consist of changing the page titles to use less paper, a modification in phase calculations to keep the arctan function from underflowing for zero argument, and removal of tests for skew and variance, allowing all data to be used in the final averages.

AVETEL

The changes affecting the AVETEL run deck are

(1) Use of high density 7-track tape

(2) Storage of absolute element of AVETEL (compiled, ready to execute) on disk file.

A.5.1 AVETEL runstream deck

The following EXEC and data cards are required for running AVETEL. The program is modified according to the listing in section 10.5.3. The standard value we use on the AVETEL control cards is underlined.

@RUN user name, project number, user ID number, $ dollar limit, page limit

@ASG,HT, 20., T, $ reel ID of output tape

If one or more AVETEL runs are on the tape already, add here

@ MOVE 20., N N = number of runs already on AVETEL output tape

---

@ ASG,AX FILENAME. File on which compiled AVETEL is stored

@ ASG,HT 11., T, reel ID These logical unit numbers 11, 12, etc., correspond to the numbers on the TAPE cards which appear in the AVETEL cards. There should be 1 ASG card for each input tape specified.

@ ASG,HT 12., T, reel ID

up to 19. as needed

@ XQT FILENAME.AVETEL

AVETEL data cards: see below

@ FIN

A.5.2 AVETEL data cards

Card 1: Identification Card

Cols 1-10: Site (H)

Cols 11-20: Location (H)

Card 2: Bands per decade (and controls for some tests not used)

Cols 1-10: Number of bands per decade (I10) 10

Cols 21-30: Z-ratio test, F.P., for no test use 1000. 1000.

Card 3: Level tests for rejection of data

Cols 1-48: Coherency and Z denominator tests - leave blank to not use.

Cols 49-56: Skew level of Z^H, F.P., 0, to 10 10.

Cols 57-64: Skew level of Z^E, F.P., 0, to 10 10.

Cols 65-72: Phase test of Z, F.P., Set >> 1, to not use. 1000.

Cols 73-80: Variance test, F.P., set >> 1, to not use. 1000.

Card 4: Tape and record selection card

These cards are required to specify one or more data records to be included in the averaging process. Data records can be read from up to 10 different tapes (although 3 or 4 is a recommended maximum because of UWCC tape drive limitations). The first card must be a tape selection card of this format:

Cols 1-4: 'TAPE'

Cols 9-10: tape logical unit numer, lun; $10 \leq lun \leq 19$.

The tape selection card is followed by record selection cards, one card for each record on the tape to be included in the averages. These cards are punched out by MAGTEL whenever a record is written on tape, with format:

Cols 1-6: "MAGTEL"

Cols 7-10: Record number on tape

Cols 11-15: Logical Record Number of a raw data file

Cols 16-20: Physical " " " " " " "

Cols 21-25: String Number of a raw data file

Cols 31-36: UWCC Run in which MAGTEL created the record

Cols 41-48: Date of UWCC Run in which MAGTEL created the record

Cols 51-60: Output page number for Block 1 of UWCC Run in which MAGTEL created the record

Cols 61-70: Minimum frequency in the record

Cols 71-80: Maximum " " " "

The record selection cards for a tape must be ordered so that the record numbers (cols 7-10) are strictly increasing.

After all record selection cards for one tape are included, another tape selection card may be included followed by record selection cards for that tape.

To run several sets of data from unit 11 use:

```
@ XQT
     1st set
@ REWIND
@ XQT
     2nd set
```

If MAGTEL rejected all data for a string it will not write anything on tape, but will produce a record selection card. If you try to use this card in AVETEL, it will print "position error in data record" and stop. When you do a MAGTEL carryover these strings will be deleted from the new tape.

A.5.3 AVETEL modifications listing

```
252  @RUN,/R YOUNG,40660,7768,$5.00,100
253  @ASG,AX CYAVE.
254  @ASG,MT 10.,T,TTS658
255  @MOVE 10.,3
256  @COPY,G 10.,TPF$
257  @FREE 10.
258  @FOR,U AVETEL,AVETEL
259  -233,236
260  -240,264
```

```
261  @FOR,U MTITLE,MTITLE
262  -19,19
263  60     FORMAT(' ',48X,'**********',24X,'YOUNGS AVETEL'/
264  @FOR,U RPHI,RPHI
265  -20,20
266         Q(I)=0
267         IF(X.NE.0.AND.Y.NE.0) Q(I)=DGPRAD*ATAN2(Y,X)
268  @FOR,U START,START
269  -67,68
270         IF(HSKL..LE.0.OR.HSKL.GT.100)  ERR=1
271         IF(ESKL.LE.0.OR.ESKL.GT.100) ERR=1
272  @MAP,IN ,TPF$.AVETEL
273  @COPY,A AVETEL,CYAVE.AVETEL
274  @PACK CYAVE.
275  @PRT,T CYAVE.
276  @PASS PIERRE
277  @FIN
```